UNIVERSITÄT BAYREUTH

Fakultät für Biologie, Chemie und Geowissenschaften

Biochemical and structural characterisation of mammalian deiodinases as key regulators of thyroid hormone metabolism

DISSERTATION

to obtain a doctorate in natural sciences from the Faculty of Biology, Chemistry and Earth Sciences at the University of Bayreuth

presented by
M.Sc. Biochemist

Holly Towell

from Pontefract, West Yorkshire, United Kingdom

Bayreuth, 2021

This doctoral thesis was prepared at the department of Biochemistry at the University of Bayreuth from May 2016 until June 2021 and was supervised by Prof. Dr. Clemens Steegborn.

This is a full reprint of the dissertation submitted to obtain the academic degree of Doctor of Natural Sciences (Dr. rer. nat.) and approved by the Faculty of Biology, Chemistry and Geosciences of the University of Bayreuth.

Dissertation submitted on: 30th June 2021

Date of Defence: 15th February 2022

Acting dean: Prof. Dr. Benedikt Westermann

Doctoral Committee:

Prof. Dr. Clemens Steegborn (First Reviewer)

Prof. Dr. Claus – D. Kuhn (Second Reviewer)

Prof. Dr. Matthais Ullmann (Chairman)

Prof. Dr. Rhett Kempe

List of Publications

Schweizer, U., **Towell, H**., Vit, A., Rodriguez-Ruiz, A. and Steegborn, C. 2017. Structural aspects of thyroid hormone binding to proteins and competitive interactions with natural and synthetic compounds. *Molecular and Cellular Endocrinology*. **458**, pp.57–67.

Conferences & Courses

2020	Poster presentation at the BESSY User Meeting, online. Titled 'Structural Characterisation of Iodothyronine Deiodinases.'
2019	Oral presentation at the Heart of Europe Bio-Crystallography (HEC) meeting in Obergurgl, Austria. Titled 'Structural Characterisation of Iodothyronine Deiodinases.'
2019	Poster presentation at the Thyroid Trans Act in Berlin, Germany. Titled 'Structural Characterisation of Iodothyronine Deiodinases.'
2018	BCA/CCP4 Crystallography Summer School held at Diamond Light Source, Oxfordshire, United Kingdom.
2018	Oral presentation at the Thyroid Trans Act in Berlin, Germany. Titled 'Biochemical and Structural Characterization of mammalian deiodinases.' Joint presentation in collaboration with Alfonso Rodrigues-Ruiz.

Contents

Abbreviations

Amp^R – Ampicillin resistance
AQUA – Advanced quick assembly
BRET – Bioluminescence resonance energy transfer
CMC – Critical micellar concentration
CNS – Central nervous system
ddH_2O – Double distilled water
DDM - n-Dodecyl β-D-Maltoside
dH_2O – Distilled water
Dio - Iodothyronine deiodinases
DMSO - Dimethyl sulfoxide
DNA – Deoxyribonucleic acid
dNTP – 2'-desoxyribonucleoside-5'-triphosphate
DTT – Dithiothreitol
ER – Endoplasmic reticulum
FBS – Foetal bovine serum
FITC - Fluoresceinthioisocyanate
FRET - Fluorescence resonance energy transfer
GTG - Gold thioglucose
hDio – Human Deiodinase construct
HEPES - 4-(2-hydroxyethyl)-1-piperazineethanesulfonic acid
I^+ - iodine cation
IMAC – Immobilised affinity chromotography
IPTG - Isopropyl β-D-1-thiogalactopyranoside
LB – Lysogeny broth
LZ – Leucine zipper
LZ_D3C – Mouse Deiodinase 3 and leucine zipper construct
mDio – Mouse Deiodinase construct
MMI – Methimazole
MOI – Multiplicity of infection
MST – Microscale thermophoresis
MTU – Methylthiouracil
ON – Overnight
PACT - pH, anion- and cation testing
PBS – Phosphate buffered saline
PCR – Polymerase chain reaction
PFU – Plaque forming units
PMSF - phenylmethylsulphonyl fluoride
PTU - Propylthiouracil
RF – Restriction free
rT_3 – reverse 3,3',5'-triiodothyronine
SAXS – small angle x-ray scattering
SDM – Site directed mutagenesis
SDS-PAGE – sodium dodecyl sulphate–polyacrylamide gel electrophoresis
Se^- - Selenolate
Sec – Selenocysteine
SEC – Size exclusion chromotography
SeI – Selenium iodide
SOB – Super optimal broth
SUMO - small ubiquitin-related modifier
T_2 - 3,5-Diiodothyronine
T_3 - 3,3',5-triiodothyronine
T_4 - 3,3',5,5'-tetraiodothyronine
TB – Terrific broth
TCEP - Tris-(2-carboxyethyl)-phosphine
TEMED - N,N,N',N'-tetramethylethylendiamine
TEV - Tobacco Etch Virus
TFs – Transcription factors
Tg – Thyroglobulin
TH – Thyroid hormones
THR – Thyroid hormone receptor
TPO - Thyroid peroxidase
TRIS - Tris(hydroxymethyl)aminomethane
Trx – Thioredoxin
TSA – Thermal shift denaturation assay

Zusammenfassung

Iodothyronin-Deiodinasen (DIO) sind eine Familie Selenocystein-abhängiger Transmembranenzyme, die den Spiegel des aktiven Schilddrüsenhormons regulieren. Alle drei Deiodinase-Isoformen (Dio1-3) besitzen homologe katalytische Domänen und eine ähnliche homodimere Architektur. Sie katalysieren eine einzigartige Selen-abhängige reduktive Halogeneliminierung an aromatischen Ringen von Schilddrüsenhormonen, unterscheiden sich jedoch in ihren Regioselektivitäten der Deiodierung und ihren regulatorischen Eigenschaften. Eine zuvor gelöste Kristallstruktur des katalytischen Kerns der Dio3 aus *mus musculus* ($Dio3_{cat}$) zeigt eine Peroxiredoxin-Faltung und eine Substratbindetasche. Allerdings kristallisierte das Protein als Monomer und war somit nicht in der Lage, das Substrat oder Inhibitoren im aktiven Zentrum zu binden. Das Ziel dieser Arbeit war, Einblicke in die Unterschiede der Deiodinase-Isoformen bezüglich ihrer spezifischen Regioselektivitäten, die mögliche Dimerisierungstelle und Interaktionsdetails mit dem Substrat zu erhalten, um so die Entwicklung verbesserter Substrate/Inhibitoren für die Behandlung der Schilddrüse und schilddrüsenbezogener Krankheiten zu ermöglichen.

Die Kristallstruktur der katalytischen Dio2 Domäne aus *mus musculus* wurde gelöst und weist stark ähnliche Sekundärstrukturelemente zu Dio3 auf, was den vorgeschlagenen gemeinsamen Mechanismus unterstützt. Weiterhin zeigt die Struktur auch Dio2-spezifische Merkmale, die vermutlich die einzigartigen katalytischen Eigenschaften vermitteln, einschließlich des Zusammenhangs mit der Ubiquitinierung und dem proteasomalem Abbau. Weitere Arbeiten, basierend auf Grundlage der zuvor gelösten Strukturen, führten zur Entwicklung eines Dio1-Homologiemodells. Dies ermöglichte weitere Einblicke in die Gemeinsamkeiten und Unterschiede aller drei Isoformen, insbesondere bezüglich der Reste im und um das aktive Zentrum, was zu möglichen Erklärungen der unterschiedlichen Spezifität und allgemeinen Aktivität führte.

Obwohl Dio2 in erster Linie monomer vorliegt, dimerisierte auch ein kleiner Anteil. Nachfolgende Tests zeigten, dass das Dio2 Dimer relativ stabil und reproduzierbar war. Durch chemische Quervernetzung konnten die an der Dimerisierung beteiligten Lysine bestimmt werden, die das vorhergesagte Modell des Homodimers bestätigen. Da Kristallisationsversuche von dimerisiertem Dio2 erfolglos waren, wurde ein Dio3 Dimer mittels eines artifiziellen Leucin-Zipper-Fusionsproteins stabilisiert.

Aktivitätsassays mit dimerisiertem Dio3 zeigten, dass das Dimer in Gegenwart von TH-Substrat (T_4) aktiv und DTT-abhängig ist, was die Enzymkinetik der Dio-Isoformen bestätigt. Kristallisationsversuche des Dio3 Dimers ergaben Mikrokristalle, die leider weder optimiert werden konnten noch Diffraktion zeigten. Weitere Bindungsarbeiten mit dimerem Dio3 deuteten auch auf eine Bindung des Inhibitors Xanthohumol hin und wurden für weitere Kristallisationsexperimente neben monomerem Dio2 Protein verwendet.

Diese Arbeit liefert weitere Einblicke in die strukturellen Merkmale der Dio-Isoformen und zeigt, dass die Dimerisierung durch den N-Terminalen Bereich und den katalytischen Kern des Enzyms vermittelt wird, wobei der N-Terminus hauptsächlich zur Stabilisierung des Dimers beiträgt und die Gesamtaktivität unterstützt. Durch Quervernetzungsstudien wurde die zur Dimerisierung beitragende Oberfläche bestimmt, was weitere Einblicke in die Architektur des gesamten Dio-Homodimers ermöglicht.

Summary

Iodothyronine Deiodinases (DIO) are a family of selenocysteine-dependent transmembrane enzymes that regulate the levels of active thyroid hormone. All three deiodinase isoforms (Dio1-3) feature homologous catalytic domains and a related homodimeric architecture. They all catalyse a unique selenyl-dependent, reductive halogen elimination on the thyroid aromatic rings, but differ in their regioselectivies for the deiodination and regulatory features. A previously solved crystal structure of the mouse Dio3 catalytic core ($Dio3_{cat}$) revealed a peroxiredoxin fold and a substrate binding pocket. However, the protein crystallised as a monomer which is unable to bind substrate or active-site inhibitors. The aim of this work was to obtain insights into deiodinase isoform differences that causes their specific regioselectivities, the potential dimerization interface and function, and the interaction details with the substrate, enabling improved substrates/inhibitors to be developed for the treatment of thyroid and thyroid-related diseases.

The crystal structure of the mouse Dio2 catalytic domain was solved, which revealed highly similar secondary structure elements to Dio3 supporting the proposed common mechanism. However, the structure also indicated Dio2 specific features likely mediating its unique catalytic properties, including the correlation with ubiquitination and proteasomal degradation. Further structural work led to the development of a Dio1 homology model based on the previous solved structures. This allowed further insight into the similarities and differences between all three isoforms, in particular the residues in and around the active site region indicating possible explanations for differences in specificity and general activity.

Although Dio2 yielded primarily monomer proteins, a small proportion of dimeric Dio2 was produced. Subsequent testing signified that the dimeric Dio2 species was relatively stable and reproducible and further work with cross-linking studies revealed lysine residues implicated in the dimerization interface reinforcing the predicted homodimer model. However, as crystallisation trials for the dimeric Dio2 were unsuccessful, an enforced Dio3 dimer was created with the use of a Leucine zipper fusion. Activity assays with the Dio3 dimer showed that the dimeric protein is active in the presence of TH substrate (T_4) and DTT dependent supporting the enzyme kinetics of the Dio isoforms. Crystallisation trials with the Dio3 dimer produced micro crystals, which either produced no diffraction or unfortunately could not be optimised. Further

binding work with the dimeric Dio3 also indicated binding with the inhibitor Xanthohumol and has been used in additional ongoing crystallisation screenings alongside Dio2 monomeric proteins.

This work provides further insight into the structural features of the Dio isoforms and reveals that dimerization is mediated by the enzyme's N-terminus and catalytic core, with the N-terminus mainly contributing to stabilisation of the dimer and supporting the overall activity. Cross-linking studies revealed the surface mediating dimerization, providing further insights into the architecture of the complete Dio homodimer.

1.0 Introduction

1.1 Background – The Thyroid Hormones

Thyroid hormones (TH) are tyrosine-based hormones produced by the thyroid gland that have become iodinated; an important component in the amount of active and inactive THs circulating throughout the body. They are essential for any normal development of the tissues and growth in almost all vertebrates, and are crucial modulators of energy metabolism. (Bianco and Kim, 2006; Mullur *et al*., 2014; Mondal and Mugesh, 2017). THs play an important role in many bodily functions, for example they can prompt the processes of glycolysis and gluconeogenesis and they can increase the production of thermal energy (Mullur *et al*., 2014). THs also influence gene expression, this is especially important during developmental stages (de Escobar *et al*., 2008), by binding to the thyroid hormone receptors (THRs) (Samuels *et al*., 1988). THRs are transcription factors (TFs), which are a subfamily of nuclear receptors, that can recruit activator and repressor proteins which in turn can affect gene transcription (Martínez-Iglesias *et al*., 2014). This is due to THRs interacting with complexes containing histone deacetylases or acetyltransferases resulting in activation or inactivation of transcription (Wu and Koenig, 2000), respectively. This can then also affect the production of mRNAs and ultimately the translation of proteins (Martínez-Iglesias *et al*., 2014). THRs are ultimately very sensitive to the serum levels of the THs and so a balance is required within the body to ensure healthy functionality. Relatively small deviations from normal TH levels can result in various thyroid associated diseases with the most well-known being decreased (hypo-) or increased (hyperthyroidism) TH levels. Hypothyroidism results in the inability to tolerate the cold, feeling tired and depressed, as well as experiencing weight gain (National Institute of Diabetes and Digestive and Kidney Diseases, 2013). While hyperthyroidism can cause a patient to suffer from muscle weakness, a faster heart rate, an inability to tolerate heat, significant weight loss and the most noticeable side effect; an enlarged thyroid gland (National Institute of Diabetes and Digestive and Kidney Diseases, 2016).

Hypothyroidism can be treated via hormone replacement therapy however, hyperthyroidism, if left untreated, can ultimately progress into a life-threatening disease with a last resort being a thyroidectomy (Mandel and Davies, 2011). And so, the inhibition of thyroid hormone action would be an attractive therapeutic option.

1.2 Function of Iodothyronine Deiodinases on the Thyroid hormones

The thyroid gland synthesises the prohormone 3,3',5,5'-tetraiodothyronine (T_4/thyroxine) using the precursor thyroglobulin (Tg). Tg's tyrosine residues become iodinated in the thyroid gland and selective tyrosine residues can lead to the favoured formation of T_4 (Citterio *et al*., 2019). T_4 is distributed to peripheral tissues, where it can be deiodinated into the main active form, 3,3',5-triiodothyronine (T_3) and the potentially inactive forms diiodothyronine (T_2) and reverse T_3 (rT_3) (Bayse *et al*., 2020). Despite T_2 and rT_3 being considered inactive, they are also substrates of deiodinases (Visser, 1988) and have been implicated in some metabolic functions i.e. increasing resting metabolic rate (Celi *et al*., 2018). Deiodination can occur on the tyrosol (5-/inner) or phenolic (5'-/outer) rings (Fig 1) and is catalysed by a family of enzymes called iodothyronine deiodinases (Dio), which comprises of three members: Dio1, Dio2 and Dio3. These enzymes are responsible for the activation and inactivation of the THs throughout the body.

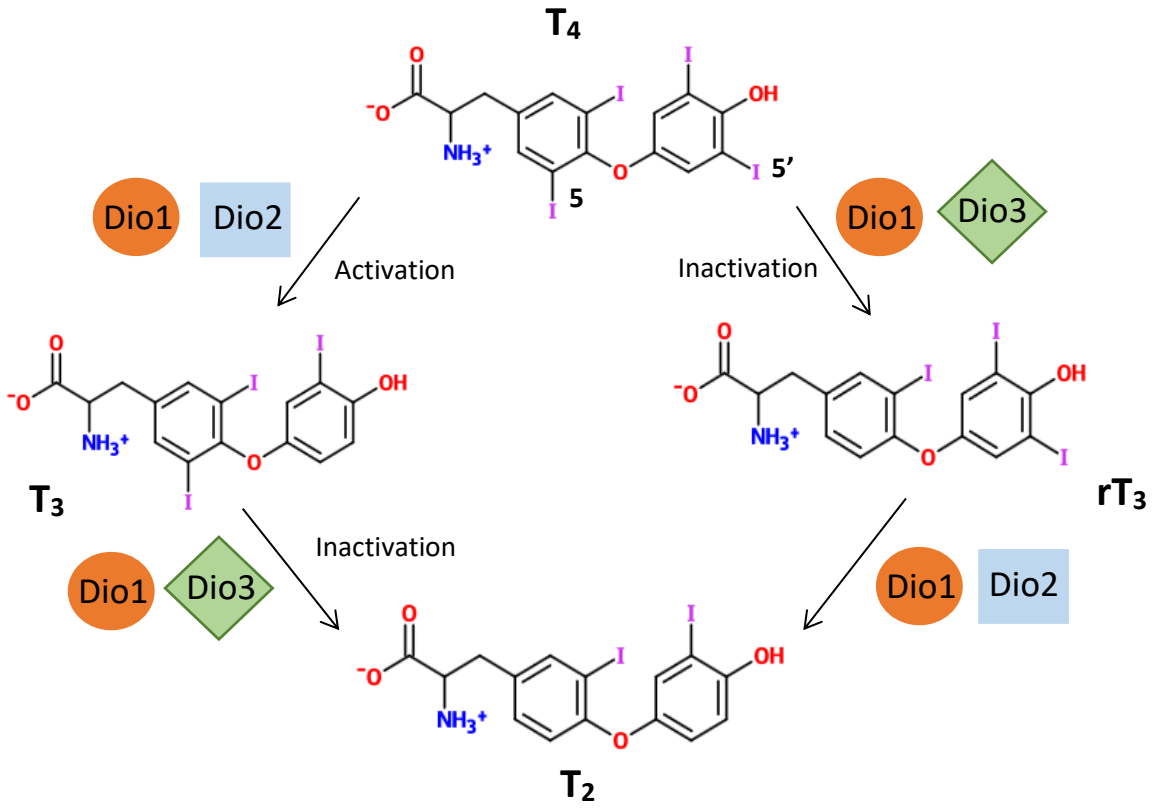

Figure 1. ***Deiodination of Thyroid Hormones.*** *Reactions catalysed by deiodinases, resulting in the removal of iodine from the substrates, creating active and inactive forms of the thyroid hormones. Adapted from Schweizer and Steegborn, 2015.*

1.3 Biochemical & molecular properties of Iodothyronine Deiodinases

All three deiodinase isoforms have differing regioselectivities for the THs but feature homologous catalytic domains (Bianco *et al*., 2002; Schweizer *et al*., 2014) and transmembrane regions with a related homodimeric architecture. The short transmembrane region is connected to the catalytic core via a linker, which mediates the proposed dimerization (Fig 2). All Dio isoforms are type-1 thioredoxin (Trx) folded integral membrane proteins with an active site pocket of β1-α1-β2 motifs of the Trx fold (Callebaut *et al*., 2003).

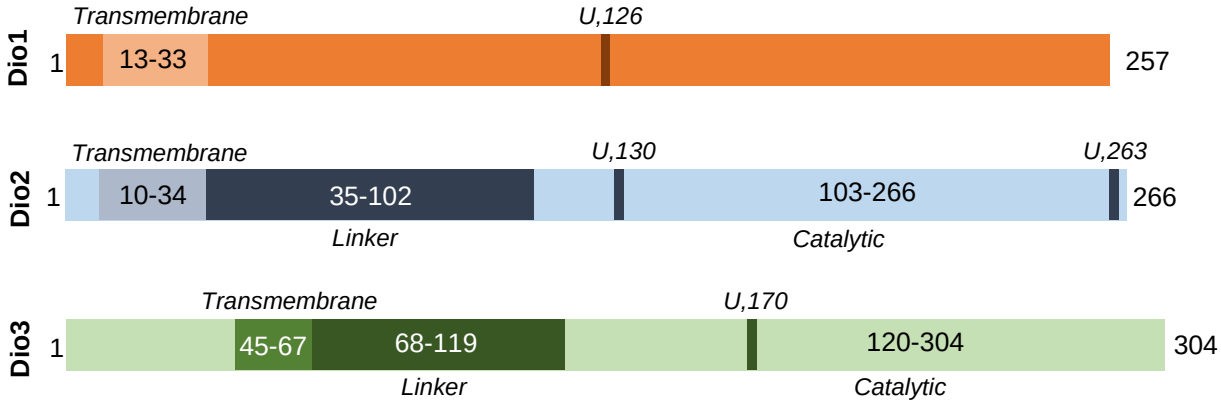

Figure 2. ***Schematic representation of Dio protein domains in mus musculus.*** *Dio1 (orange) currently has very little information about the linker or catalytic sites whereas, Dio2 (blue) and Dio3 (green) sequences have more experimental data and structural information. U represents selenocysteine and indicates the active sites of the deiodinases.*

1.3.1 The Iodothyronine Deiodinase active site

The unique component of these enzymes is the presence of a selenocysteine (Sec/U) within the active site for each isoform, discovered towards the end of the 1990s via the cDNAs. Dio1 and Dio3 have only one UGA Sec codon in the active site; the Dio1 Sec is conserved in position 126 and the Dio3 is present at position 170, both in humans, mice and rats (Maria J. Berry *et al*., 1991; St. Germain *et al*., 1994; Croteau *et al*., 1995). Dio2 varies by having two Sec residues present in the sequences for humans, mice, rats and chickens (Davey *et al*., 1995). The first Sec residue is in the active site (similarly to Dio1/3) at position 130 in mice and 133 in humans, whereas the second Sec residue is close to the C-terminus of the protein but does not appear to play a role in the catalytic activity of the enzyme (Salvatore *et al*., 1999). This suggests that the second Sec is in fact an artefact that appears after the stop codon in Dio2 and that the isoforms with only one Sec represent the canonical form. This is further supported by

the second Sec residue not being present in the Dio2 sequences of fish and frogs (Davey *et al*., 1995; Croteau *et al*., 1996; Valverde-R *et al*., 1997).

The active site Sec catalyses a unique selenyl-dependent reductive halogen elimination from the thyroid aromatic rings. Dio1 has the ability to catalyse both the phenolic and tyrosol ring deiodinations, whereas Dio2 can only catalyse the phenolic and Dio3 can only catalyse the tyrosol deiodinations (Fig 1). The deiodinases are the only selenoenzymes known to catalyse halogen eliminations from aromatic rings.

1.3.2 Kinetics of Iodothyronine Deiodinases

The different mechanisms of the Dio isoforms is further supported by their kinetic differences i.e. Dio1 follows ping-pong kinetics, while Dio2 and 3 follow sequential kinetics (Schweizer and Steegborn, 2015). The Dio1 ping-pong mechanism is catalysed by two substrates, the first being Dio1 and the second, an unidentified thiol cofactor (Visser *et al*., 1976; M. J. Berry *et al*., 1991). In the first half of the reaction Dio1 transfers an iodine cation (I^+) from the TH substrate to the selenolate anion (Se^-) of the Sec within the active center, forming an intermediate compound. In the second half of the reaction, this compound is reduced by the unknown cofactor resulting in a selenium iodide (SeI) complex (Fig 3). In this reaction, the cofactor would act as a reducing agent allowing Dio1 to regenerate (M. J. Berry *et al*., 1991; Bianco *et al*., 2002; Maia *et al*., 2011).

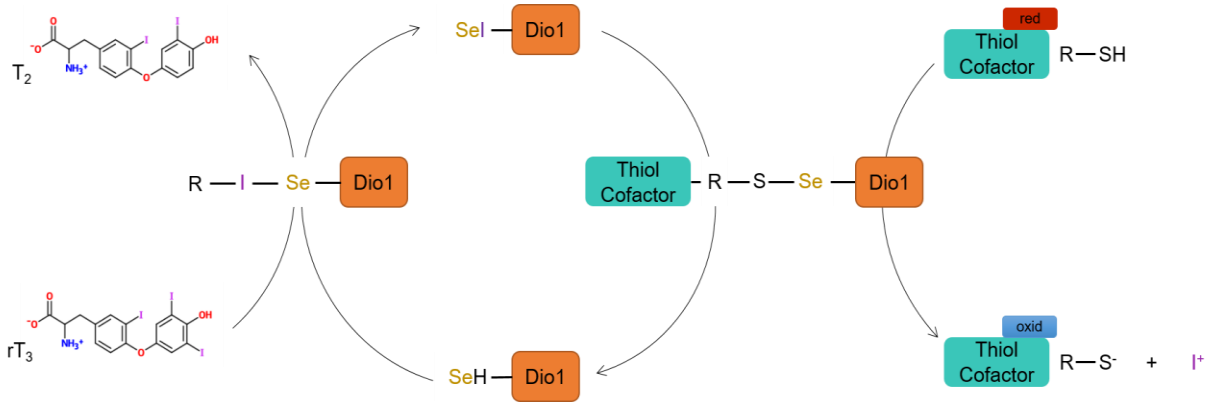

Figure 3. ***Schematic model of the D1 catalysed reaction.*** *Visualisation of the Dio1 ping-pong kinetics mechanism. rT_3, 3,3',5'-triiodothyronine; T_2, diiodothyronine; D1, deiodinase type 1; Se, selenium; I, iodide. Based on figure from Maia, 2011.*

Unlike Dio1, Dio2 and 3 follow sequential reaction kinetics, whereby both the substrate and the thiol cofactor are thought to bind to the enzyme simultaneously for a deiodinase reaction to take place (Visser *et al*., 1982; Luiza Maia *et al*., 2005). Particularly for Dio3, it is surmised that the Sec is oxidised within the active site causing the enzyme to become inactive until an unidentified cofactor can reduce the Sec within the endosome environment, theoretically reactivating Dio3.

The affinity of the Dio isoforms to the TH substrates (Table A1) also strengthens their proposed function and role. Dio2 has a high substrate affinity for T_4, with a K_M of ~ 2.2 nM, while Dio1 has a K_M of ~ 1 µM (Visser *et al*., 1982; Campos-Barros *et al*., 1996; Bianco *et al*., 2002). Dio2 also has a high affinity for rT3 with a K_M of ~ 2.4 nM, suggesting that Dio2 can also recover iodine (like Dio1) but that its main function is activation of the THs (Campos-Barros *et al*., 1996). Dio3 can deiodinate both T_3 and T_4 and has an affinity for these substrates in the nM range with a particular low K_M for T_3 (6 nM in rats, 1 nM in frogs and 12 nM in humans) compared to that of T_4 (K_M of ~ 37 nM in rats) (St. Germain *et al*., 1994; Salvatore *et al*., 1995; Bianco *et al*., 2002).

1.3.3 Iodothyronine Deiodinase structure

Although the biochemical and molecular properties of Dio3 are not as well-known as the other Dio isoforms, it is the only deiodinase structurally characterised (Fig 4a). This not only provides insight into the structural and possible catalytic properties of Dio3 but also of Dio1 and 2 due to similar sequence homologies. In the Dio3 structure, the N-terminal transmembrane and part of the linker region were omitted, and the Sec was mutated to cysteine within the active site. This resulted in reduced enzyme activity but allowed the crystallisation of the monomeric Dio3 catalytic domain to take place, giving more insight into the wildtype protein. This structure was solved at a resolution of 1.9 Å and confirmed the prediction of a Trx-folded protein; however the structure also revealed similarity to a 2-Cys peroxiredoxin from the peroxiredoxin (Prx) family (Fig 4b), but with deiodinase specific modifications and insertions (Schweizer *et al*., 2014). The resultant structure was a five-stranded mixed β-sheet surrounded by four α-helices (Fig 4a and b) with an N-terminal Prx-like module consisting of a two-stranded antiparallel β-sheet (βN) followed by a 3_{10}-helix (Θ1). The specific deiodinase insertion (residues 201-225) forms loop-D followed by an α-helix (αD) and a short β-sheet (βD). The catalytic Sec^{170} (replaced by cysteine) is located in the loop between α1 and β1, which points towards the protruding deiodinase specific loop-D, supporting the idea that this is important for TH binding.

Further investigation into the structure revealed two conserved histidine residues (Dio3, His^{202} and His^{219}) similar to those of Dio1 (His^{158} and His^{174}). These histidine residues are important for Dio1 catalytic activity (Berry, 1992) and the corresponding Dio3 histidines also appear to contribute to the catalysis. The structure of Dio3 showed that the His^{202} (corresponds to Dio1-His^{158}) projects out from the deiodinase insertion on loop-D into the substrate binding site (Fig 4c). Schweizer *et al*., 2014 suggested that the His^{202} position on the loop-D and the distance from the Sec^{170} shows that the histidine acts as a binding partner for the phenolic end of the substrate, similarly to His^{435}-Arg^{282} clamp in the T_3-receptorβ ($T_3Rβ$) complex. This was used to model the potential binding of iodothyronine in the Dio3 binding site (Fig 4c). Dio3-His^{219} (corresponds to Dio1-His^{174}) was shown to be between loop-D and αD. When combined with the conserved Glu^{200}, it suggested a proton transfer cascade could contribute to the catalysis of iodothyronine upon deiodination. It is proposed that the proton passes along conserved residues His^{219}, Glu^{200} and Ser^{167}, with Tyr^{197} and Thr^{169} supporting this H-bond network, before reaching the tyrosol position on the TH (Schweizer *et al*., 2014). This is also supported by previous mutagenesis experiments on the other Dio isoforms, whereby these essential residues are needed to maintain a binding affinity to the THs and thereby activity (Berry, 1992; Callebaut *et al*., 2003).

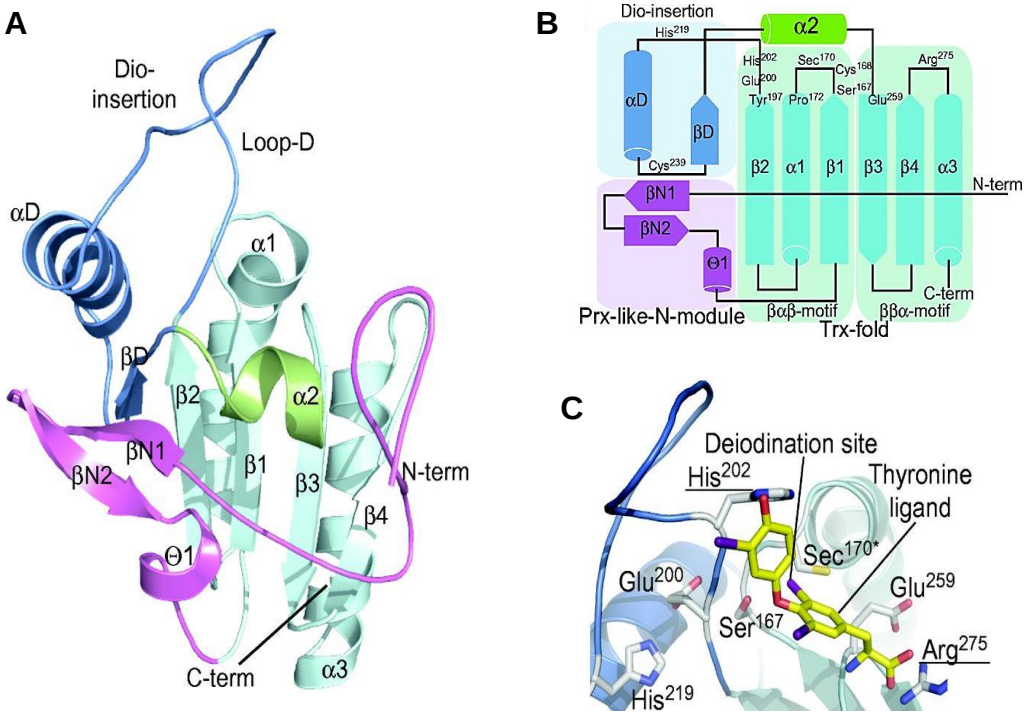

Figure 4. ***Structure of mammalian Deiodinase 3 catalytic domain.*** *(A) Crystal structure of mus muculus $Dio3_{cat}$ resolved to 1.9Å. (B) Topology of $Dio3_{cat}$. (C) $Dio3_{cat}$ active site with modelled Thyronine ligand. Figure taken with permission from Schweizer et al, 2014.*

1.4 Physiology of Iodothyronine Deiodinases

Dio1 was the first deiodinase to be implicated in the T_4 to T_3 conversion (Bianco *et al*., 2002) and the first to be cloned (Maria J. Berry *et al*., 1991; Mandel *et al*., 1992). Therefore, Dio1 biochemistry has been investigated more significantly compared to the other two deiodinases. Dio1 is the only selenodeiodinase that can catalyze both the tyrosol and phenolic ring deiodination, supplying a large portion of the circulating plasma T_3 in the body (Maia *et al*., 2011). However, Dio2 is also responsible for the activation of the THs by deiodination of the phenolic ring and contributes a significant amount of the circulating T_3 in the body. Studies of Dio2 showed that this enzyme delivers a large portion of serum T_3 levels, due to a 700-fold greater catalytic efficiency of T_4 deiodination compared to the inefficient Dio1 (Salvatore *et al*., 1996; Bianco *et al*., 2005; Luiza Maia *et al*., 2005) and so Dio2 is now considered to be the dominant isoform responsible for producing T_3. In contrast, Dio3 has no role in the activation of the THs and is instead considered to be the major inactivator of TH function (Bianco *et al*., 2002; Salvatore, 2011). Dio3 deiodinates the tyrosol ring catalysing the conversion of T_4 to rT_3 and T_3 to T_2, which are considered biologically inactive but play a role in controlling the homeostatic mechanism to protect tissues from excessive amounts of THs (Visser, 1988; Gomes-Lima *et al*., 2019).

1.4.1 Regulation & degradation of Iodothyronine Deiodinases

The Dio isoforms in a healthy individual must be regulated correctly to ensure that the active THs are only provided where they are needed. This is done via feedback regulation through TH signaling. Dio1 is upregulated by T_3 but has a higher affinity for rT_3 and the sulphated THs (Toyoda *et al*., 1997; Maia *et al*., 2011) suggesting that the main function of Dio1 is to deiodinate rT_3 ultimately to scavenge and recover iodine, rather than deiodinate T_4. It has also been shown that Dio1 cannot be ubiquitinated (Gereben *et al*., 2000) and so Dio1 activity may be maintained via protein synthesis (Maia *et al*., 2011). On the other hand, Dio2 which is considered to be the main activating TH, has a very short half-life (~20 minutes) which is exacerbated by Dio2 interaction with T_4, rT_3 and even high concentrations of T_3 in the cell, leading to an activity-induced inactivation (Halperin, 1994; Steinsapir *et al*., 1998; Bianco *et al*., 2002; Schweizer and Steegborn, 2015). This inactivation involves the use of ubiquitination and ultimately proteasomal degradation resulting in an inactive Dio2 conformation (Gereben *et al*., 2000; Sagar *et al*., 2007). Alternatively, the enzyme can be reactivated through deubiquitination (Sagar *et al*., 2007; Schweizer and Steegborn,

2015). This suggests that there is a dynamic equilibrium between increased activities of Dio2 at a lower concentration of T4 versus inactive ubiquitinated Dio2 at higher levels of substrate (Bianco *et al*., 2002). Less is known about the regulation of Dio3, but it is predicted that it can become internalised in endosomes, from the plasma membrane. This suggests that Dio3 could be relocated and recycled for further use where needed (Baqui *et al*., 2003; Bianco and Larsen, 2005). This hypothesis is supported by the long half-life of Dio3 at approximately 12 hours (Baqui *et al*., 2003).

1.4.2 Cellular localisation of Iodothyronine Deiodinases

Much like the differing regioselectivities of the Dio isoforms, the location of each individual Dio varies within cells. Dio2 is the only isoform located in the endoplasmic reticulum (ER) membrane (Baqui *et al*., 2003; Arrojo E Drigo and Bianco, 2011). Protease protection assays indicated that the N-terminus is found in the ER lumen, with the catalytic domain and C-terminus in the cytoplasm (Baqui *et al*., 2000; Bianco *et al*., 2002). The location of Dio2 is critical for generating intracellular T_3 for the THR-containing nuclear compartment (Arrojo E Drigo and Bianco, 2011). Unlike Dio2, immunohistochemical and immunofluorescence studies have shown that Dio1 is localized in the plasma membrane with the catalytic site located in the cytosol (Leonard and Rosenberg, 1978; Baqui *et al*., 2000; Leonard *et al*., 2001) and has a hydrophobic N-terminal extension into the ER lumen. This N-terminus acts as a signal recognition sequence but does not contribute to the catalytic activity, although mutating the amino acids results in reduced efficiency of transient expression and optimal formation/folding of the protein (Toyoda *et al*., 1995; Bianco *et al*., 2002; Bianco and Larsen, 2005). Dio3 is also believed to be located in the plasma membrane (Bianco and Larsen, 2005; Marsili *et al*., 2011). However, less is known about the localisation of Dio3 compared to the other Dio isoforms, but further tests revealed that although Dio3 could be localised in the plasma membrane, this is only for a short amount of time (Baqui *et al*., 2003).

1.4.3 Tissue localisation of Iodothyronine Deiodinases

The Dio isoforms are also present in different tissues and this relates to where the active or inactive THs are needed most. Dio1 is a ~27 kDa protein and is mainly expressed in the liver and kidneys but has also been identified in the thyroid, pituitary gland, intestine, placenta and gonads of adults (Bates *et al*., 1999). It is notably absent in the central nervous system (Campos-Barros *et al*., 1996). Dio1 activity is only present at low levels in the early stages of development in mammals but increases in

the later stages i.e. after birth. However, specifically in rat tissues, Dio1 is expressed in the liver, kidneys and intestine at all development stages (Bates *et al*., 1999).

Dio2 is a ~31 kDa protein and is mainly expressed in the brown adipose tissue, skeletal muscles, brain, pituitary gland, heart, skin, thyroid gland and smooth muscle cells in humans (Salvatore *et al*., 1996; Eravci *et al*., 2000; Bianco *et al*., 2005; Marsili *et al*., 2011). Interestingly, Dio2 appears to have a species-specific difference in expression and function e.g. Dio2 is the only deiodinase present in the CNS (central nervous system) for humans, whereas Dio2 and Dio3 are present in the CNS of rats (Campos-Barros *et al*., 1996). Furthermore, Dio2 is absent in the livers of humans and rats (unlike Dio1) but present and active in the liver of adult chickens and fish (Valverde-R *et al*., 1997; Gereben *et al*., 1999). Dio2 activity in tissues is markedly increased during the final stages of pregnancy and in the first few months after birth, reaching higher levels than seen in adults. This suggests that high levels of Dio2 are required for the production of T_3 in developmental processes (Bernal, 2016) e.g. Dio2 is present at high levels in the mouse cochlear postnatally (Campos-Barros *et al*., 2000).

Dio3 is a ~31.5 kDa protein and is expressed predominantly in the skin, placenta and the CNS in adults but is highly expressed in the intestine, liver and skeletal muscle neonatally, indicating that Dio3 may protect developing organs from exposure to the maternal THs (Visser, 1988; Bates *et al*., 1999; Tu *et al*., 1999; Bianco *et al*., 2002; Bianco and Larsen, 2005). Dio3 activity has also been known to reactivate in tissues during periods of injury, illness or disease (e.g. hypoxia, starvation or inflammation) and also shows an increased expression in tumours (e.g. gliosarcoma) (Visser, 1988; Huang and Bianco, 2008; Casula and Bianco, 2012; Aw *et al*., 2014). This gives rise to the idea that expression levels of certain deiodinases could contribute to tumour development by the increased proliferation of cells (Visser, 1988; Gereben *et al*., 2008; Casula and Bianco, 2012).

1.5 Iodothyronine Deiodinase dimerization

As previously stated, the Dio isoforms appear as homodimers in nature (Sagar *et al*., 2008) and that the dimerization is required for deiodination to occur (Sagar *et al*., 2007). The N-terminal transmembrane and linker region is required not only for cell localisation but also for the mediation of dimerization (Sagar *et al*., 2007; Schweizer *et al*., 2014). The previous work on Dio3 has only provided structural insights for the inactive, monomeric form of the protein (Schweizer *et al*., 2014) using a truncated

recombinant Dio3. This work reinforces the idea that the N-terminal region is needed to support dimerization and that the catalytic domain has only weak intrinsic dimerization properties (Schweizer *et al*., 2014). The structure revealed clear electron density for Phe^{258} from the α2/β3 loop and that it obstructs the active site. This is also the only residue in the disallowed region of a Ramachandran plot (Schweizer *et al*., 2014) indicating that this is not the recommended conformation of Phe^{258}.

A model of a potential $Dio3_{cat}$ dimer was produced by basing the catalytic domain dimer on rat heme-binding protein (HBP23) that belongs to the 2-Cys Prx family and fusing this to a homology model of the transmembrane region (Schweizer *et al*., 2014) (Fig 5a). This model inferred that the N-terminal loop and the β4 of one of the monomers could have close contacts with the β4/α3-loop and substrate site on the second monomer (Schweizer and Steegborn, 2015). This form of dimerization could cause a relaxation of the α2/β3-loop allowing T_3 (or other thyroid ligands) to bind to the active site (Sec^{170} for Dio3 model) that as a monomer would have been shielded by Phe^{258}, with an auto-inhibitory conformation (Fig 5b).

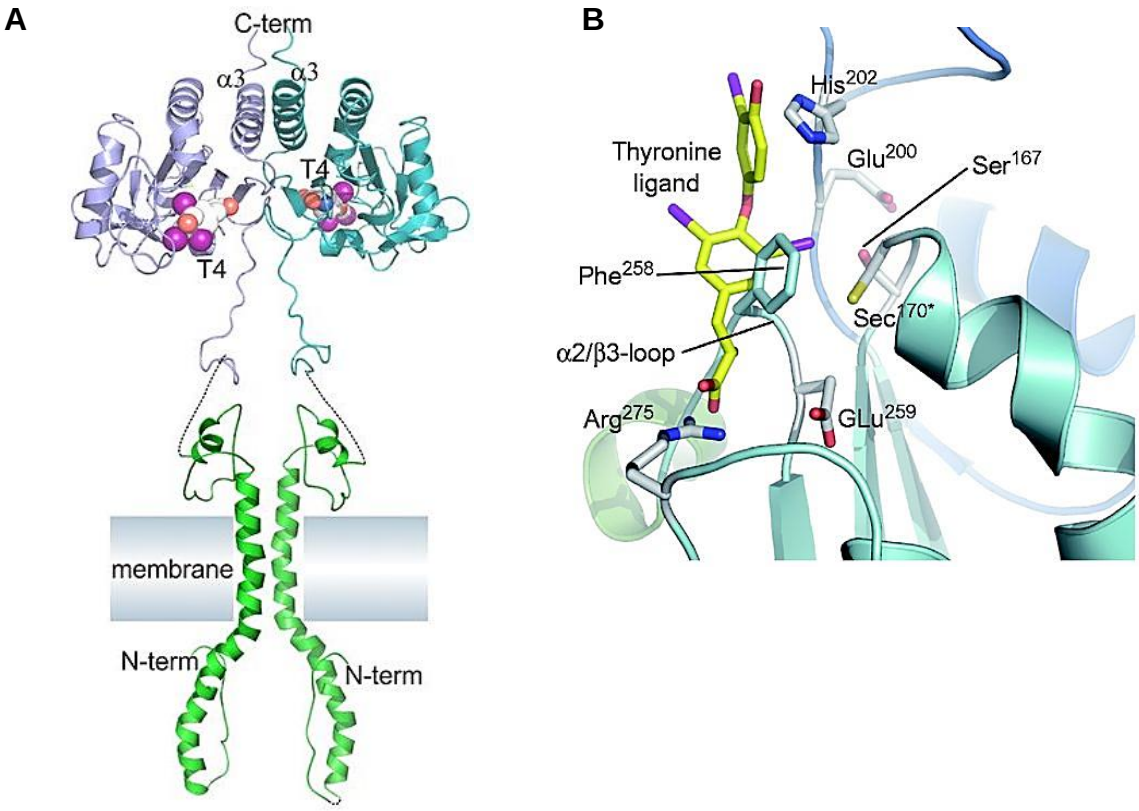

Figure 5. ***Dimerization model of Dio3*** *(A) Model of full length Dio3 dimer, based on HBP23 and fused to a homology model for the transmembrane region. (B) Model of* $Dio3_{cat}$ *complex with thyronine ligand. Figures taken with permission from Schweizer et al, 2014.*

1.6 Deiodinase modulating compounds

As deiodinases are the key activators and inactivators of the THs, they are a desirable drug target to help normalise TH levels preventing serious illnesses or life-threatening diseases. Current methods of controlling dangerously fluctuating TH levels are either through synthetic forms of hormone replacement or by blocking the synthesis of THs altogether. Therefore, the inhibition of the Dio isoforms could be a potentially less invasive and more focussed form of treatment.

All three Dio isoforms are potentially important drug targets however, Dio2 and Dio3 are arguably the key isoforms to inhibit as the main activating and inactivating TH enzymes. Dio2 is responsible for converting the majority of T_4 into T_3 and so inhibiting Dio2 could reduce the amount of circulating active THs, this could be particularly important in patients with an overactive thyroid i.e. Grave's disease. Dio3 could also be an attractive drug target as although it is associated with the inactivation of THs it is also linked to cell proliferation in tumours (Huang and Bianco, 2008; Dentice *et al*., 2013). An inhibition of Dio3 could potentially reduce the malignancy in tumours (Mondal and Mugesh, 2017). Further structural information of the Dio isoforms could provide renewed interest in potential new drugs as well as revisiting compounds. The dimerization interface of the Dio isoforms could also shine more light on potential compounds and further the development of potential drugs.

1.6.1 Natural compounds

There are many natural compounds that have been discovered over the years, some with no similarity to the TH substrates, which have shown significant data on the inhibition of Dio catalysis. This includes gold, a competitive inhibitor of all three Dio isoforms, and gold-containing drugs i.e. gold thioglucose (GTG) (Figure A2a). Gold can interact with the selenium active center of all isoforms (M. J. Berry *et al*., 1991; Marsili *et al*., 2011), while GTG in particular can inhibit Dio2 by interacting with the Sec to produce a gold-selenolate complex. However, this would need to be developed further as it seems to rely on gold ions to form this intermediate and is non-specific (Kuiper *et al*., 2005; Schweizer and Steegborn, 2015; Mondal and Mugesh, 2017). Most recently, xanthohumol (Figure A2b), a prenylated chalconoid, was identified as a potent inhibitor of all three Dio isoforms (IC_{50} 1.5-3 µM) and genistein (Figure A2c), an isoflavonone, is an inhibitor specific to Dio1 (IC_{50} 3 µM) (Renko *et al*., 2015; Schweizer and Steegborn, 2015)

Furthermore, a vast variety of compounds with structural similarities to the THs have been found to be inhibitors of the Dio isoforms, these include plant metabolites, flavonoids and halogenated dyes (Auf'mkolk *et al*., 1986; Ferreira *et al*., 2002; Shimizu *et al*., 2013). However, these compounds have not been studied on specific Dio isoforms leading to a lack of detailed information but also an opportunity to develop new compounds from these starting points.

1.6.2 Synthetic compounds

There are also various Dio inhibiting synthetic compounds available that have been studied and used for the treatment of thyroid related diseases. Propylthiouracil (PTU) (Figure A2d) and methylthiouracil (MTU) (Figure A2e) are considered potent uncompetitive inhibitors of Dio1, as they interact with the SeI intermediate compound to form an irreversible complex, competing with the thiol cofactor (Mandel *et al*., 1992; Sanders *et al*., 1997; WW *et al*., 2001; Kuiper *et al*., 2005; Bianco and Kim, 2006; Maia *et al*., 2011). These drugs can have adverse side effects relating to hepatotoxicity (Glinoer and Cooper, 2012) and so are only available to patients when there are no other alternatives. Furthermore, both Dio 2 and Dio3 are insensitive to PTU and MTU, most likely due to the lack of an intermediate compound formed from the sequential reaction or a less accessible active site due to a proline residue near the Sec (Kuiper *et al*., 2005; Bianco and Kim, 2006; Schweizer and Steegborn, 2015). PTU, MTU and methimazole (MMI) (Figure A2f) have also been shown to irreversibly inhibit thyroid peroxidase (TPO), an essential enzyme that oxidises iodide into iodine atoms which can then be added to the tyrosine residues of thyroglobulin for the formation of T_4 (Ruf and Carayon, 2006). However, this means that these drugs, in particular PTU and MTU, have a specificity to both Dio1 and TPO which would need to be investigated further for the development of other potential compounds (Schweizer and Steegborn, 2015; Mondal and Mugesh, 2017). All three Dio isoforms can also be inhibited by iopanoic acid (IA) (Figure A2g), which is an iodine-containing radiocontrast medium that is non-specific – this compound can therefore be used as a starting point for more specific similar inhibitors to be produced (Leonard and Visser, 1986; St. Germain, 1988; Renko *et al*., 2012; Renko *et al*., 2015; Schweizer and Steegborn, 2015). Another synthetic compound is 'Amiodarone' (Figure A2h), an anti-arrhythmic drug which is a weak non-competitive inhibitor of both Dio1 and Dio2. But a metabolite produced from this reaction, desethyamiodarone, can become a strong inhibitor of these Dio isoforms (Rosene *et al*., 2010). However, this also gives rise to an increase

in TH plasma levels and so more tests would need to be performed to understand any potential side effects.

Further compounds have been developed related to the active site of the Dio isoforms that mimic the catalytic activity and since the Sec is a crucial part of the active site many organo-sulphur and selenium compounds have been produced over the years to study the catalytic function of the Dio isoforms e.g. Sodium hydrogen selenide, NaHSe and sodium selenide, Na_2Se (Vasil'ev and Engman, 1998; Mondal and Mugesh, 2017). With the addition of structural information from the Dio isoforms, all the compounds described above could be investigated more with a clinical setting in mind, to hopefully produce better therapies for TH related diseases.

1.7 Aims of this Study

1.7.1 Mechanistic & Structural Deiodinase isoform differences

Despite the Dio3 catalytic structure providing many insights into the mechanism of these enzymes, there is still very little information on the differences between the isoforms and how these differences infer specificity regarding the TH substrates. One of the goals of this project was to successfully produce a structure or structures of the Dio1 and/or Dio2 isoforms to elucidate how the active site differs and what residues contribute to this differentiation. Therefore, Dio1/2 constructs were overexpressed in insect or *E.coli* cells, purified using a combination of affinity and size exclusion chromatography and taken into crystallisation trials.

1.7.2 Dimerization interface & function

Although it is believed that the Dio isoforms are homodimers and that dimerization ensures functionality, there has been no structure at this time to show how dimerization occurs and how this enables the THs to enter the active site. Hence, the aim was to create a pseudo-dimer construct, then express and purify the protein. This construct was analysed for activity and ligand interaction using thermophoresis and mass spectrometry. Crystallography was also used to determine the dimerization interface and how this could potentially interact with THs for deiodination to occur.

1.7.3 Interaction with substrates

As deiodinases are attractive drug targets, understanding how these enzymes interact with substrates is essential to the development of new potential drugs. Consequently, all Dio isoform constructs were studied via thermophoresis and thermal shift assays with the TH substrates (specifically T_3 and T_4) and an inhibitor, xanthohumol. Furthermore, the substrates were added to crystallisation trials to try and obtain a structure containing a ligand to further understand how individual residues contribute to the interaction.

2.0 Materials & Method

2.1 Materials

2.1.1 Chemicals, Enzymes, Standards

If not stated differently, all chemicals were purchased from *Applichem*, *Roth*, *Promega*, *Serva* and *Sigma-Aldrich*. DNA-modifying enzymes and DNA standards came from *New England Biolabs* or *Fermentas*. Protein standards were purchased from *Bio-Rad* or *New England Biolabs*. Enzymes and inhibitors for activity assays were obtained from *Sigma* and *Cayman Chemical*. Detergents were purchased from *Anatrace*. *Tobacco Etch Virus* (TEV) protease, small ubiquitin-related modifier (SUMO) protease and all deiodinases were purified in the laboratory using established protocols. Human deiodinase 1 plasmids and viral stock for insect cells was provided by Prof. Dr. Ulrich Schweizer's laboratory at the University of Bonn.

2.1.2 Bacterial Strains

Vectors and plasmids were amplified in *E.coli* DH5α, *E.coli* TOP10 and *E.coli* XL1blue. For heterologous expression of proteins, *E.coli* Codonplus (DE3) pLysS and *E.coli* Tuner (DE3) pREP GroESL were used. For small scale expression trials *E.coli* BL21 (DE3), *E.coli* Rosetta 2 (DE3), *E.coli* Rosetta (DE3) pLysS RARE, *E.coli* BL21 Lobstr (DE3), *E.coli* Tuner (DE3) and *E.coli* Overexpress™ C43 (DE3) were also used.

Genotypes of the *E.coli* strains used:

DH5α (*Invitrogen)*	F- Φ80lacZ Δ M15 Δ (lacZYA-argF) U169 recA1 endA1 hsdR17 (rK-, mK+) phoA supE44 λ - thi-1 gyrA96 relA1
Top10 (*Invitrogen*)	F- mcrA Δ(mrr-hsdRMS-mcrBC) φ80lacZΔM15 ΔlacX74 nupG recA1 araD139 Δ(ara-leu)7697 galE15 galK16 rpsL(Str^R) endA1 λ^-
XL1blue (*Stratagene*)	endA1 gyrA96(nal^R) thi-1 recA1 relA1 lac glnV44 F'[::Tn10 $proAB^+$ $lacI^q$ Δ(lacZ)M15] hsdR17(r_K^- m_K^+)
BL21 Codonplus (De3) pLysS (*Agilent Technologies*)	F- *omp*T *hsd*S(rB- mB-) *dcm*+ TetR *gal λ endA Hte* [*argU ileY leuW*] (Cam^R)
Tuner (DE3) pREP GroESL (*Novagen*)	F- *omp*T *hsd*S(rB- mB-) *gal dcm lac*Y1(DE3) (Kan^R)

Genotypes of the *E.coli* strains used continued:

BL21 (DE3) (*Novagen*)	F- *dcm omp*T *hsd*S(rB-mB-) *gal* λ(DE3) (-)
Rosetta 2 (DE3) (*Novagen*)	F- *omp*T *hsdS*B(rB- mB–) *gal dcm* λ(DE3) pRARE2 (Cam^R)
Rosetta (DE3) pLysS RARE (*Novagen*)	F- *omp*T *hsd*SB(rB- mB-) gal dcm λ(DE3 [*lac*I *lac*UV5-T7 *gene* 1 *ind*1 *sam*7 *nin*5]) pLysS RARE (Cam^R)
BL21 Lobstr (*Kerafast*)	F- *dcm omp*T *hsd*S(rB-mB-) *gal* λ(DE3) (-)
Tuner (DE3) (*Novagen*)	F^- *ompT hsdS*$_B$ (r_B^- m_B^-) *gal dcm lacY1*(DE3)
Overexpress™ C43 (DE3) (*Lucigen*)	F- *omp*T *gal dcm hsd*SB(rB- mB-) pREP4 λ(DE3) (Kan^R)

2.1.3 Plasmids

All deiodinase isoforms and constructs used for crystallisation and assays were expressed in a pET151/D_TOPO, pET19b SUMO or pET32a TEV vectors. All vectors contained an ampicillin resistance (Amp^R), an N-terminal His_6-tag and a T7 RNA polymerase promoter. Dio1 expressed in insect cells was provided by Alfonso Rodrigues-Ruiz (Schweizer lab, University of Bonn) in a pUltraBac1 vector, which contained a polyhedron promoter, with a C-terminal enterokinase site, a His_8-tag, and an Amp resistance.

2.1.4 Growth media & antibiotics

E.coli cells were grown in lysogeny broth (LB), terrific broth medium (TB), 2x yeast extract-tryptone medium (2xYT) or super optimal broth (SOB). All medias were prepared with desalted water (dH_2O) and sterilised at 121°C and 2 bar for 20 minutes.

LB Medium:	1% (w/v) tryptone, 0.5% (w/v) yeast extract, 171 mM NaCl
TB Medium:	12% (w/v) tryptone, 24% (w/v) yeast extract, 0.1% (v/v) glycerol, 0.07 M KH_2PO_4, 0.072 M K_2HPO_4 (KH_2PO_4 and K_2HPO_4 sterilised separately and added before inoculation)
2xYT Medium:	3.5% (w/v) tryptone, 2% (w/v) yeast extract, 86 mM NaCl
SOB Medium:	2% (w/v) tryptone, 0.5% (w/v) yeast extract, 10 mM NaCl, 2.5 mM KCl, 20 mM $MgSO_4$

All growth media was supplemented with the appropriate antibiotics; 100 mg/L ampicillin (Amp), 34 mg/L chloramphenicol (Cam), or 30 mg/L kanamycin (Kan).

2.1.5 Oligonucleotide primers

Oligonucleotide primers for PCR were purchased from Eurofins (HPLC purified). All primers used are listed in Table A3 and A4.

2.1.6 Additional Materials

All expandable materials were purchased from *Bio-Rad*, *Corning*, *Eppendorf*, *GE Healthcare*, *Greiner Bio-One*, *Hampton Research*, *Jena Bioscience*, *Millipore*, *Molecular Dimensions*, *NanoTemper*, *Promega*, *Qiagen*, *Serva Electrophoresis Starstedt*, *StarLab* or *VWR* unless stated otherwise.

2.1.7 Equipment

Table 1: Equipment used and their manufacturers.

Device Name	*Manufacturer*
ÄKTA Purifier	*GE Healthcare (DE)*
Analytical scale ACJ 120-4M	*Kern & Sohn (DE)*
Analytical scale TE15025	*Sartorius (DE)*
Autoclave Systec DX-150	*Systec (DE)*
Avanti centrifuge J-30I, rotor: JA-30.50	*Beckman Coulter (DE)*
Avanti centrifuge J-30I, rotor: JLA 16.250	*Beckman Coulter (DE)*
Avanti R centrifuge J-26 XP, rotor: JLA-8.1000	*Beckman Coulter (DE)*
Bio-Rad mini Sub cell GT	*Bio-Rad Laboratories (USA)*
Bio-Rad mini-PROTEAN tetra system	*Bio-Rad Laboratories (USA)*
Branson Sonifier 250	*Emerson (USA)*
Centrifuge 5804R	*Eppendorf (DE)*
Epoch 2 microplate spectrophotometer	*BioTek Instruments (USA)*
Eppendorf thermomixer 5436	*Eppendorf (DE)*
EPS 3500 power supply (agarose gels)	*Pharmacia Biotech (SWE)*
EV243 power supply (SDS-PAGE)	*Consort (USA)*
FlexCycler	*Analytik Jena (DE)*
FluoDia T70 spectrophotometer	*Photal Technology Int (USA)*
Formulatrix Rock Imager 1000	*Formulatrix (USA)*
Heidolph unimax 1010	*Heidolph Instruments (DE)*
Heraeus Labofuge 400R, rotor: 8179	*Thermo Scientific (DEU)*
Ice machine	*Ziegra (DE)*
Infors HT Multitron Pro	*Infors HT (DE)*
Innova 4200 & 40 incubator shaker	*New Brunswick Scientific (USA)*
INTAS gel imaging system	*INTAS Science Imaging (DE)*

Table 1 continued:

Intelli-Mixer RM-2S	*Elmi Ltd (LVA)*
KMO2 basic magnetic stirrer	*IKA-Werke (DE)*
LTQ Mass Spectrometer	*Thermo Fischer Scientific (USA)*
Mighty small II SE250	*Hoefer Inc*
Monolith™ NT.115	*NanoTemper Technologies (DE)*
MP220 pH detector	*Mettler-Toledo (USA)*
Nanodrop 2000 UV/Vis spectrophotometer	*Thermo Scientific (DE)*
Odyssey Sa infrared imaging system	*LI-COR (USA)*
Olympus CKX41	*Olympus (JPN)*
Phoenix Liquid Handling System	*Art Robbins Instruments (USA)*
Plate incubator	*Memmert (DE)*
Rotating anode	*Bruker (USA)*
Sorvall RC6 Plus centrifuge, rotor: SS-34	*Thermo Scientific (DE)*
Stereo microscope SZX16	*Olympus (JPN)*
System Gold programmable detector module	*Beckman Coulter (DE)*
System Gold programmable solvent module	*Beckman Coulter (DE)*
Thermoshake incubation shaker	*Gerhardt (DE)*
Thermoshaker TS100	*Peqlab (DE)*
Trans-blot SD Semi-Dry Transfer cell	*Bio-Rad Laboratories (USA)*
Vakuum concentrator BA-VC 300H	*H.Sauer Laborbedarf (DE)*
Vortex Genie 2	*Roth (DE)*
VWR ultrasonic cleaner USC-T	*VWR International (USA)*
X-ray Detector MAR 345	*MarXperts (DE)*
X-ray source	*Incoatec (DE)/ MarXperts (DE)*

2.1.8 Buffers & Solutions

All buffers were prepared with ddH_2O. Markers used for electrophoresis were either the 1 kb ladder (NEB, #N3232S) or the 100 bp ladder (NEB, #N3231S). The marker for sodium dodecyl sulphate–polyacrylamide gel electrophoresis (SDS-PAGE) was protein test mixture 6 (Serva, #39207, containing phosphorylase B (97.4 kDa), bovine serum albumin (67 kDa), ovalbumin (45 kDa), carbonic anhydrase (29 kDa), soy trypsin inhibitor (21 kDa), cytochrome C (12.5 kDa) and bovine lung trypsin inhibitor (6.5 kDa)). The marker for Native PAGE was a custom composition for the protein MW standard for non-denaturing systems (Serva, #39064). The marker for the Western blot was a blue pre-stained standard marker 11-190 kDa (NEB, #P7706S).

Table 2.1: Components and their compositions for electrophoresis.

Gel components	Composition
Agarose gel Electrophoresis	
Agarose gel	0.5-2% (w/v) agarose, 100 ml 1x TAE buffer, 5 µl Midori Green
1x TAE running buffer	50 mM Tris/HCL pH 8.0, 20 mM acetic acid, 1 mM EDTA
DNA sample buffer (6x)	30% (v/v) glycerol, 0.25% (w/v) Bromophenol blue, 0.25% (v/v) Xylene Cyanol FF
SDS-PAGE	
Stacking gel	5% (w/v) 37.5:1 Acrylamide, 125 mM Tris/HCl pH 6.8, 0.1% (w/v) SDS, 0.1% (v/v) TEMED, 0.65% (w/v) APS
Separating gel	15% (w/v) 37.5:1 Acrylamide, 375 mM Tris/HCl pH 8.0, 0.1% (w/v) SDS, 0.1% (v/v) TEMED, 0.6% (w/v) APS
10x Running buffer	25 mM Tris/HCl pH 6.8, 0.1% (w/v) SDS, 192 mM glycine
Sample buffer (5x)	250 mM Tris/HCl pH 6.8, 10% (w/v) SDS, 50% (v/v) glycerol, 0.02% (w/v) bromophenol blue, 10% (v/v) β-ME
Staining solution	30% (v/v) ethanol, 10% (v/v) acetic acid, 0.25% (w/v) Coomassie Brilliant Blue G250
Fast staining solution	67 ml ethanol (>99%), 52 ml phosphoric acid (85%), 115 mg Coomassie Brilliant Blue G250, 10 g β-Cyclodextrin
Blue Native PAGE	
Glycerol buffer 0%	150 mM Bis-Tris/HCl pH 7.0, 600 mM Ɛ-aminocaprone acid
Glycerol buffer 60%	150 mM Bis-Tris/HCl pH 7.0, 600 mM Ɛ-aminocaprone acid, 60% (v/v) glycerol
Cathode buffer	15 mM Bis-Tris/HCl pH 7.0, 50 mM Tricine, 0.02% (w/v) Coomassie-blue G250
Anode buffer	50 mM Bis-Tris/HCl pH 7.0
5% stacking gel	1.3 ml 0% glycerol buffer, 2 ml ddH_2O, 0.7 ml 37.5:1 Acrylamide, 40 µl 10% APS stock, 4 µl TEMED
12.5% resolving gel	3 ml 60% glycerol buffer, 2.1 ml ddH_2O, 3.8 ml 37.5:1 Acrylamide, 50 µl 10% APS stock, 15 µl TEMED
Western blot	
TBST buffer	20 mM Tris/HCl pH 7.5, 150 mM NaCl, 0.05% (v/v) Tween 20
Blocking buffer	5% milk powder, 50 ml TBST buffer
10x Transfer buffer	250 mM Tris pH 8.5, 190 mM glycine, 0.05% (v/v) SDS
1x Transfer buffer	50 ml 10x stock, 20% Methanol, 350 ml dH_2O
Primary antibody	Mouse anti-His tag (*Invitrogen*), diluted 1:1000 in Blocking buffer
Secondary antibody	Goat anti-mouse (IR-Dye LT689, LICOR), diluted 1:5000-1:20000 in 1x TBST buffer

All buffers for purification (Table 2.2) were prepared with ddH_2O and filtered through a 0.45 µm filter. Buffers used for gel filtration were degassed prior to use.

Table 2.2: Buffers used in the purification of recombinant proteins.

Buffers	Composition
hDio1	
Lysis buffer	50 mM NaH_2PO_4 pH 8.0, 300 mM NaCl
mDio2	
Lysis buffer	50 mM Tris/HCl pH 7.5, 500 mM NaCl, 2 mM DTT
SEC buffer	20 mM Tris/HCl pH 7.5 or 20 mM HEPES pH 7.5, 200 mM NaCl, 1 mM TCEP
LZ_D3C	
Lysis buffer	50 mM Tris/HCl pH 7.8, 500 mM NaCl, 2 mM DTT
SEC buffer	20 mM Tris/HCl pH 7.8 or 20 mM HEPES pH 7.8, 200 mM NaCl, 1 mM TCEP

All buffer used in assays (Table 2.3) were prepared with ddH_2O and filtered through a 0.45µm filter. Highest grade stock solutions were used where possible.

Table 2.3: Buffers used in assays.

Buffers	Composition
Activity assay	
General buffer	100 mM KPO_4 pH 8.0
Crosslinking	
Reaction buffer	20 mM HEPES pH 7.5, 200 mM NaCl, 1 mM TCEP
Stop solution	1 M Tris/HCl pH 8.0
Mass Spectrometry	
MS running buffers for peptide analysis on a C18 column (TOF/LTQ)	buffer A: 0.1% (v/v) FA, 5% (v/v) acetonitrile; buffer B: 0.1% (v/v) FA, 95% (v/v) acetonitrile; buffer C: 0.1% (v/v) FA, 5% (v/v) acetonitrile
MS running buffers for intact protein analysis on a C4 column (TOF)	buffer A: 0.1% (v/v) TFA, 99.9% (v/v) ddH2O; buffer B: 0.1% (v/v) TFA, 99.9% (v/v) acetonitrile; buffer C: 0.1% (v/v) FA, 5% (v/v) acetonitrile
Microscale thermophoresis	
Labelling buffer	1x PBS pH 7.4

2.2 Molecular Biology Methods

2.2.1 Restriction free (RF) cloning

RF cloning is a polymerase chain reaction (PCR) based method that negates the use of restriction enzymes allowing custom DNA plasmids to be created by the user. Hybrid primers are designed that are both complementary to the insert and the chosen plasmid. These are used in a primary PCR to amplify the insert creating a 'mega-primer' that can then be taken into a secondary PCR with the plasmid acting as a template (Van Den Ent and Löwe, 2006; Unger *et al*., 2010).

RF cloning was used to produce constructs for the Dio isoforms in a FlexCycler PCR machine (*analytik jena*). The primary PCR (Table 3.1) had a total volume of 50 µl consisting of 50-250 ng of genomic DNA, 0.5 µM of the forward and reverse primers, 200 µM dNTPs and 0.5 µl of *Phusion High Fidelity* (2U/µl *NEB*) polymerase and the corresponding polymerase buffer. After PCR, the 'mega-primer'/ template DNA was purified (2.2.4) and used in a secondary PCR (Table 3.2). The reaction sample for the secondary PCR had a total volume of 20 µl consisting of an insert:plasmid ratio of 20 with the aim of ~100 ng of plasmid, 200 µM dNTPs and 0.2 µl of *Phusion High Fidelity* polymerase and the corresponding buffer. After the secondary PCR, the DNA is digested with DpnI (20 U, 1-2 hours at 37°C) before transformation (2.3.1).

Table 3.1: Primary PCR for RF cloning.

Step	Temperature	Duration
Start	98°C	30 sec
Cycles	x35	
Denaturation	98°C	10 sec
Annealing	55-60°C	20 sec
Elongation	72°C	15 – 30 sec/kb
End	72°C	5 min
	4°C	∞

Table 3.2: Secondary PCR for RF cloning, two-step.

Step	Temperature	Duration
Start	98°C	30 sec
Cycles	x15	
Denaturation	98°C	8 sec
Elongation	72°C	30 sec/kb
End	72°C	5 min
	4°C	∞

2.2.2 Advanced Quick Assembly (AQUA) Cloning

AQUA cloning is another PCR based method for producing seamless cloning without the use of enzymes (Beyer *et al*., 2015). Four primers are designed; a forward and reverse primer for the amplification of the vector, this is a universal primer pair which can be used for subsequent cloning experiments with different inserts. A forward and reverse primer is also required for the amplification of the insert, these primers are insert and vector specific and require a 24 bp overlap.

The vector and insert are amplified in two separate PCRs (Table 4), using the same amounts of products for the RF primary PCR, before a DpnI digest is performed (2 U, 1-2 hours at 37°C). The vector and insert are then purified (2.2.5) and mixed in a molar ratio of 1:3 or 1:5 (vector:insert). This mixture is incubated for 1 hour at 37°C and up to 10 µl is then used for transformation into competent cells (2.3.1).

Table 4: PCR for vector and insert:

Step	Temperature	Duration
Start	98°C	30 sec
Cycles	x30	
Denaturation	98°C	10 sec
Annealing	55 - 65°C	20 sec
Elongation	72°C	15 – 30 sec/kb
End	72°C	5 min
	4°C	∞

2.2.3 Mutagenesis

Site-directed mutagenesis (SDM) was used to introduce mutations (substitutions of residues) into the Dio constructs using a PCR-based method (Table 5). The primers were designed 25-30 nucleotides long, with the substitution in the middle. The total volume of the sample was 50 µl consisting of 50 ng of the plasmid DNA, 0.2 µM of the forward and reverse primers, 200 µM dNTPs and 0.5 µl of *Phusion High Fidelity* polymerase and the correct polymerase buffer. Up to 5% of Dimethyl sulfoxide (DMSO) could be added to the PCR mixture if the SDM was not producing the correct results, as this helps to disrupt base pairing and strand separation. After PCR, DpnI was added to the mixture (20 U, 1 hour at 37°C) to digest the DNA before taking into transformation.

Table 5: PCR protocol for SDM.

Step	Temperature	Duration
Start	95°C	30 sec
Cycles	x18-20	
Denaturation	95°C	30 sec
Annealing	55-60°C	1 min
Elongation	68°C	1 min/kb
End	68°C	5-7 min
	4°C	∞

2.2.4 Colony PCR

After ligation/transformation of the Dio constructs, the presence of the insert was confirmed by colony PCR. A single colony from the transformation was picked with a sterile pipette tip and resuspended in ddH_2O. This bacteria-water suspension was then used to inoculate the PCR sample composed of 0.2 µM forward and reverse primers (primers used for the insertion in the original PCR), 200 µM dNTPs, 0.5 µl of *Taq DNA* polymerase (5U/µl *NEB*) and the corresponding buffer for a total volume of 50 µl. Once the PCR was complete, the samples were run on an agarose gel to check for the insert. If a positive result was obtained, the bacteria-water suspension was used to inoculate 10 ml of LB culture supplemented with the appropriate antibiotics.

2.2.5 Purification of PCR products & plasmid DNA

Products from PCR were purified using the FavorPrep™ GEL/PCR Purification Mini Kit (*Favorgen® Biotech Corp.*) according to the manual. The purified DNA was eluted with ddH_2O.

After confirmation of a positive PCR result, the plasmids were transformed (2.3.1) and grown in LB media. The FavorPrep™ Plasmid Extraction Mini Kit (*Favorgen® Biotech Corp.)* was used to obtain the plasmid from the LB culture according to the manufacturer's manual.

2.2.6 Agarose gel electrophoresis

Agarose gel electrophoresis was used to separate DNA and assess the results of the PCRs. Gels were comprised of 0.5 – 2% (w/v) agarose in 1x TAE buffer supplemented with 5 µl of Midori Green (*Biozym®*) per 40 ml of gel. Once the gel had set, the DNA samples (with the addition of 6x DNA sample buffer) and a marker (2.1.8) were pipetted into the wells and the gel was run at 100 V for 30-40 min. After electrophoresis, the agarose gel could be viewed under UV light with an INTAS imaging system.

2.2.7 Sequencing

To verify the DNA sequence of positive clones, the purified plasmid was sent to *Eurofins MWG Operon*. *Eurofins* required DNA concentrations of 50-100 ng/µl, with an amount of 15 µl. Vector specific primers were added by *Eurofins*. Sequencing was also verified at *Microsynth AG*, which required 12 µl of plasmid DNA with 1.5 µl each of the forward and reverse primers (10 µM).

2.3 Microbiological Methods

2.3.1 Transformation of competent cells

Chemically competent cells in 50 µl aliquots (2.1.2) were transformed by adding 100-200 ng of circular DNA followed by 15-30 min incubation on ice. The cells were then heat shocked for 45 sec at 42°C and then placed back on ice for 1-3 min while 500 µl of LB media was added. The cells were then incubated at 37°C for 1 hour (600 rpm) before the transformed cells were plated on an LB agar plate supplemented with appropriate antibiotic. The plates were then inverted and placed in a 37°C incubator overnight (ON).

2.3.2 Sterilisation

All instruments, media and buffers were sterilised at 121°C and 2 bar for up to 20 min in a DX-150 autoclave (*Systec*).

2.3.3 *E.coli* Cultivation & heterologous overexpression of recombinant proteins

For overexpression of Dio2 constructs in *E.coli* Tuner (DE3) pREP GroESL, LB medium supplemented with 100 mg/L of Amp and 30 mg/L of Kan was inoculated 1:1000 with cells from an ON culture and incubated at 37°C and 120 rpm. At an OD_{600} of 0.6-0.8, the cells were cold shocked on ice for at least 20 min and the expression was induced with the addition of 0.5 mM IPTG. The cultures were shaken for 3-6 hours at 30°C before the cells were harvested.

Before overexpression of Dio3 constructs in *E.coli* BL21 (DE3) CodonPlus pLysS (Codon+), precultures were set up by scraping the colonies of one LB agar plate (containing the Dio3 construct) into ~10 ml of LB medium and incubating at 37 °C and 120 rpm until the culture was turbid. TB medium supplemented with 1 mM $MgSO_4$, 100 mg/L of Amp and 34 mg/L of Cam was then inoculated 1:1000 with the cells from the preculture and incubated at 37°C and 120 rpm. At an OD_{600} of 0.6-0.8, the cells were cold shocked on ice for at least 20 min and the expression was induced with the addition of 0.5 mM IPTG. The cultures were shaken ON at 20°C before the cells were harvested the next morning.

2.3.4 Cell harvesting & disruption

After overexpression, cells were harvested by centrifugation for 10 min at 6000 rpm in a JLA 8.1000 rotor. If cells were not disrupted directly, the cell pellet was snap frozen in liquid nitrogen and stored for future use at -80°C. For disruption, cell pellets were thawed on ice for 10 min before lysis buffer was added (5 ml per g of pellet) and supplemented with 1 mM phenylmethylsulphonyl fluoride (PMSF), *1 cOmplete EDTA-free* inhibitor tablet (*Roche*), 300 µg/g lysozyme, 10 µg/µl DNase and 5 mM $MgSO_4$. The cells in this mixture were resuspended at 4°C while stirring for up to 1 hour. The cells were then disrupted either by sonication or homogenisation, depending on the volume of cells.

For sonication, the cells are disrupted by a sonifier using a medium/big tip at duty cycle 60-70%, output ≤7 for 2 min (repeated 4-6 times). The cell suspension is kept on ice throughout sonication and left to cool between each interval. Cell debris is cleared by centrifugation for 1 hour at 4°C in a JLA 16.250 rotor at 13000 rpm.

For homogenisation, after the cells are resuspended, the mixture is filtered and then the cells are disrupted using an Emulsiflex C3 (Avestin) that has been primed with the lysis buffer. The cell suspension is run through twice and then the cell debris is cleared by the same centrifugation process as for sonication.

2.4 Insect Cells

For all experiments with insect cell cultures the HighFive™ cell line was used. These cells were kindly provided by Dr. Claus D. Kuhn (Faculty of Biology, Chemistry and Earth Sciences, University of Bayreuth). Viral stocks for protein expression were kindly provided by Prof. Dr. Ulrich Schweizer and Alfonso Rodriguez-Ruiz (Institute for Biochemistry and Molecular biology, University of Bonn).

2.4.1 Cultivation of insect cells

Cells were cultivated in SF4 Baculo Express Insect cell medium (*BioConcept*) supplemented with 10 µg/ml Gentamycin. Cells were initially grown in 125 ml disposable baffled Erlenmeyer flasks (*Corning*) for small cultures (≤ 50 ml) but were transferred to sterilised glass flasks (*Neolab*®) when the cultures were upscaled (> 50 ml). The cells were grown in a 28°C incubator at 120 rpm and were split every two days to a density of $1x10^6$ cells/ml, never allowing the cells to grow over $4x10^6$ cells/ml. Cells were counted using a Neubauer hemocytometer (*Marienfeld*) and a microscope.

2.4.2 Storage of insect cells

For storage, 10 ml of cell suspension were grown to a density between $0.5\text{-}1.0x10^6$ cells/ml, these could be obtained after splitting the cells and removing the medium. The cells were spun down at 700-800 rpm for 3-5 min and the media was aspirated. The pellet was then resuspended in 1 ml of freezing media (2-8°C) and placed into a cryo-vial. The cryo-vial was placed on ice immediately and transferred into a *Mr. Frosty* freezing container (*Nalgene*®) and stored at -80°C overnight. The cells were then transferred into liquid nitrogen storage the next day.

Freezing Media: 42.5% (v/v) conditioned medium, 42.5% (v/v) fresh media, 10% (v/v) DMSO and 5% (v/v) Foetal bovine serum (FBS).

For thawing, one cell aliquot was removed from the liquid nitrogen and placed in room temperature water. When the cells are half-thawed, they are added to 10 ml of pre-warmed (37°C) media in a 15 ml falcon tube. The cells are then centrifuged at 700-800 rpm for 3-5 min and the media is aspirated. The cell pellet is resuspended in

10 ml of media and placed into a TC-75 cm^2 flask (*Techno Plastic Products*) at 28°C. Once the cells have reached over 80% confluency, they are passaged to three TC-75 cm^2 flasks. The cells are then left to adhere for 2-3 days and resuspended to $0.4x10^6$ cell/ml for suspension cultures.

2.4.3 Protein expression in insect cells

An initial protein expression test was performed to find the correct multiplicity of infection (MOI) for larger scale expression. HighFive™ cell cultures (≤ 50 ml) were infected with five different MOIs from the viral stock e.g. 0 (negative control), 1, 3, 6, and 10. The MOI is calculated using the virus infectivity in plaque forming units (pfu) and the number of cells (Equation 1). The cells were grown over 3 days, with a sample taken every day for western blot analysis. Once the best MOI and incubation period for expression had been established (MOI of 1 and incubation for 48 hours), the expression was moved to large scale (≥ 50 ml). After expression, the cultures were centrifuged, and the cell pellets were flash frozen and kept at -80°C.

Equation 1: $$MOI = \frac{\text{pfu of virus used for infection}}{number\ of\ cells}$$

2.5 Purification of recombinant proteins

2.5.1 Affinity Chromatography

Removal of the N-terminal His_6-tag from the recombinant proteins was completed by using immobilised metal ion affinity chromatography (IMAC). A *Glass Econo-Column* (*Bio-Rad Laboratories*) was filled with ca. 5 ml *cOmplete His-Tag Purification Resin* (*Roche*) and equilibrated with the appropriate lysis buffer. The supernatant after cell harvesting and disruption (2.3.4), along with 10 mM imidazole, was applied to the resin and incubated for 1 hour at 4°C while stirring. The low concentration of imidazole is added to interfere with any weak binding. After incubation, the mixture was filtered through the gravity flow column and then the beads were washed with lysis buffer, followed by increasing concentrations of imidazole (the proteins eluted at various concentrations of imidazole) with a final 1 M imidazole wash to remove all remaining bound proteins. All flowthroughs were collected and ran on an SDS-PAGE (2.6.2). The concentrations of the fractions were measured with a Nanodrop 2000 (Thermo Scientific).

2.5.2 Proteolytic cleavage and dialysis

After IMAC, the His_6-tag was removed by proteolytic cleavage. Fractions containing the protein were mixed in dialysis tubes with either TEV protease (1:100 molar ratio) or SENP2 (1:20 molar ratio) depending on the cleavage site used in the vector. The dialysis tubes (10 kDa molecular weight cut-off) were placed in 4 L of lysis buffer overnight at 4°C to remove the imidazole.

2.5.3 Reverse affinity chromatography

A reverse affinity chromatography was performed after dialysis to remove the protease and affinity tags. Resin equilibrated with lysis buffer was incubated with the dialysis mixture for 1 hour at 4°C. The mixture was then filtered through the gravity column and washed with lysis buffer, 20 mM imidazole and 1 M imidazole. All flowthroughs were collected and analysed on an SDS-PAGE (2.6.2) and a Nanodrop. Fractions containing protein were pooled and concentrated (10 kDa cut-off) for size exclusion chromatography (SEC).

2.5.4 Size exclusion chromatography

SEC assesses the purity of the protein and the oligomerisation state. SEC was performed using either a Superdex (S) 200 or S75 column of varying dimensions; 10/300, 16/60 or 26/60 (*GE Healthcare*) in combination with an ÄKTApurifier (*GE Healthcare*). All columns were equilibrated with ≥1 column volumes (CV) of degassed gel filtration (GF) buffer; the concentrated protein was then centrifuged at 14,000 rpm for 10 min at 4°C and loaded onto the column. The protein was eluted with 1 CV of GF buffer in fractions of 0.5-1 ml and collected for SDS-PAGE. The fractions containing the target protein were pooled and concentrated to a suitable concentration before being flash frozen in liquid nitrogen and stored at -80°C in 10-50 µl aliquots.

2.5.5 Deiodinase 1 purification from insect cells

Insect cell pellets are resuspended in phosphate buffered saline (PBS) at 4°C and this mixture is centrifuged for 10 min at 6000 rpm. The cell pellet is then resuspended in lysis buffer and supplemented with 1 mM PMSF, *1 cOmplete EDTA-free* inhibitor tablet (*Roche*), 300 µg/g lysozyme, 10 µg/µl DNase. The sample is sonicated and then centrifuged for 1 hour at 4°C in a JLA 16.250 rotor at 13,000 rpm. The pellet is resuspended in lysis buffer and supplements as well as the addition of n-Dodecyl β-D-Maltoside (DDM) detergent at a concentration of 1x critical micellar concentration (CMC). This is left stirring over night at 4°C.

The mixture is then centrifuged the next day for 1 hour at 4°C in a JLA 16.250 rotor at 13,000 rpm. The pellet is resuspended in the lysis buffer, supplement, DDM detergent mix and loaded onto *cOmplete His-Tag Purification Resin* (*Roche*) equilibrated with the lysis buffer (2.5.1). All supernatant, samples and fractions from affinity chromatography are kept and ran on an SDS-PAGE and used for further Western blotting.

All following purification steps follow the same method for *E.coli* recombinant proteins with the exception of the proteolytic cleavage of an enterokinase His_8-tag and the use of DDM detergent (1 x CMC) in the lysis buffer.

2.6 Biochemical Methods

2.6.1 Photometric determination of concentration

Concentrations of nucleic acids and proteins were measured with a NanoDrop 2000 spectrophotometer (Thermo Scientific) in combination with the absorbance at 260 nm for nucleic acids and the appropriate extinction coefficient, molecular weight and the Lambert-Beer equation (Equation 2) for proteins. Extinction coefficients and molecular weights were based on the sequence of the proteins calculated by ProtParam (ExPASy) (Gasteiger *et al*., 2005). An overview of the molecular weights and extinction coefficients for each protein is given in Table A5.

Equation 2: Lambert Beer's law. A = absorbance value (nm), c = concentration of the protein solution (M), ε = extinction coefficient at 280 and d = path length (cm).

$$A = \varepsilon \times c \times d$$

2.6.2 SDS-PAGE

Discontinuous denaturing SDS-PAGE was used to separate proteins according to their molecular weight on a 15% (w/v) SDS gel. Before electrophoresis, all samples being run were mixed with 5x sample buffer and denatured at 95°C for 5 min. Once the samples were loaded alongside a marker (2.1.8), the electrophoresis was run at 150 V for 5 min for the samples to pass through the stacking gel, the voltage was then increased to 180-200 V for a further 40-50 min. After the SDS-PAGE, gels were briefly washed with dH_2O and either covered in staining solution and heated for 1 min in the microwave or the gel was covered in fast staining solution for 20-30 min at room temperature. Destaining was done via washing with dH_2O; this was not required for the fast staining solution.

2.6.3 Western blot

Prior to western blotting, samples were run on an SDS-PAGE (2.6.2) in combination with a pre-stained marker (2.1.8). The gel was washed in transfer buffer for 10-20 min before being placed on a polyvinylidene fluoride (PVDF) membrane cut to the same size, this membrane was activated in ≥50% alcohol and washed in transfer buffer for 10-15 min. The membrane and gel were packed tightly between both electrodes using Whatman filters soaked in transfer buffer. The proteins were transferred at 10 V for 30 min using a Semi-dry Transfer cell (2.1.7). After protein transfer, the membrane was dried for 20 min, followed by an overnight incubation with primary antibody at 4°C. Secondary antibody incubation was performed at room temperature for 2 hours in a black box. After each antibody step, the membrane was washed three times with 1x TBST buffer for 15 min at room temperature. The membranes were analysed by fluorescence scan on the Odyssey imaging system (2.1.7).

2.6.4 Blue Native PAGE

Blue Native PAGE (BN-PAGE) was used to analyse the oligomerisation state of the proteins. Once the gel had been prepared and polymerised, the protein samples were mixed with 10% (v/v) glycerol and applied to the gel. Cathode buffer was added to the inner chamber of the Mighty small II SE250 mini electrophoresis system (*Hoefer Inc*) and the anode buffer was added to the lower, outer chamber. Electrophoresis was performed for 15 min at 150 V before increasing the voltage to 200 V for 2-4 h, this was all run at 4°C. The gels were destained in dH_2O.

2.6.5 Thermal shift denaturation assay (TSA)

The TSA was performed as described (Reinhard *et al*., 2013). For the set-up, 6 µl of protein for a final concentration of 1-10 µM was supplemented with 50x Sypro Orange (*Invitrogen*) with a final concentration of 5x, 8 µl of dH_2O and 40 µl of a 1.5x solvent/compound. Samples were sealed with 15 µl of mineral oil in each well to prevent evaporation. The TSA was performed at 0.5-1°C increments in a FluoDia T70 spectrophotometer (*Photal*, λ_{ex} = 465nm, λ_{em} = 580nm). The Tm was determined in GraphPad Prism (*GraphPad Software*) using a Boltzmann model.

2.6.6 Microscale thermophoresis (MST)

The interaction between deiodinases and ligands was analysed by MST using a Monolith NT.115 *(Nanotemper Technologies*) in combination with fluoresceinthioiso-cyanate (FITC). This technique analyses protein/ligand interactions using the

thermophoretic effect via the proteins fluorescence change (Wienken *et al*., 2010; Jerabek-Willemsen *et al*., 2011).

For protein labelling of lysine residues, the protein was incubated with FITC (dissolved in 1x PBS pH 7.4) in a molar ratio of 1:2 overnight at 4°C or at room temperature for 1-2 hours. Any free FITC was removed by an illustra NAP-5 gravity flow column (*GE Healthcare*) and the concentration of the labelled protein and FITC was checked via a UV/Vis spectrum at 280 nm and 495 nm. 1-5 µM of the labelled protein was used in a 2x stock concentration in the chosen buffer for the assay in combination with 2x stock of varying concentrations of the titrant/ligand. The mixtures were placed into standard treated capillaries for NT.115 (NanoTemper Technologies Inc.). MST was carried out at 25°C, 20-30% LED power and 20/30/40% laser power. Raw MST data was background corrected and normalised to the upper baseline (=100% bound) and fitted using Equation 3.

Equation 3: [Bound] = concentration of bound ligand, Capacity = amplitude of binding curve, [Free] = concentration of free ligand, K_d = dissociation constant, Background = background signal.

$$[Bound] = \frac{Capactiy\ x\ [Free]}{Kd + [Free]} + \text{Background}$$

2.6.7 Activity assays

To assess whether the Dio constructs were active, an activity assay was performed with T_4 at various time points. 100 mM KPO_4 at pH 8.0, 20 mM DTT, 0-20 µg of enzyme and 1 µM of T_4 were mixed with dH_2O for a total volume of 100µl. All components were mixed and incubated at various time points ranging from 0-3 hours, the reactions were stopped with the addition of 10 µl of 100% acetic acid. The samples were then sent to Prof. Dr. Josef Köhrle's lab (Institute of Experimental Endocrinology, Charité Universitätsmedizin Berlin) where they were analysed by mass spectrometry for the product rT_3, an increase of this product over time would indicate that the Dio construct is active. The rT_3 ratio was plotted against time on a graph and fitted using linear regression.

2.6.8 Cross linking

Cross linking is used to identify interactions between proteins and when combined with mass spectrometry, this can reveal the specific interaction sites. Initially proteins were transferred into a HEPES buffer (2.1.8) via SEC and the cross-linkers were prepared;

10% formaldehyde stock, 0.2% glutaraldehyde stock, 20 mM DSS stock and 100 mM DSSO stock (all in HEPES buffer). In total volumes of 15-30 µl, proteins were cross-linked at room temperature to an individual cross-linker at various time points e.g. T_0, T_{15}, T_{30}, T_{60} and T_{ON}. Samples were taken for each time point and the reaction was stopped with the addition of 1 µl of Tris/HCl pH 8.0 (T_0 was removed before the cross-linker was added). NADOX protein was used as a positive control. All the samples were run on an SDS PAGE and subjected to tryptic digest for mass spectrometry.

2.7 Mass Spectrometry

2.7.1 Tryptic digest of proteins

To identify specific proteins or to obtain a detailed analysis of a mixture by mass spectrometry, a tryptic digest was performed. The samples could be digested either from bands cut from a gel, or in solution.

Any protein from an SDS PAGE that were to be investigated further were excised, cut into 1 mm x 1 mm cubes, and transferred into an Eppendorf. The reduction, alkylation and destaining of the proteins follows the protocol as described (Shevchenko *et al*., 2007). The gel pieces can be stored at -20°C or the digestion step can be continued. For digestion, ≥ 50 µl of 25 mM ammonium bicarbonate was added to each sample along with the addition of 1 µl of a trypsin solution (200 ng trypsin in 0.01% formic acid). This mixture was placed at 4°C for 30 min up to 2 hours, with any additional 25 mM ammonium bicarbonate needed to cover the gel pieces. The samples are placed in an incubator overnight at 37°C. The next day, the samples are chilled, spun down at 10,000 rpm for 10 min and the supernatant is extracted into a clean eppendorf for mass spectrometry analysis.

For in solution digests, 20-70 µM of protein was supplemented with 1 µl of trypsin solution for a total volume of up to 50 µl, this was performed overnight at 37°C. Samples from both tryptic digest methods were injected onto a pre-column for desalting before being injected onto a C18 column for peptide separation on a LTQ or TOP mass spectrometer.

2.7.2 Limited proteolysis

Limited proteolysis is a technique used to identify stable fragments of proteins that can be produced for further structural and functional studies. The proteases used to perform proteolysis included trypsin, elastase, subtilisin A and proteinase K, all at 1mg/ml. The protein was digested in molar ratios of 1:100 and 1:500 with the individual

proteases at room temperature for 30 min. The reactions were stopped with the addition of 5x SDS sample buffer and incubated at 95°C for 5 mins before being run on an SDS PAGE. Selected bands were cut out for tryptic digest and mass spectrometry analysis.

2.8 Crystallographic Methods

2.8.1 Crystallisation

Proteins were crystallised using the sitting-drop vapor diffusion method at both 4°C and 20°C. Crystallisation screens from *Qiagen* (e.g. *JCSG+, JCSG Core I – IV, Classics I & II, Classics lite and PACT* [pH, anion- and cation testing screen]) and lab-made screens (PEG smear I & II) (Chaikuad *et al*., 2015) were used for initial crystallisation set-ups by using MRC2 or MRC3 crystallisation plates (*Molecular Dimensions*). The initial screens were composed of 35 µl of reservoir solution and 0.2 µl drops (a ratio of 1:1 was used for protein to reservoir solution) that were set up via a *Phoenix* liquid handling system (*Art Robbins Instruments*). Plates were then closed with *Crystal Clear* tape and placed at 20°C in a *ROCK IMAGER* (*Formulatrix*) or at 4°C for manual viewing.

Once a crystallisation condition yielded a crystal, the condition was optimised in a 24 well VDX greased 18/22mm hanging drop plate (*Hampton Research*) or in a 48 well MRC maxi sitting drop plate (*Swissci*). These plates were sealed with glass cover slips (*Hampton Research*) or *Crystal Clear* tape, respectively. The chosen conditions were optimised by varying the precipitant and/or the salt concentration. The experiments consisted of 200-500 µl of reservoir solution and 1-2 µl drops (with the ratio of protein to reservoir solution varied e.g. 2:1).

Seeding was performed by crushing the identified crystals with a glass probe before mixing with 50 µl of reservoir solution in an eppendorf containing a *Seed Bead.* This tube is vortexed for 3 mins in 30 second intervals while resting on ice. This seed stock can then be further diluted via serial dilutions and frozen at -80°C (Bergfors, 2003; D'Arcy *et al*., 2007). The seed stocks were used in optimisation experiments and were used instead of or in conjunction with the reservoir solution in the drop.

2.8.2 Data Collection

Any crystals obtained were mounted with a *Cryo-loop* (*Hampton Research*) and then flash cooled with liquid nitrogen in a cryo-protectant solution (e.g. the reservoir solution with additional glycerol at a minimum of 25%, if needed). Diffraction and data sets

could be tested and collected in-house with a marμX micro beam system (*MAR Research)*. Diffracting crystals were sent to BESSY II beamline 14.1 or 14.2 (Helmholtz Zentrum Berlin-Adleshof, Berlin, Germany) or to the SLS PX III (Paul Scherrer Institute, Switzerland), using 100 K liquid nitrogen cooling. These data sets collected produced higher resolution structures.

2.8.3 Data reduction, model building and structure refinement

Data processing was performed with XDSAPP (Sparta *et al*., 2016), a graphical interface of XDS (Kabsch *et al*., 2010), for indexing, integration, scaling, sorting and data conversion. The molecular replacement for the Dio2 structure was calculated with Phaser (McCoy *et al*., 2007) from the Phenix Suite (Adams *et al*., 2010; Echols *et al*., 2012) using a published Dio3 structure as a model (PDB code:4TR3). The molecular replacement for the structure was checked via refinement cycles with Refine (Echols *et al*., 2014; Afonine *et al*., 2018) from the Phenix suite. Coot (Emsley and Cowtan, 2004; Emsley *et al*., 2010) was used for model building after each cycle of refinement until the R and R_{free} could no longer be improved. Graphical representations of the structure were generated using PYMOL (*Schrödinger*). Any compounds used during modelling were drawn using *marvinsketch* (*Chemaxon*) and loaded into Coot for a 3D representation of the interaction.

3.0 Results

3.1 Optimisation of Deiodinase 1 from insect cells

Prof. Dr. Ulrich Schweizer's lab prepared a C-terminal His tagged, full length human Dio1 (hDio1) construct in a pUltraBac1 plasmid (Sec replaced by Cys in the active site). The protein was expressed in the HighFive™ insect cell line and optimal expression was previously established between 48-72 h post infection. Viral stocks obtained from preliminary small-scale expressions were forwarded to our lab and starter cultures of ≤50 ml were initiated before increasing the volume (>50 ml per flask) resulting in a final volume of 2.5 L of hDio1 expressed in HighFive™ cells. The expression was confirmed by western blot (Fig 6a). The western blot clearly indicated that the hDio1 protein (~30.5 kDa) was expressed in all five flasks (Exp_{2-6}) at 48 h post infection and that there was no other His-tagged contaminants or false positives as shown by the negative control (Exp_1). The hDio1 protein was pooled for purification.

The original purification protocol provided by Alfonso Rodríguez Ruiz had to be modified to accommodate a larger protein amount with the final goal of achieving successful crystallisation. This involved purifying in a shorter time frame, a change of detergent (UDM to DDM) and the His-tag to remain intact. However, the results were difficult to see on a western blot and so a further step of methanol precipitation was used on the samples to remove any interfering reagents (i.e. detergent) that could affect the final blot (Fig 6b). The western blot shows that the protein is present in the fractions from the 400mM to 1M imidazole wash, albeit at much lower concentrations compared to the positive control. This suggests that although the purification was successful, it could be optimised further to improve the hDio1 protein yield and prevent the loss of protein in some of the initial purification steps. Unfortunately, the insufficient amounts of hDio1 protein obtained from this purification could not be taken further into crystallisation trials yet.

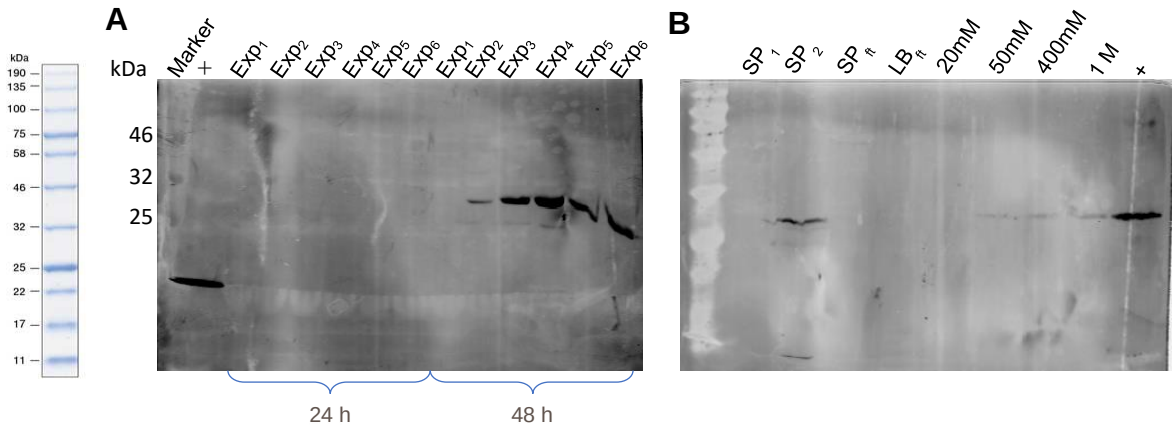

Figure 6. ***Expression & purification of hDio1 in insect cells****. (A) Expression of hDio1 over a 48-hour time period shown on an anti-His western blot. + represents positive control, a 17 kDa His-tagged protein obtained from Sandra Weiß. Exp_1 is the negative control, no viral stock added. Exp_{2-6} are individual expression flasks with the addition of the viral stock at an MOI of 1. (B) Purification of hDio1 on an anti-His western blot after methanol precipitation. + represents positive control, a sample from the Dio1 expression, Exp_5 48 h. SP_{1-2} is the supernatant collected after initial purification steps, Sp_{ft} & LB_{ft} is the supernatant and lysis buffer flow through from IMAC, 20 mM-1 M are the imidazole concentrations used to obtain the fractions collected from IMAC.*

3.2 Structural Characterisation of Deiodinase 2

3.2.1 Recombinant expression & purification of Deiodinase 2 constructs

For expression, Dio2 constructs were either designed via sequence alignment (Fig 7a) or were obtained from stocks previously produced by Christine Schlicker (former student working on the project). The result was several Dio2 constructs of varying length (Fig 7b) that could potentially mimic the construct of the crystallised Dio3 protein (aa 131-301). The selenocysteine within the constructs (Sec^{130}) was replaced with cysteine or serine, denoted by a C or S in the construct name.

A

```
Dio2     1 MGLLSVDLLI----------------------------------TLQILPVEFSNCLFLA
Dio3     1 MPRQAASRLVVGEGEGPPGASGPAATMLRSLLLHSLRLCAQTASCLVLFPRFLGTAFMLW

Dio2    27 LYDSVILLKHVALLLSRSKSTRGEW-----------------------RRMLTSEGLRCV
Dio3    61 LLDFLCIRKHFL---RRRHPDHPEPEVELNSEGEEMPPDDPPICVSDDNRLCTLASLKAV

Dio2    64 WNSFLLLAYKQVKLGEDAPNSSVVHVSNPESGNNYASEKTADGAECHLLDFASAERPLVV
Dio3   118 WHGQKLLPFKQAHEGGPAPNSEVVRPDGFQ------S--------QRILDYAQGTRPLVL

Dio2   124 NFGSATUPPFTRQLPAFRQLVEEFSSVADFLLVYIDEAHPSDGWAVPGDSSLSFEVKKHR
Dio3   164 NFGSCTUPPFMARMSAFQRLVTKYQRDVDFLIIYIEEAHPSDGWVTT-DS--PYVIPQHR

Dio2   184 NQEDRCAAAHQLLERFSLPFQCQVVADRMDNNANVAYGVAFERVCIVQRRKIAYLGGKGP
Dio3   221 SLEDRVSAARVLQQ---GAPGCALVLDTMANSSSSAYGAYFERLYVIQSGTIMYQGGRGP

Dio2   244 FSYNLQEVRSWLEKNFSKRUILD----
Dio3   278 DGYQVSELRTWLERYDEQLHGTRPHRF
```

Continued next page

Figure 7 continued:

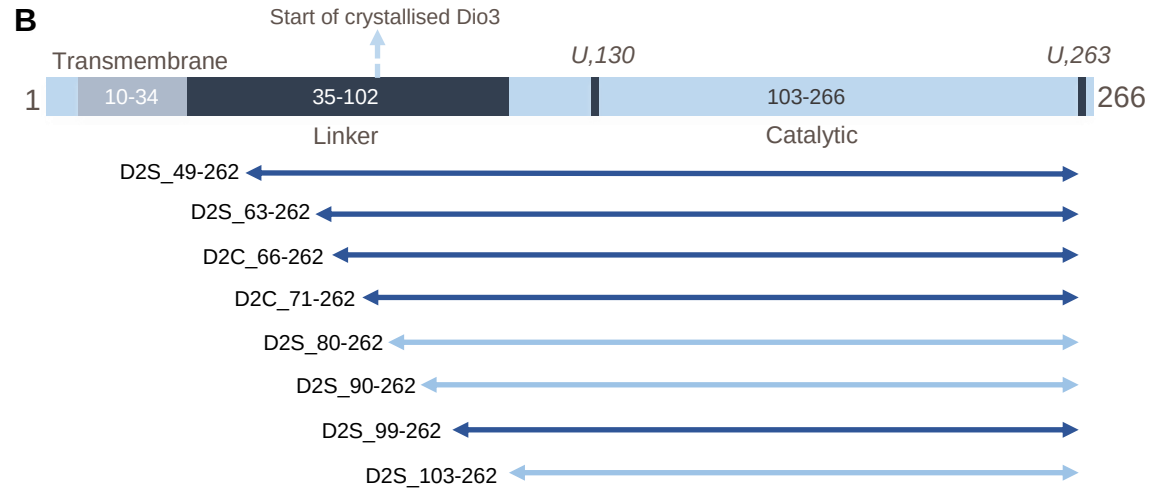

Figure 7. ***Dio2 construct design for expression*** *(A) Sequence alignment of Dio2 (mus musculus) & Dio3 (mus musculus), generated using T-Coffee and Boxshade server on Expasy (Notredame et al., 2000). (B) Scheme of full length Dio2 with construct designs; dark blue arrows indicate previously designed constructs & light blue arrows indicate constructs designed via sequence alignment for this project. Start of crystallised Dio3 protein is at aa 79 in the Dio2 alignment.*

All the Dio2 constructs were initially tested for expression using the methods described in Schweizer *et al*., 2014; expression in Rosetta2 cells (*Merck*) overnight at 20°C after induction with 0.5 mM IPTG. However, preliminary expression of the constructs resulted in a low yield of soluble protein and so small-scale expression trials were carried out to obtain the optimal media, cells and overall protocol for Dio2 protein expression (Fig 8). Nevertheless, some of the Dio2 constructs still had poor expression and these unsuccessful constructs (D2S_99 and D2S_103) were not taken further into purification steps.

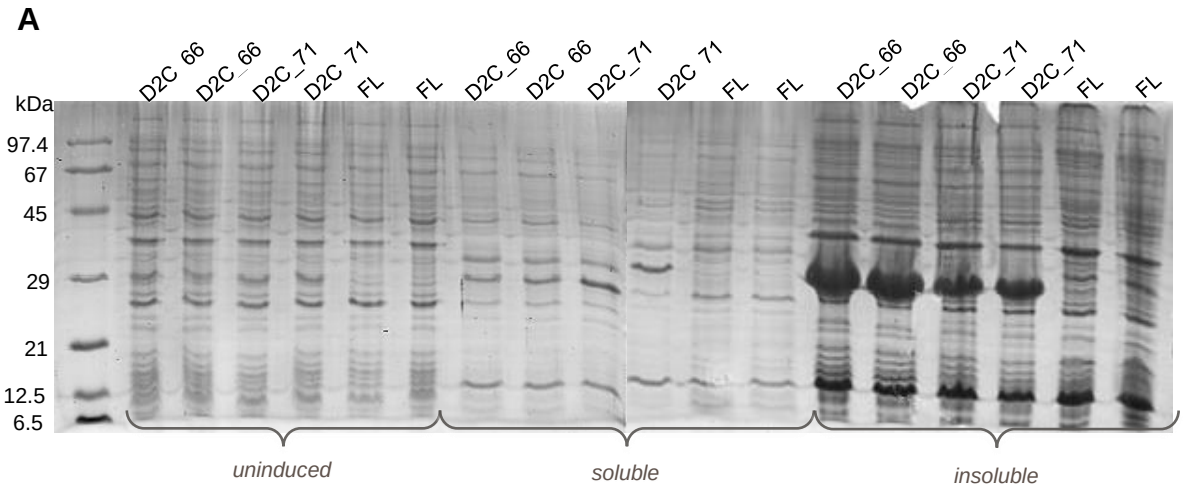

Continued next page

Figure 8 continued:

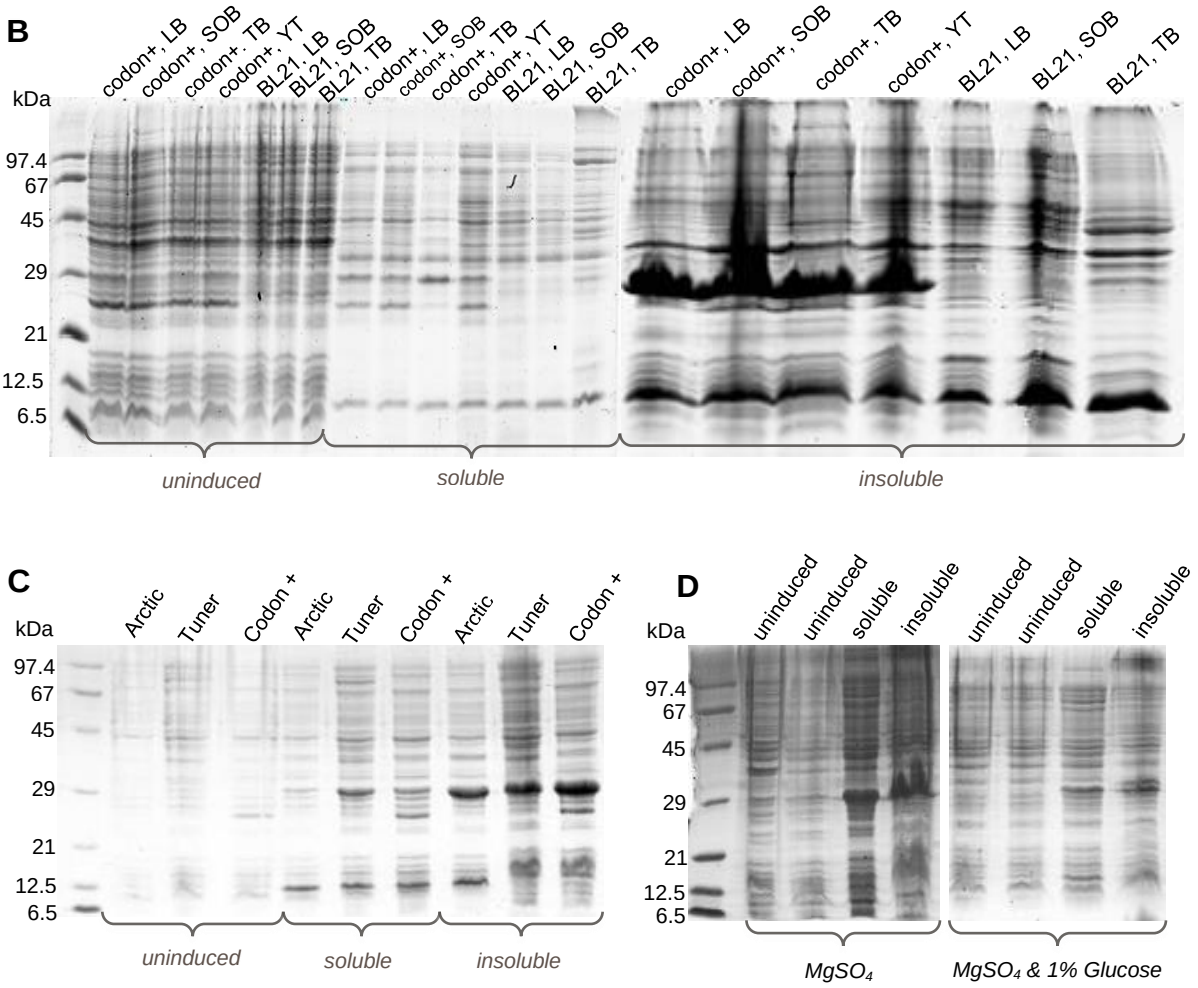

Figure 8. ***Small-scale expression trials of Dio2 constructs.*** *A number of variables were tested in the small-scale expression trials, this figure demonstrates some of the experiments that took place. (A) Initial construct test expression indicating the high yield of insoluble protein. (B) Expression test with different cell types and media. (C) Expression test with different cell types in LB media. (D) Addition of $MgSO_4$ and glucose to expression media. Dio2 has a molecular weight of 22 kDa but all constructs run higher on SDS PAGE.*

Alongside the small-scale expression trials, a different expression protocol was also tried; this involved scraping the colony plate directly into the final culture media (no starter culture was prepared) and a reduced expression time at a higher temperature. The overall results of the experiments indicated that the use of Tuner cells in LB media (with no starter culture), the addition of 1 mM $MgSO_4$, induction with 0.5 mM IPTG and expression for 2-3 h at 30°C produced the best yield of soluble protein for several constructs (Fig 9).

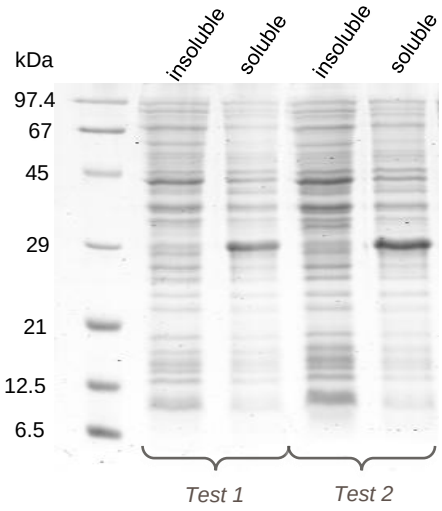

Figure 9. ***Optimised expression of D2C_71*** *(~ 21 kDa) construct shown on an SDS PAGE. D2C_71 was expressed using the updated and improved protocol in two simultaneous expression tests, resulting in a high yield of soluble protein.*

Initially, the purification method previously used for the crystallised Dio3 protein (Schweizer *et al*., 2014) was tested for the purification of the Dio2 constructs. However, the outcome was low amounts of unstable, degraded protein and so an optimisation of the purification protocol was also required. The first step was to increase the amount of salt in the initial purification buffer from 200 mM to 500 mM NaCl (the final size exclusion buffer would have a reduced concentration of salt, as not to interfere with further experiments). This change improved the purity of the proteins slightly throughout the purification. However, during the later stages of purification (i.e. after SEC), the protein produced still contained some degradation products and impurities. Therefore, a range of buffers were tested using a buffer screen in a TSA denaturation assay (Fig 10) with a total of 24 buffer solutions (all containing NaCl). The buffer solutions were produced in lab as described (Reinhard *et al*., 2013).

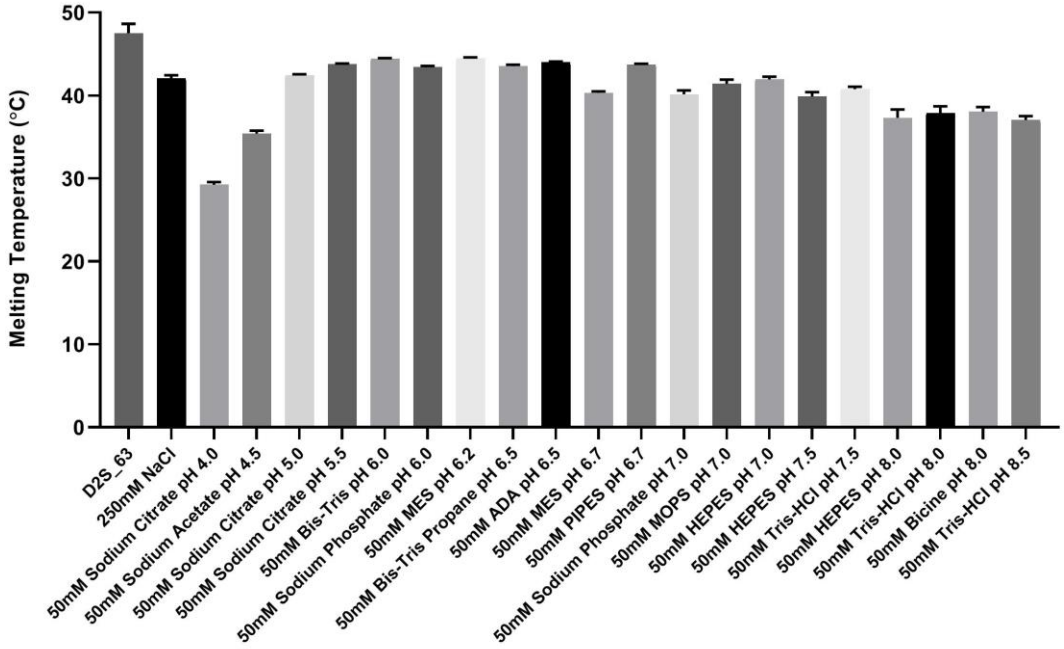

Figure 10. ***TSA buffer screen with D2S_63****. D2S_63 (concentration of 2.5 µM) protein sample in 20 mM Tris/HCl pH 7.5, 500 mM NaCl. All buffer solutions contained an additional 250 mM NaCl. Performed as described in 2.6.5.*

The TSA results indicated that the buffer solutions screened did not produce a better result than the buffer that was currently being used, and so the continued use of the lysis buffer; 50 mM Tris/HCl pH 7.5, 500 mM NaCl and 2 mM DTT was maintained during the initial purification stages. The next step was to introduce additional additives, specifically during cell disruption. This included protease inhibitors; 1 mM PMSF and 1 *cOmplete™ EDTA-free inhibitor* cocktail tablet; as well as 5 mM $MgSO_4$ and 300 µg/g lysozyme. These additions plus working quickly and solely at 4°C (compared to room temperature for the crystallised Dio3 purification) produced cleaner protein with much less degradation (Fig 11).

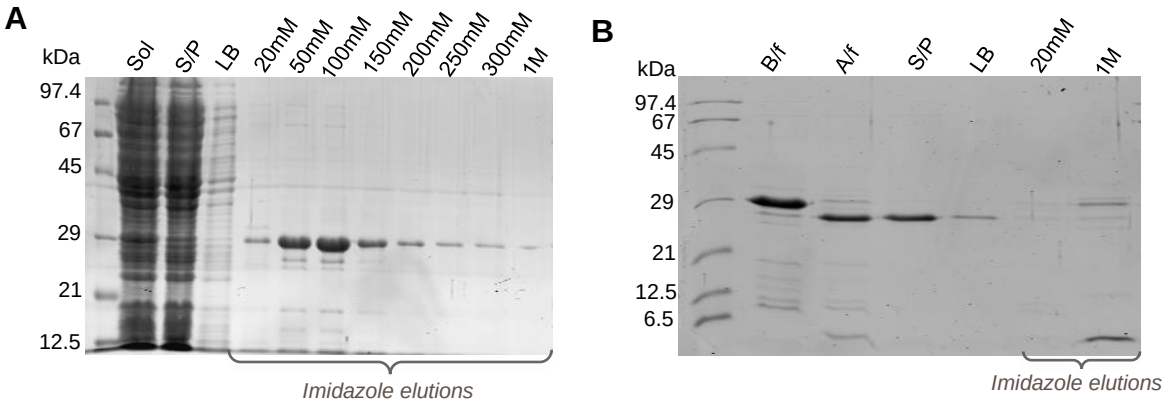

Continued next page

Figure 11 continued:

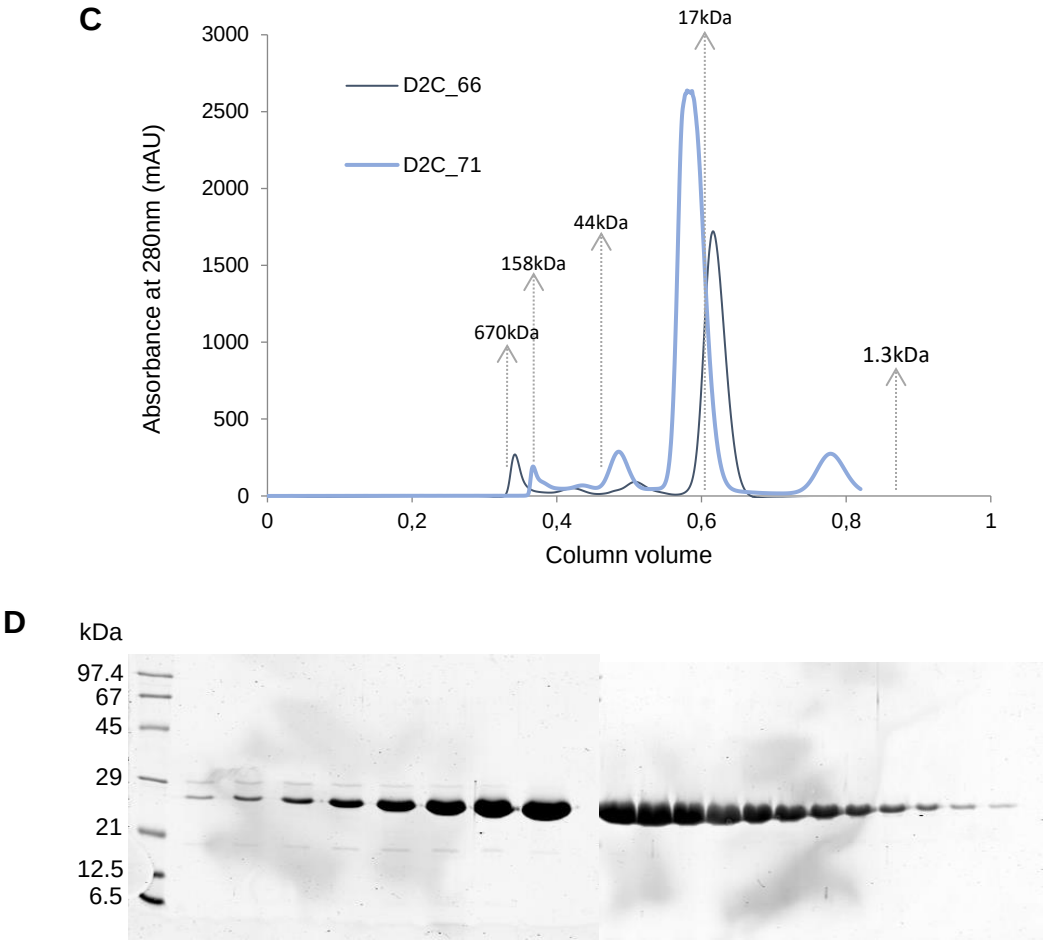

Figure 11. ***Purification of Dio2 constructs*** *(~ 22 kDa). (A) Ni-NTA of D2C_66 on SDS PAGE, protein starts to elute from 100 mM imidazole. Sol is the soluble sample after expression but before IMAC, S/P is the supernatant after cell disruption and applied to the Ni-NTA column & LB is the elutant after lysis buffer wash. (B) D2C_66 after dialysis and reverse Ni-NTA on SDS PAGE, clear band of protein seen for S/P. B/f is the sample before the protein was dialysed overnight, A/f is a sample of the dialysed protein, S/P is the elutant after the protein was ran on the Ni-NTA column & LB is the elutant from the lysis buffer wash. (C) SEC of D2C_66 and D2C_71 with protein marker shown. Proteins were applied to different columns. (D) SDS PAGE of D2C_66 monomeric peak from SEC.*

Although the new methods of expression and purification worked well for some of the constructs, other constructs still had poor expression and some degraded quickly during purification. Furthermore, none of the protein from the remaining constructs produced diffracting crystals and so limited proteolysis was performed on the full length Dio2 protein to try and obtain a more structurally stable Dio2 construct for crystallisation (Fig 12).

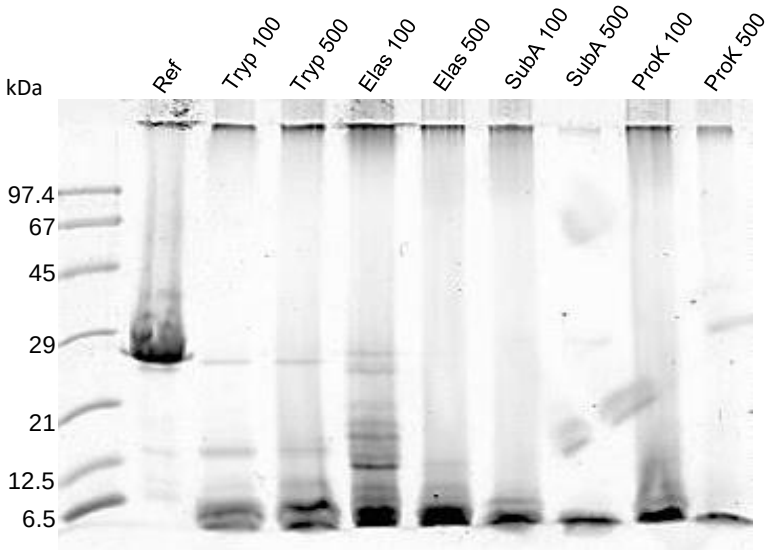

Figure 12. ***Proteolysis of full length Dio2*** *on an SDS PAGE. Ref is D2C_66 construct. The full-length protein was digested in molar ratios of 1:100 and 1:500 (represented by 100 or 500) with trypsin (Tryp), elastase (Elas), subtilisin A (SubA) and proteinase K (ProK)for 30 minutes.*

Unfortunately, the limited proteolysis result indicated that although fragments were produced, they were very small with no dominant fragment being identified. As the size of these fragments would not have garnered enough structural information, it was clear that the established constructs could not be improved upon and so some of the longer constructs that were stable during expression and purification (D2S_63, D2S_66 & D2C_71) were taken forward into mutagenesis experiments.

New constructs were designed using surface entropy reduction predication (Goldschmidt *et al*., 2007) with full length Dio2 (Fig 13a), which produced a number of specific mutations that could theoretically improve the crystallisation by replacing clusters of two to three surface residues, that have high conformational entropy, with Ala. Several mutation predictions were produced but two clusters of double mutants were taken forward; $Glu^{101}Lys^{102}$ and $Lys^{180}Lys^{181}$ mutated to Ala (Fig 13b). These mutants were introduced in D2S_63, D2C_66 and D2C_71, then expressed and purified according to the established protocol and set up into crystallisation trials.

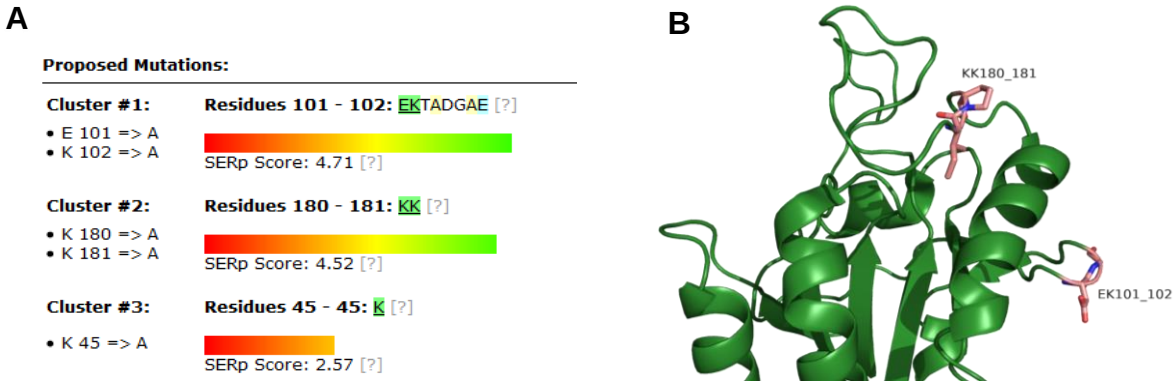

Figure 13. ***Mutagenesis of Dio2 constructs.*** *(A) Output of the SERp sever indicating the clusters proposed for mutagenesis. (B) Glu^{101}Lys^{102} and Lys^{180}Lys^{181} clusters shown on aligned amino acids on Dio3 model.*

3.2.2 Structure determination of Deiodinase 2

Although all the successfully purified Dio2 constructs were set up in crystallisation experiments, only a small number of constructs produced diffracting crystals and only one Dio2 mutant construct (D2C_71_KK180AA) produced crystals that were sufficient for structure determination. This construct crystallised exclusively at 4°C in several crystallisation set-ups in the shape of large rods as well as an array of small rods emanating from one point (which could be optimised further) (Fig 14a & b). These appeared within 3-4 days and diffracted inhouse up to 2.0 Å but were improved upon at the BESSY II beamline to obtain a 1.1 Å structure (Fig 14c). The structure was solved in space group P32 and refined to final R and R_{free} values of 15.8% and 18.4%, respectively (Table 6).

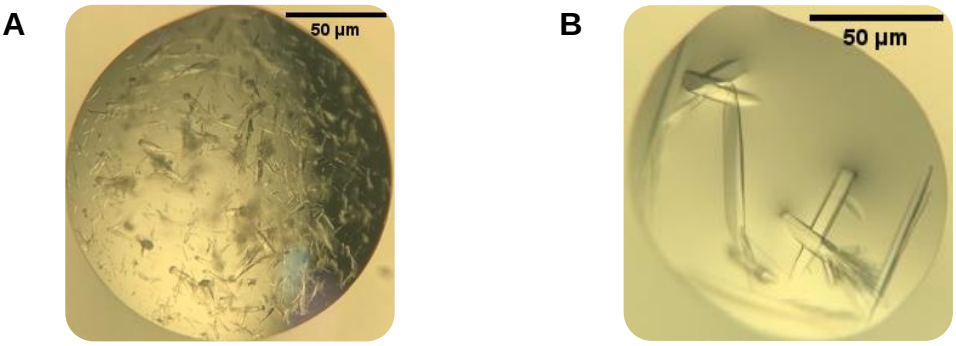

Continued next page

Figure 14 continued:

C

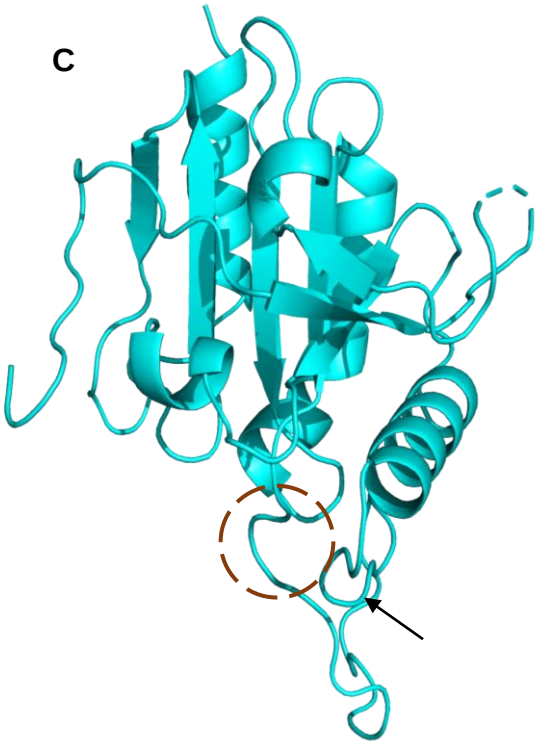

D2C_71 KK110AA Data processing & Refinement statistics	
Data Processing	
Space group	P 3(2)
Unit Cell	47.8 47.8 64.7, 90 90 120
Unique Reflections	65565 (4435)
Completeness (%)	94.85 (64.62)
Multiplicity	5.4 (3.6)
Wilson B-factor	14.23
Mean I/sigma(I)	9.45 (0.39)
CC1/2	0.999 (0.117)
Refinement	
Resolution range (Å)	34.85 – 1.089 (1.128 – 1.089)
Number of macromolecules	1465
Number of solvent atoms	192
R-work	0.1449 (0.3703)
R-free	0.1696 (0.4002)
Ramachandran favoured (%)	97.77
Ramachandran allowed (%)	2.23
Clashscore (Molprobity)	1.73
Average B-factor	21.19

D

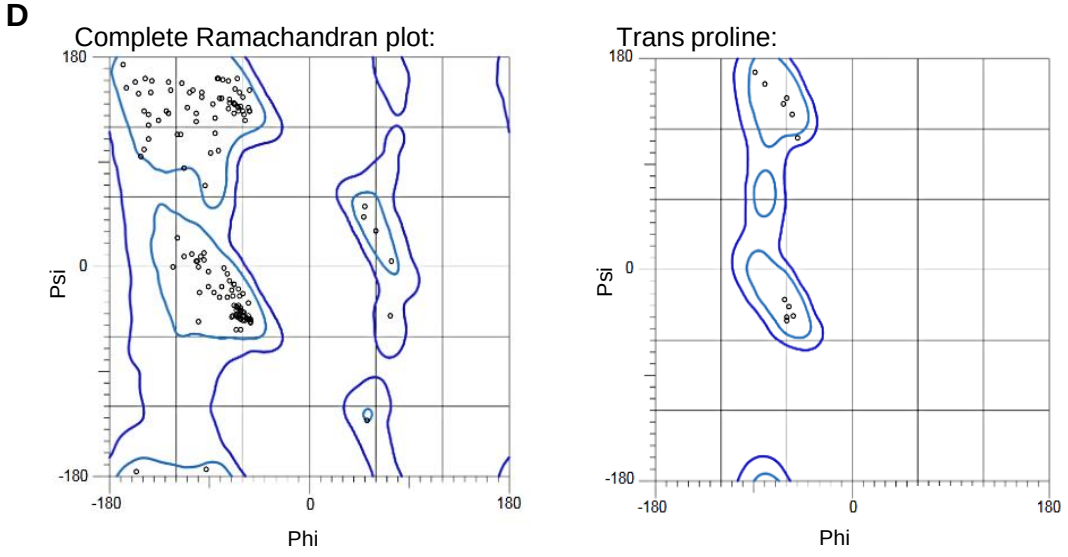

Figure 14. ***Crystals & structure of D2C_71_KK180AA****. (A) Crystallisation drop from PACT (Qiagen) of 0.1 M MMT (DL-malic acid:MES:Tris base) buffer pH 8 & 25% (w/v) PEG 1500, at 4°C. (B) Crystals grown from PACT (Qiagen) in 0.1 M SPG (succinic acid:sodium dihydrogen phosphate:glycine)buffer pH 7 & 25% (w/v) PEG 1500 at 4°C, these crystals were used to obtain the final structure. (C) Final structure of truncated Dio2 mutant, nine amino acids are missing from the loop region, the circled area indicates the active site and the arrow indicates the location of the mutated residues. (D) Ramachandran plots of structure indicating no outliers from MolProbity (Davis et al., 2007).*

Table 6. ***Data processing & refinement statistics for truncated Dio2 mutant.***

3.2.3 Structural features of Deiodinase 2

The resultant structure produced for $Dio2_{cat}$ allowed regions to be identified comparable to those proposed for Dio3 enabling a topology diagram to be produced (Fig 15) similar to that in Schweizer *et al*, 2014 (Fig 4). The topology of the Dio2 structure indicates a Trx-fold with deiodinase specific modifications and insertions, confirming the generic Dio fold similar to $Dio3_{cat}$. The structure has an N-terminal Prx-like module consisting of a small two-stranded antiparallel β sheet, βN1/2, and a 3_{10}-helix, Θ1. This is followed by the Trx-fold, a four stranded mixed β-sheet, surrounded by two α-helices and another 3_{10}-helix, Θ2, which appears to be Dio2 specific compared to a longer α-helix, α2, in the $Dio3_{cat}$ structure (comprised of four Ser residues). The deiodinase specific insertion (residues 161-188) is flanked by an α-helix, αD, and a short β-sheet, βD, which protrudes out of the structure and contributes to the iodothyronine binding. Overall, the $Dio2_{cat}$ structure supports the previous work that the isoforms have homologous catalytic domains (Bianco *et al*., 2002; Schweizer and Steegborn, 2015).

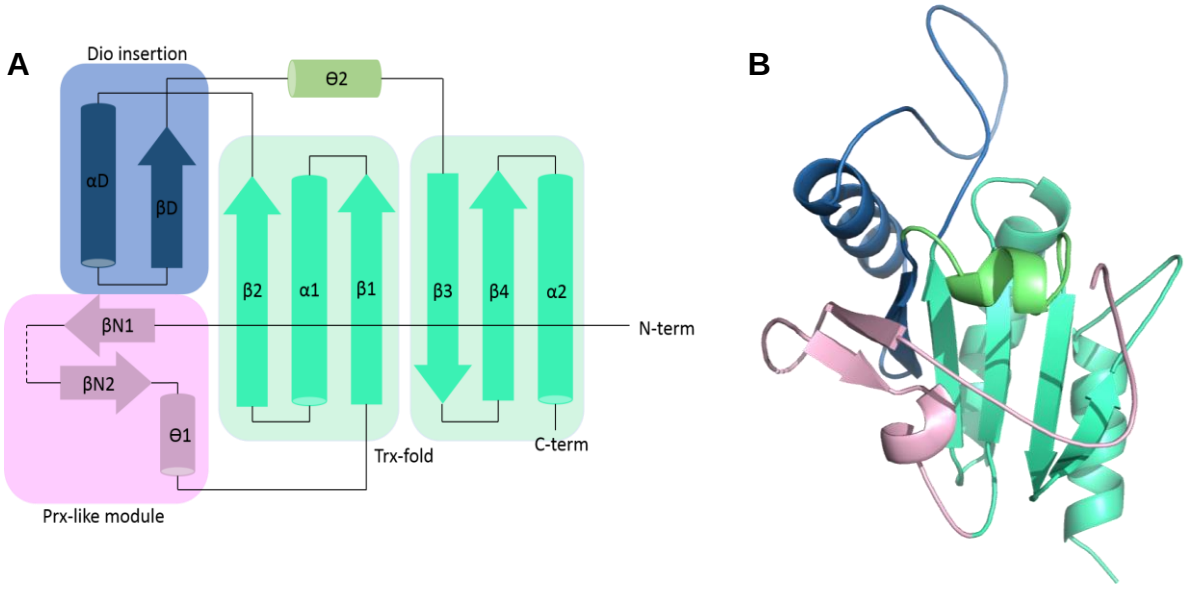

Figure 15. *$Dio2_{cat}$ secondary structure.* *(A) $Dio2_{cat}$ topology based on figure from Schweizer et al, 2014, with relevant residues highlighted, dashed line indicates missing residues. (B) Overall structure of the truncated monomeric form of Dio2; trx fold coloured in cyan, prx-like module coloured in pink, the Dio insertion coloured in a dark blue and the Θ2 in light green.*

3.2.4 Homology Modelling of Deiodinase 1

Further investigation into the structural differences of the isoforms led to the alignment and homology modelling of the Dio1 catalytic domain. Initially, all the isoform sequences were aligned, to highlight any immediate differences or similarities (Fig 16a) between them. This indicated that the Dio3 protein has an extended transmembrane sequence compared to Dio1 or 2 suggesting a possible role in the internalisation and recycling of Dio3 in endosomes (Baqui *et al*., 2003; Bianco and Larsen, 2005). The Dio2 and Dio3 structures were then aligned in PYMOL (*Schrödinger*) using ClustalW2 (Larkin *et al*., 2007). A homology model was generated for Dio1 (Fig 16b and c) using both aligned structures as a template in MODELLER with standard parameters (Eswar *et al*., 2006). The predicted model of $Dio1_{cat}$ indicated an analogous size and similar secondary structure elements as the other isoforms with a particular high similarity to Dio3. It also revealed a difference in two loop regions (highlighted on Fig 16b) between all three isoforms that could reveal specific Dio isoform features. However, the results are limited as the only structures available are truncated monomeric versions. The dimeric forms of the proteins could possibly provide more insight into the significant differences and substrate specificities of the isoforms.

A

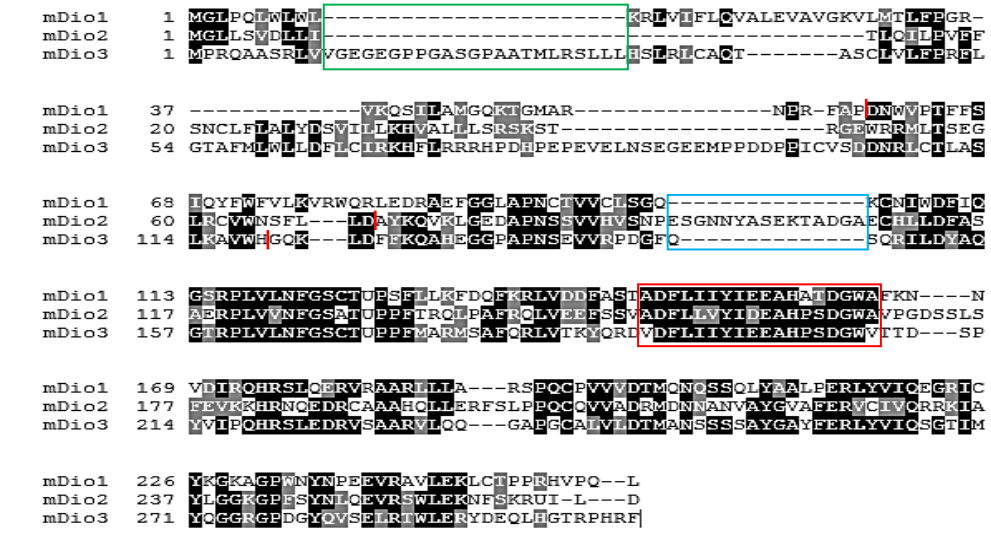

Continued next page

Figure 16 continued:

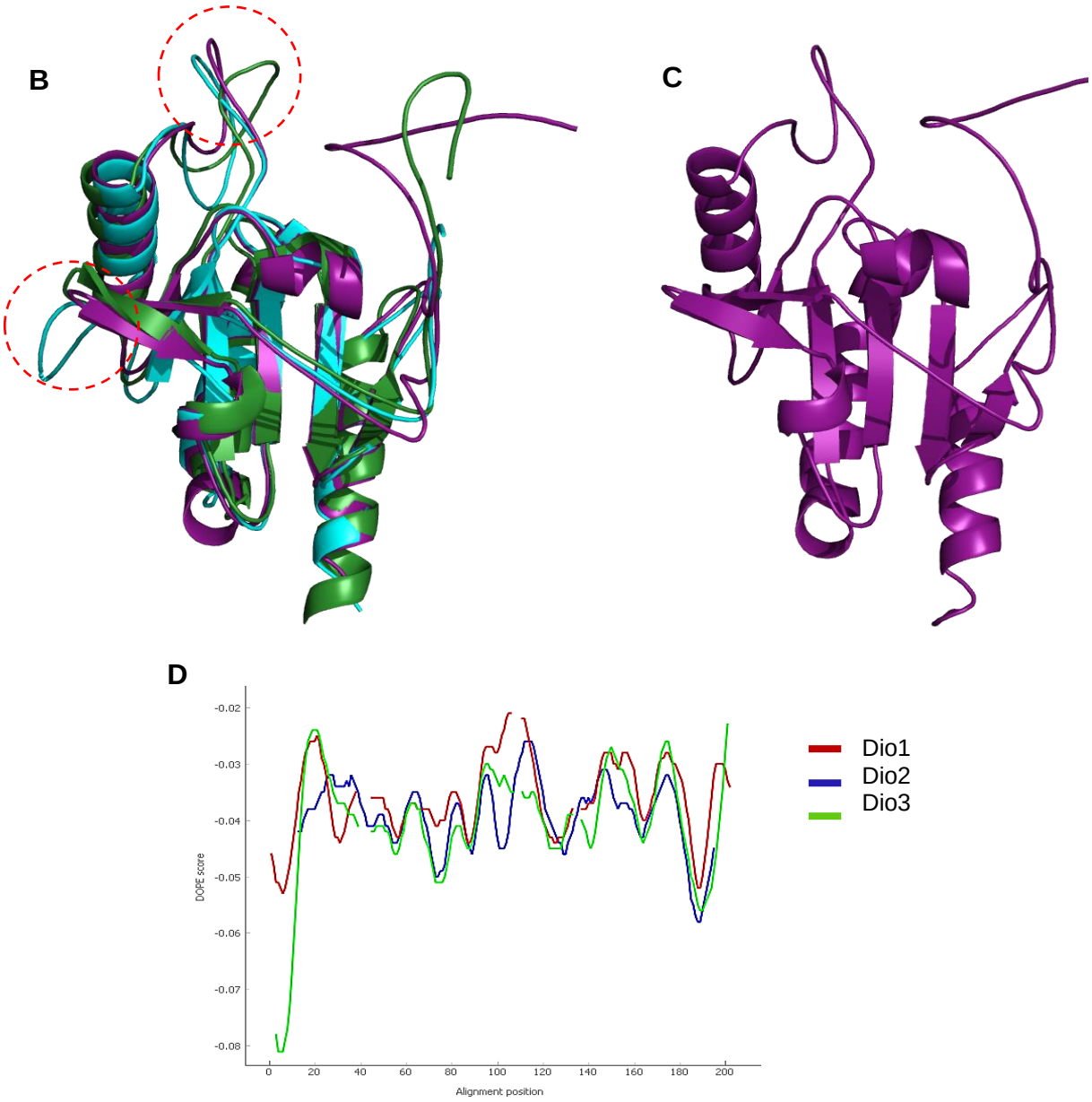

Figure 16. ***Homology Modelling of Dio1.*** *(A) Alignment of Dio1-3 sequences. Start of structures indicated by red lines, different transmembrane region indicated by green box, Dio2 specific sequence indicated by blue box and highly conserved Dio specific residues indicated by red box. (B) Alignment of Dio2 (cyan) & Dio3 (green) plus the model produced for Dio1 by MODELLER (purple). Circles indicate loop differences (C) Model of Dio1 predicted from the solved Dio structures. (D) DOPE (Discrete optimised protein energy) score comparison of the Dio1 model, indicating similarities and differences in the residues.*

3.3 Dimerization

3.3.1 Deiodinase 2 native dimer

Unexpectedly, while expressing and purifying Dio2, a native dimer appeared for several constructs allowing additional information to be garnered about the deiodinase dimers. To ensure that the Dio2 dimer formation were not artefacts but stable dimers that could be used for further analysis, the samples were initially tested via SEC. Aliquots corresponding to the dimer on the original SEC (Fig 11c) were pooled and left at 4°C before being applied back on to the same SEC column 24-48 hours later (Fig 17).

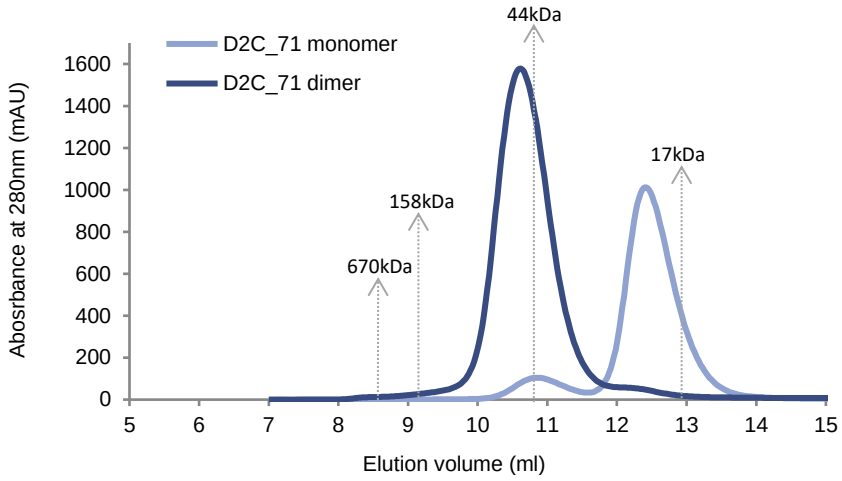

Figure 17. ***SEC of D2C_71 monomer and dimer fractions****. Both the monomer and dimer fractions were run on separate SEC columns and the data was combined for the graph representation.*

The result from the second SEC indicated that the dimer produced was stable but also implied that there could potentially be a monomer/dimer dynamic equilibrium albeit through a slow transitioning, as seen by the small peaks for both monomer and dimer protein. The dimer fractions were pooled, concentrated and flash frozen for further use.

Further analysis comparing the Dio2 monomer and dimer was carried out via blue native PAGE (Fig 18) in combination with a Dio3 dimer protein (3.3.2). This experiment confirms the presence of dimeric forms for both the Dio2 and Dio3 constructs and supports the SEC result of a potential dynamic between the Dio2 monomer and dimer proteins, indicated by the faint bands observed for monomer and dimer in both samples.

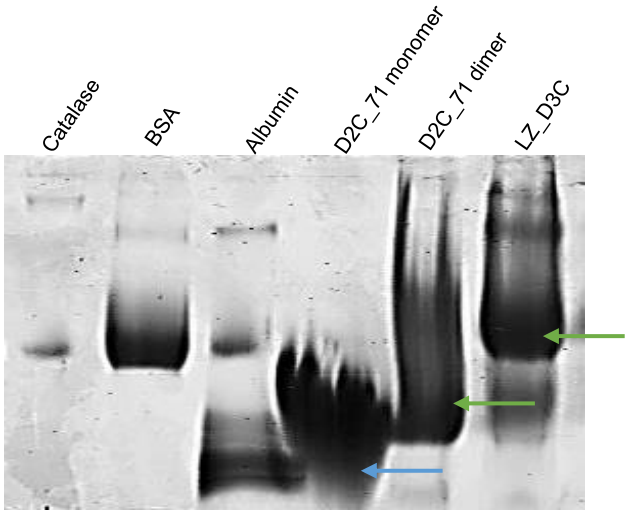

Figure 18. ***Blue Native PAGE analysing Dio2 monomer, dimer & Dio3 dimer****. Catalase (240 kDa), BSA (67 kDa) and chicken egg albumin (45 kDa) are markers. Green arrows indicate presence of dimer and the blue arrow indicates the monomer.*

3.3.2 Recombinant production of dimeric Deiodinase 3 catalytic core

As a truncated form of Dio3 had already been solved structurally, a construct was designed to create a dimer of the truncated monomeric Dio3 via attachment to a Leucine Zipper (Fig 19 & A6). Similarly, to Dio2 the selenocysteine in the active site was replaced with a cysteine in the construct (LZ_D3C). This construct was longer than the $Dio3_{cat}$ (120-304) to accommodate the linker region, which is believed to mediate dimerization.

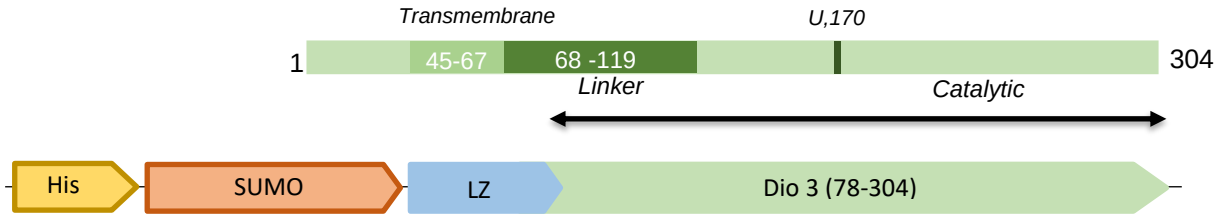

Figure 19. ***Schematic representation of LZ_D3C construct.*** *Top scheme characterises the full length Dio3, bottom scheme is of the cloning construct in pET19b SUMO.*

Once the construct had been designed, expression trials were carried out (similarly to Dio2) to determine the optimum method of obtaining a high yield of soluble protein. This included testing cell type, media, expression time and temperature (Fig 20). The results from the expression experiments indicated that TB media, Codon+ cells, the addition of 1 mM $MgSO_4$, induction with 0.5 mM IPTG and expression overnight at 20°C produced the best yield of soluble protein for the LZ_D3C construct.

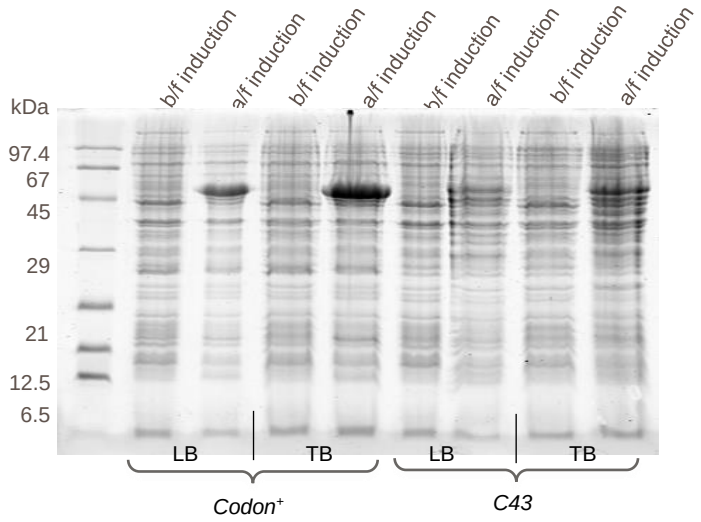

Figure 20. ***Expression trial using two different cell types & media for LZ_D3C.*** *The protein plus the His-tag would have a molecular weight of ~43 kDa. The cell type Codon+ and the media TB produced the biggest yield of soluble protein.*

For the purification protocol, likewise to Dio2, the amount of salt in the lysis buffer was increased to 500 mM NaCl. Nevertheless, the purification of LZ_D3C proved to be difficult due to the addition of chaperone proteins (Fig 21), therefore additional purification steps were required to remove them before SEC.

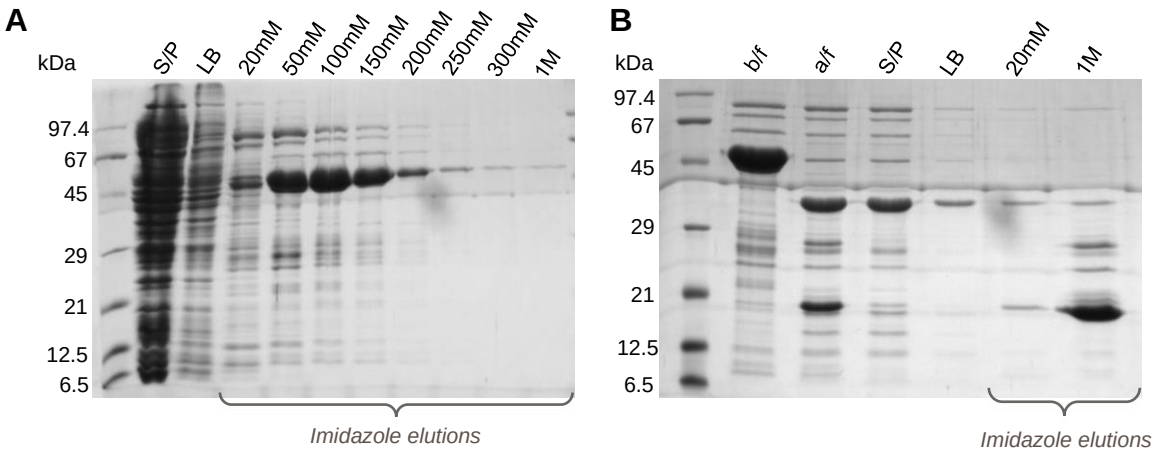

Figure 21. ***Purification of LZ_D3C on SDS PAGE****. (A) Ni-NTA of LZ_D3C (43 kDa), protein elutes early with large amounts of degradation and chaperone proteins. (B) Reverse Ni-NTA after dialysis to remove his-tag. LZ_D3C (~30 kDa) elutes in S/P but chaperone proteins are still bound, and degradation of the protein can be seen. S/P is the supernatant flowthrough, LB is the lysis buffer flowthrough, b/f is a sample before dialysis and a/f is a sample after overnight dialysis.*

The simplest method of removing the chaperone proteins without affecting the LZ_D3C protein involved an additional step in IMAC. After the lysis buffer wash, the beads were incubated at 4°C for ~ 10 mins with denatured E.coli proteins combined with MgATP, as described by the protocol in Rial and Ceccarelli, 2002. This process

successfully removed the chaperone proteins without the need for further purification methods (Fig 22).

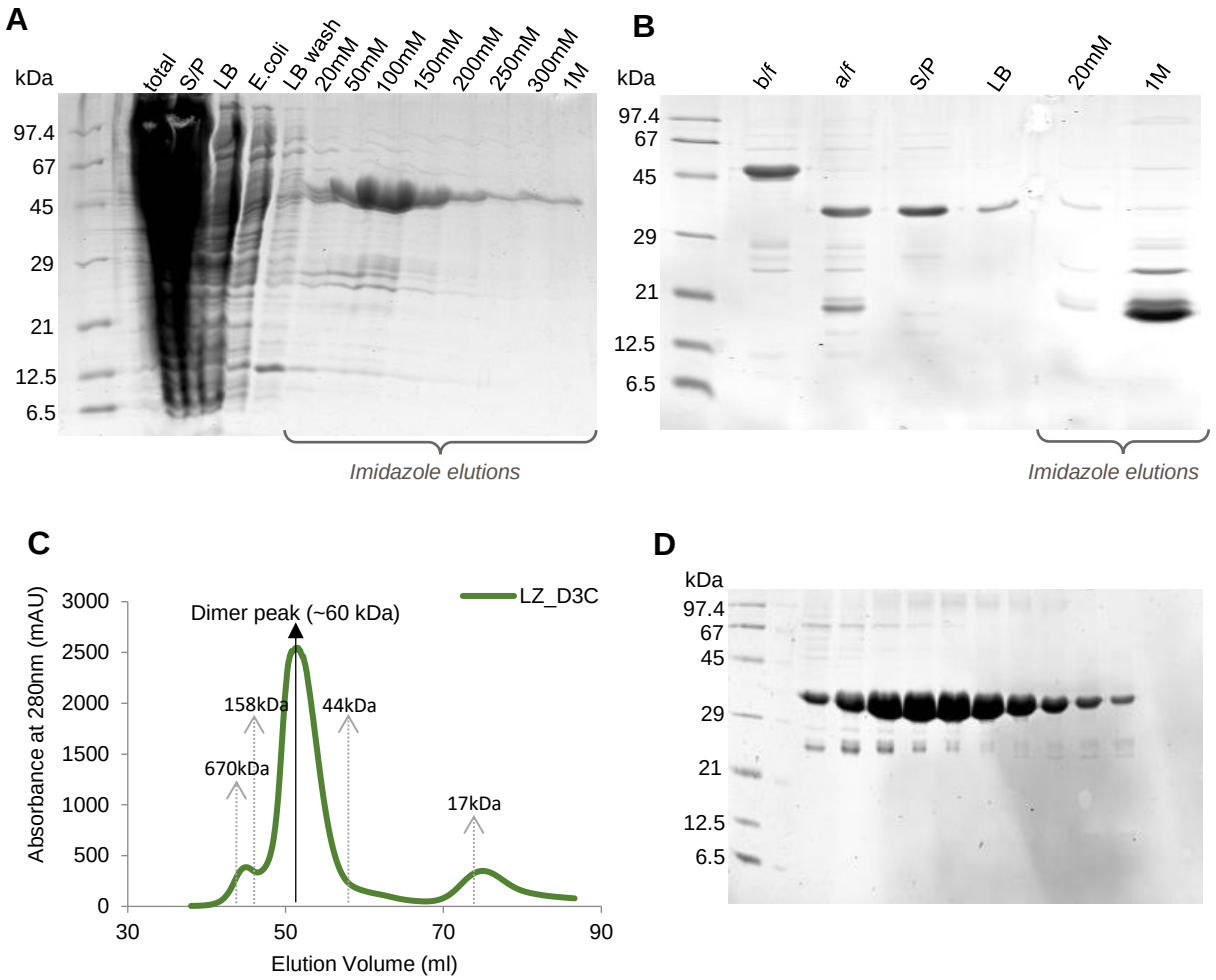

Figure 22. ***Purification of LZ_D3C with removal of chaperone proteins on SDS PAGE.*** *(A) Ni-NTA of LZ_D3C with the inclusion of the E.coli wash step. Total is the complete sample after expression, S/P is the supernatant flowthrough , LB is the lysis buffer flowthrough, E.coli is the flowthrough after incubation with denatured E.coli and LB wash is the flowthrough after an additional lysis buffer wash. (B) Reverse Ni-NTA after dialysis to remove the his-tag. b/f is the sample before dialysis, a/f is after overnight dialysis, S/P is supernatant flowthrough and LB is lysis buffer flowthrough. (C)SEC of LZ_D3C dimer at ~60 kDa (D) Fractions from the dimer peak on the SEC were ran on an SDS PAGE indicating the removal of chaperone proteins and less degradation.*

The result of the purification was an increased yield of soluble LZ_D3C dimer but crystallisation experiments did not produce diffracting crystals and with the success of site directed mutagenesis for Dio2, this was also implemented for the LZ_D3C dimer construct (these mutations were only introduced into the Dio3 part of the construct, so as not to interfere with dimer formation). Initially, the D2 and D3 alignment (Fig 7a) was used to verify if the successful mutations for D2 could be introduced to similar amino acids for LZ_D3C. Unfortunately, no similar amino acid clusters were identified

for mutagenesis and so new mutations for the D3C sequence were predicted via the surface entropy prediction server (Goldschmidt *et al*., 2007). Two clusters of mutations were mutated to Ala; $Glu^{89}Glu^{91}Glu^{92}$ and $Glu^{83}Glu^{85}$ (Fig 23), the mutations proposed were all in the linker region of the D3C construct and not in the catalytic domain and therefore could not be viewed on the $Dio3_{cat}$ structure.

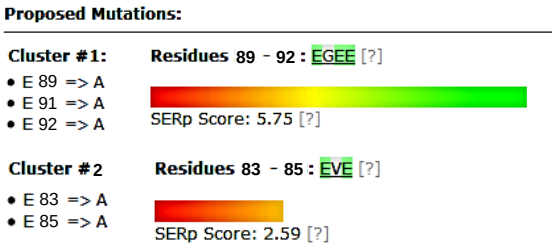

Figure 23. ***Mutagenesis of LZ_D3C.*** *Output of the SERp sever indicating the clusters proposed for mutagenesis.*

These mutants were produced, expressed and purified according to the previously established protocol, and then used in crystallisation experiments. Although some crystals were obtained (Fig 24), they were either too small to mount/test or no diffraction was seen, and the optimisation of the conditions did not improve the results. Seeding was also used with the micro crystals produced; however, these too yielded no viable crystals. Since no Dio3 dimer structure has been solved to date, other methods were used to study the LZ_D3C protein and investigate the dimer formation further.

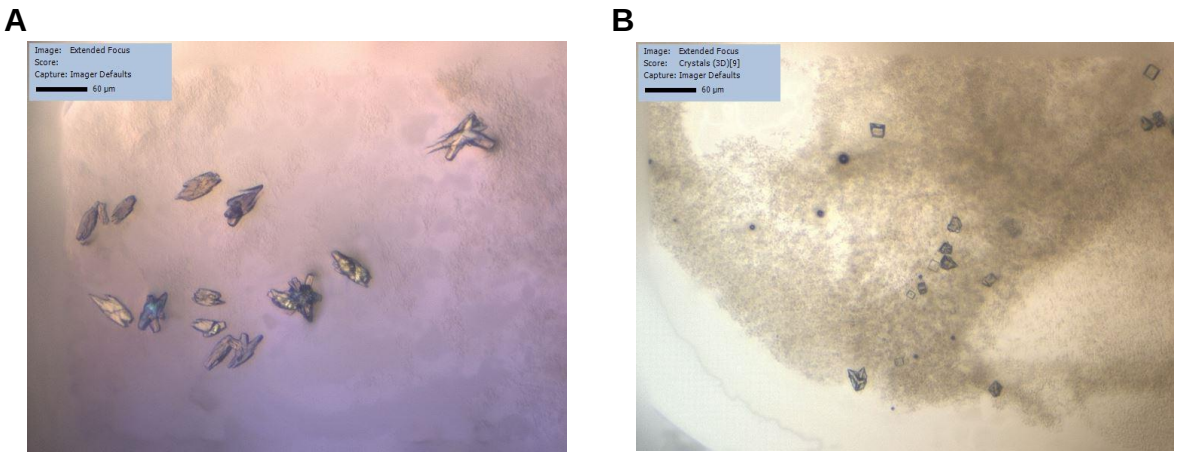

Figure 24. ***Crystallisation of LZ_D3C_EGEE^{89} mutant.*** *(A) Crystals grown from Classics suite II (Qiagen) at room temperature. 0.2 M $CaCl_2$, 0.1 M BIS-TRIS pH 5.5 & 45% (v/v) 2-Methyl-2,4-pentanediol. (B) Crystals grown from Cryos (Qiagen) at room temperature. 0.0085 M ZnSO4, 0.085 M MES pH 6.5, 21.3% (v/v) PEG 550 MME & 15% (v/v) glycerol. Both conditions were taken forward into optimisation, but bigger diffracting crystals were not produced. All images were taken with Rock imager.*

3.3.3 Active Deiodinase 3 dimer

With the creation of the LZ_D3C dimer, one of the most important aspects was a functional enzyme, meaning this constructed dimer should mimic the activity of the native dimer with a substrate. Furthermore, the introduction of a compound could stabilise the LZ_D3C protein allowing diffracting crystals to be produced for structural analysis. However, we initially needed to establish that the LZ_D3C dimer was active with a TH substrate.

An activity test was performed in collaboration with Prof. Dr. Josef Köhrle and Prof. Dr. Ulrich Schweizer's groups. The LZ_D3C dimer was prepared with the TH substrate T_4 and the formation of TH products (particularly rT_3) would be detected via mass spectrometry (Table A7). This assay required a significant amount of LZ_D3C dimer for the mass spectrometry to sufficiently distinguish rT_3 due to the lower activity level caused by the mutation of Sec to Cys. The assay was carried out at different time points, with varying concentrations of LZ_D3C dimer and with the presence/absence of DTT (Fig 25).

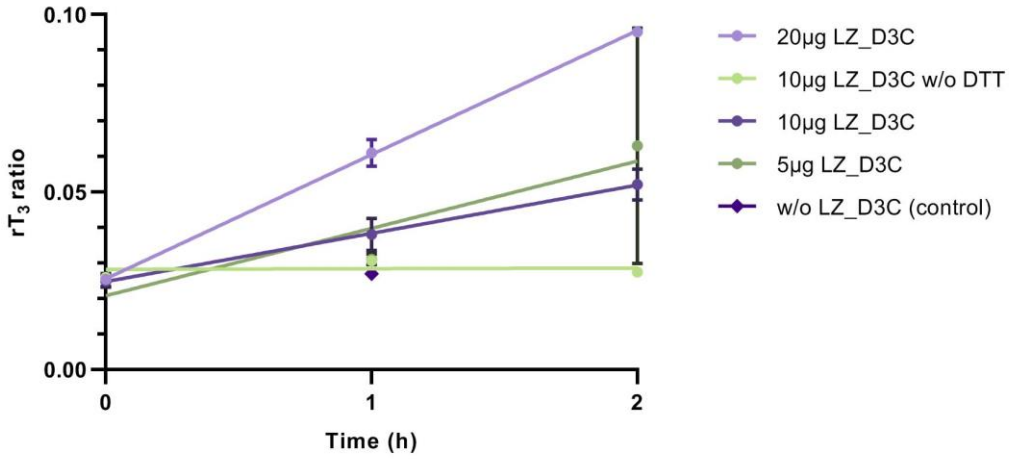

Figure 25. ***Activity assay of LZ_D3C & T4****. All TH substrates were measured by mass spectrometry in the samples and the amount of rT_3 formed was in comparison to the other substrates. High amounts of LZ_D3C required meant repeats could not be performed at the time. A correlation between increase in LZ_D3C and the production of rT_3 is evident. Results displayed using Graphpad Prism.*

The result indicates a clear increase of rT_3 with higher concentrations of enzyme but that the product was also DTT dependent – DTT is required for the enzyme as a reducing agent for in vitro tests. Overall, this assay showed that the LZ_D3C dimer was active and had the potential for further structural insights into how the dimer interacts with the substrate.

3.3.4 Supporting the homodimer model

To understand how the deiodinase isoforms dimerise and what residues are associated with this, cross-linking was performed on the native D2C_71 monomer and dimer. The protein samples (including a NADOX positive control) were tested at different time intervals with four different cross-linkers: formaldehyde, glutaraldehyde, DSS and DSSO. The resulting samples obtained were applied to an SDS PAGE (Fig 26) and the bands from the DSSO gel were analysed by mass spectrometry (Fig 27).

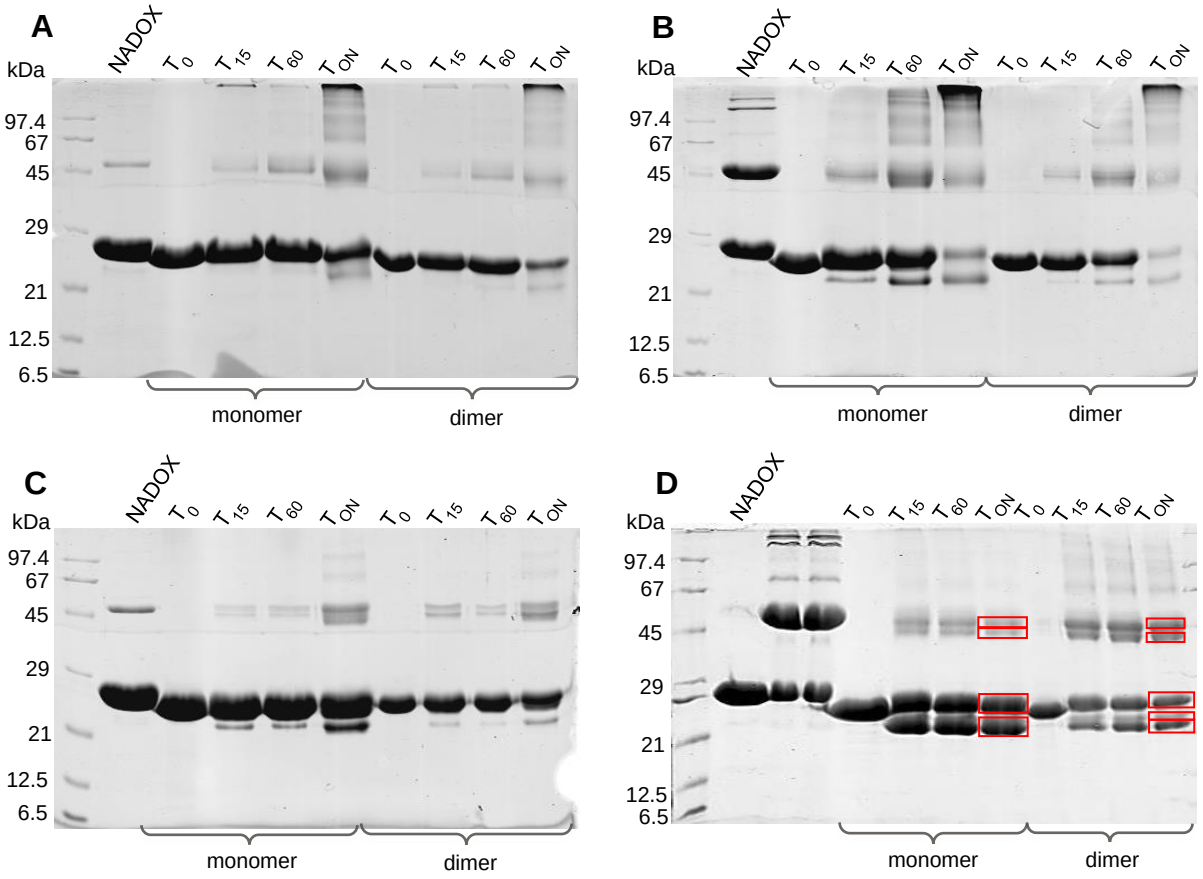

Figure 26. ***SDS PAGE of D2C_71 monomer and dimer cross-linking.*** *(A) Cross-linking with formaldehyde. (B) Cross-linking with glutaraldehyde, (C) Cross-linking with DSS. (D) Cross-linking with DSSO, bands from this experiment (highlighted with red squares) were used in mass spectrometry analysis.*

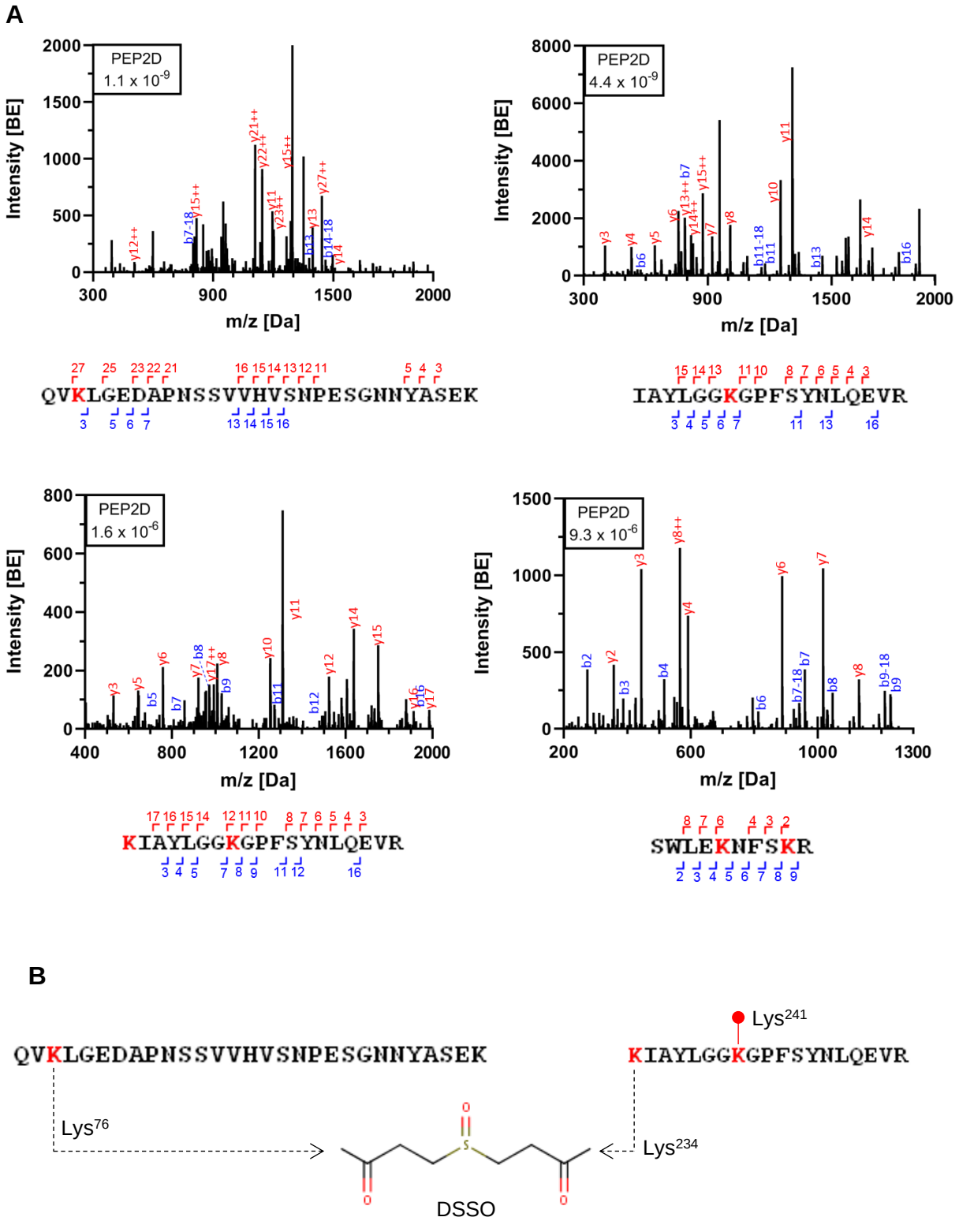

Figure 27. ***Fragment spectrums of DSSO cross-linking from mass spectrometry.*** *(A) Examples of fragment spectrums obtained from mass spectrometry identifying the cross-linked lysine residues. (B) Example of the DSSO cross-linking occurring between two lysine residues.*

The mass spectrometry results highlighted several lysine residues implicated in the dimerization of the protein: Lys^{76}, Lys^{234}, Lys^{257}, Lys^{261} and Lys^{241} as the dominant interactor. These residues were mapped on the Dio2 and Dio3 structures and allowed the identification of the interaction interface (Fig 28), supporting the proposed dimer model based on the redoxins heme binding protein, a structural homolog of $Dio3_{cat}$ (Fig 5a) (Schweizer *et al*., 2014). The result showed that all the lysine residues identified in cross-linking were along one side of the protein, indicating that this could be the dimerization interface (Fig 28c).

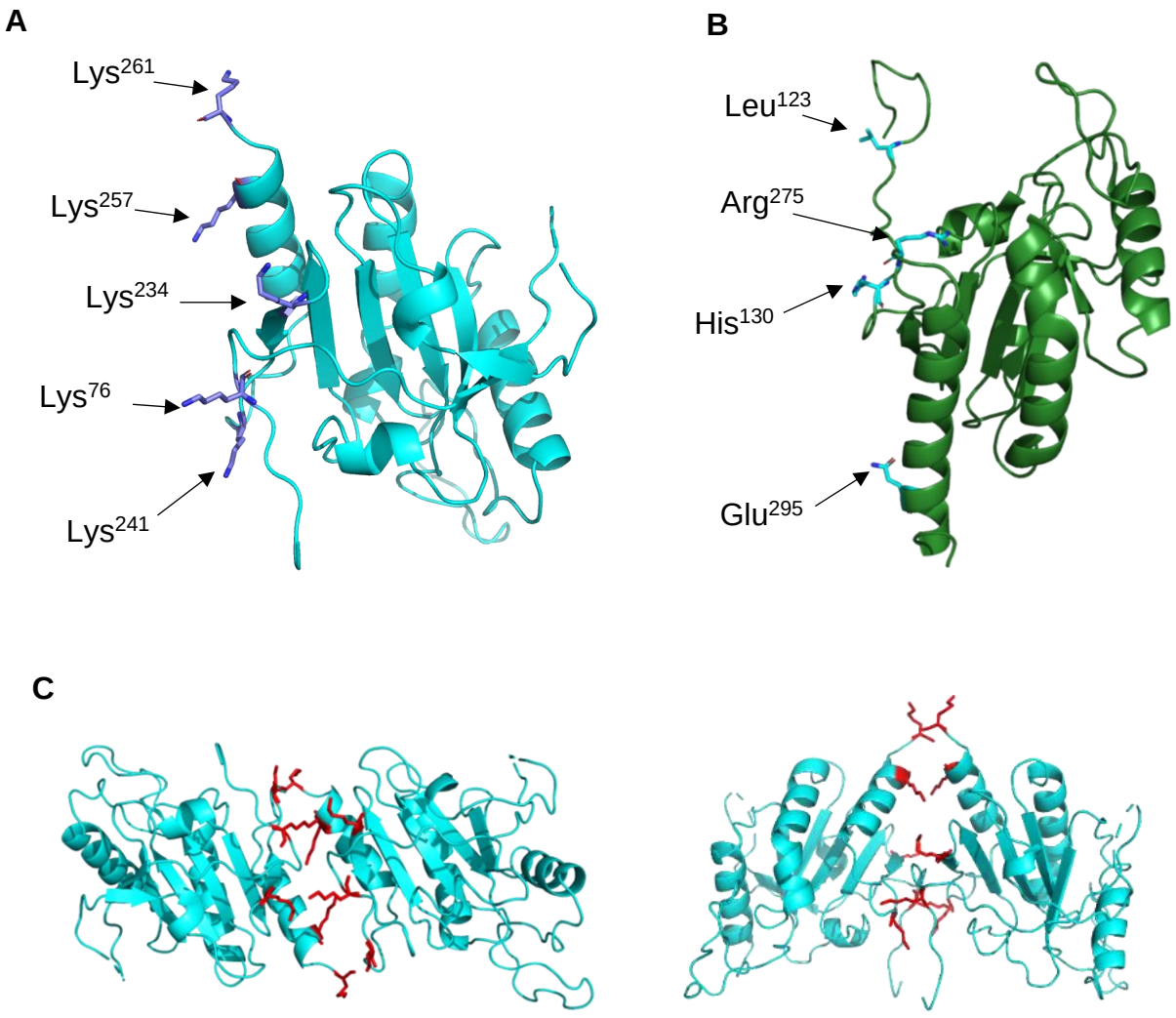

Figure 28. ***Mapping of residues implicated in dimerization on Dio2 and Dio3 structures.*** *(A) Structure of truncated, monomeric Dio2 with Lys residues emphasised. (B) Structure of truncated, monomeric Dio3 (PDB: 4TR3); sequences of Dio2 and Dio3 were aligned and the residues corresponding to the Dio2 Lys residues were highlighted on the Dio3 structure. (C) Possible dimerization interfaces of Dio2, Lys residues shown in red.*

3.4 Ligand Interaction

An important aspect of this project was to identify substrate interaction and analyse the binding of deiodinases that occurs across the different isoforms. Two assays were used to investigate protein-ligand interaction through changing melting temperature (TSA) or thermophoresis (MST), to hopefully identify a ligand that could potentially be used with the Dio isoforms for further crystallisation experiments.

3.4.1 Thermal Shift Assays

Initial TSA experiments with Dio2 protein constructs and T_4 proved to be inconsistent, and the results suggested that the T_4 solvent (NaOH) could be destabilising the protein too much and so further testing was required to determine how the set-up of the assay should be changed to accommodate the use of solvent and minimise its effects. The Dio2 proteins (final concentration of 5 µM) were tested with varying concentrations of Tris/HCl buffer (20 mM to 640 mM) and the addition of NaOH at a concentration of 46 mM (the original T_4 stock concentration). The solutions were mixed in the plate and the results from the assay were analysed (Fig 29).

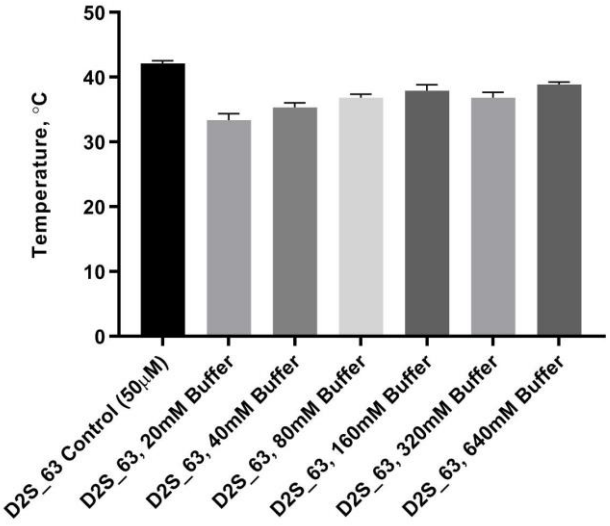

Figure 29. ***Thermal shift assay with D2S_63.*** *Increasing concentrations of Tris/HCl buffer in combination with ligand solvent, NaOH (46 mM) were tested.*

The results indicated that increasing concentrations of Tris/HCl buffer could stabilise the protein however, increasing the buffer concentration too high was not feasible for further experimentation and so the NaOH solvent concentration had to be reduced accordingly to negate the effects on the protein. It is worth noting that although Tris/HCl buffer can undergo pH change with temperature changes there was no indication in

initial TSA trials that this affected the overall results and as the crystallisation buffer was also Tris/HCl, this was preserved to keep the results as accurate as possible.

D2S_63, D2C_66, D2C_71 monomer and dimer and LZ_D3C constructs with varying concentrations of T_4 or T_3, using the method as described above, were then evaluated via thermal shift assays (Fig 30).

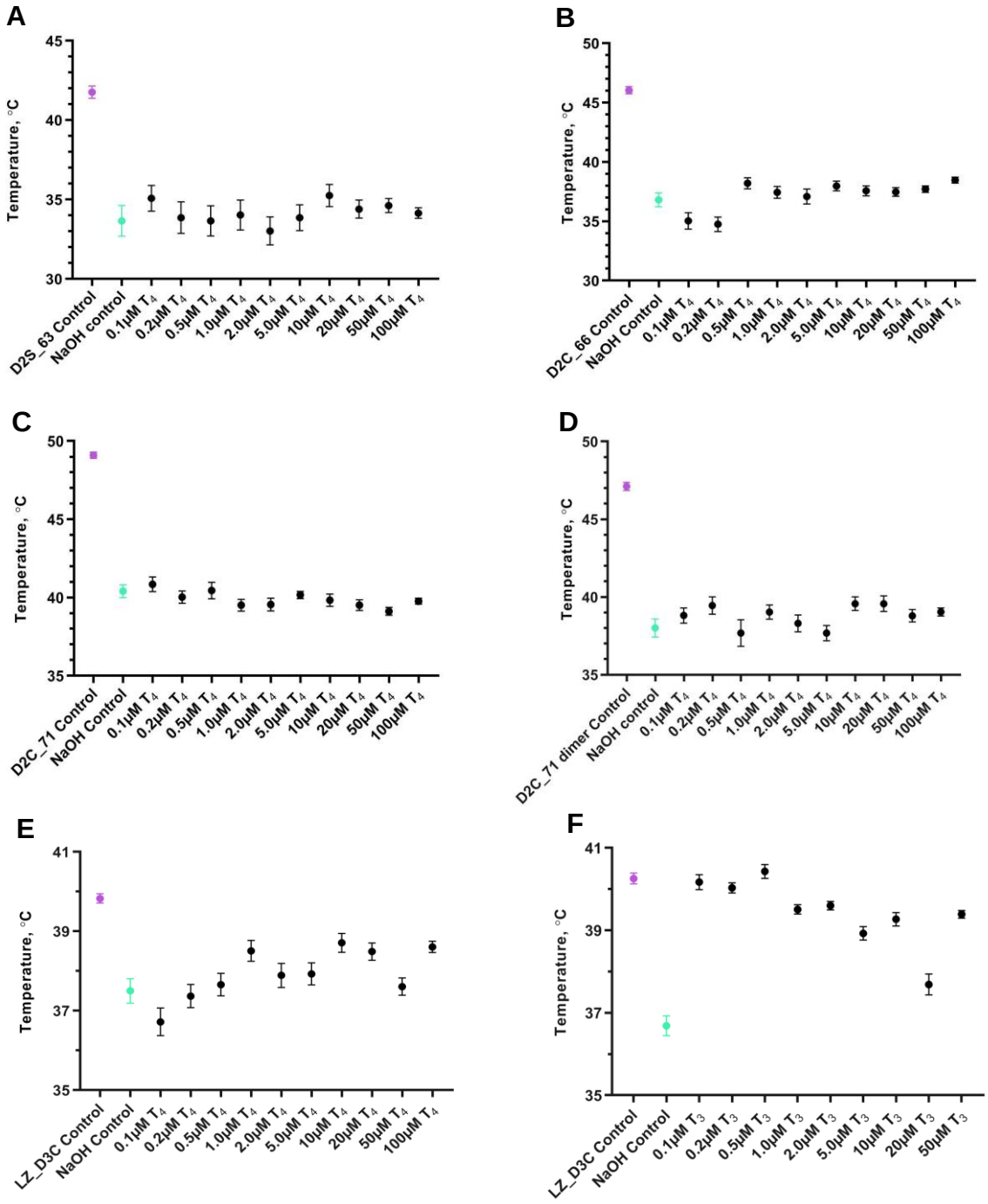

Figure 30. ***TSA of Dio2 and Dio3 construct.*** *All assays contained 5.36 mM NaOH with varying concentrations T_4 or T_3 ligand. (A) TSA of D2S_63 with T_4. (B) TSA of D2C_66 with T_4. (C) TSA of D2C_71 monomer with T_4. (D) TSA of D2C_71 dimer with T_4. (E) TSA of LZ_D3C with T4. (F) TSA of LZ_D3C with T_3.*

The results showed that there was no significant change in the melting temperature for the Dio2 and T_4 assays however, a temperature change of 2-3°C was seen for LZ_D3C T_4/T_3 assays. This indicated that T_4 and T_3 were either not binding to these constructs or were only weakly bound due to the proteins not being full length and therefore not complete native dimers. Furthermore, the T_4 and T_3 substrates had poor solubility and were difficult to work with in small sample measurements and could have hindered the final results. The next step was to incorporate a different substrate in the assays, xanthohumol, an inhibitor of the Deiodinase enzymes with better solubility (Renko *et al*., 2015), in the hope that this would provide a more significant binding result.

Similarly, to the assays for T_4/T_3, the Dio constructs were kept at the same concentration with increasing concentrations of xanthohumol (Fig 31). The same method of maintaining the concentration was applied to the solvent of xanthohumol (DMSO) as this was known from previous work of other students to interfere with the final assay results. Unfortunately, due to the limited amount of D3 dimer, this was not tested with xanthohumol in the TSA.

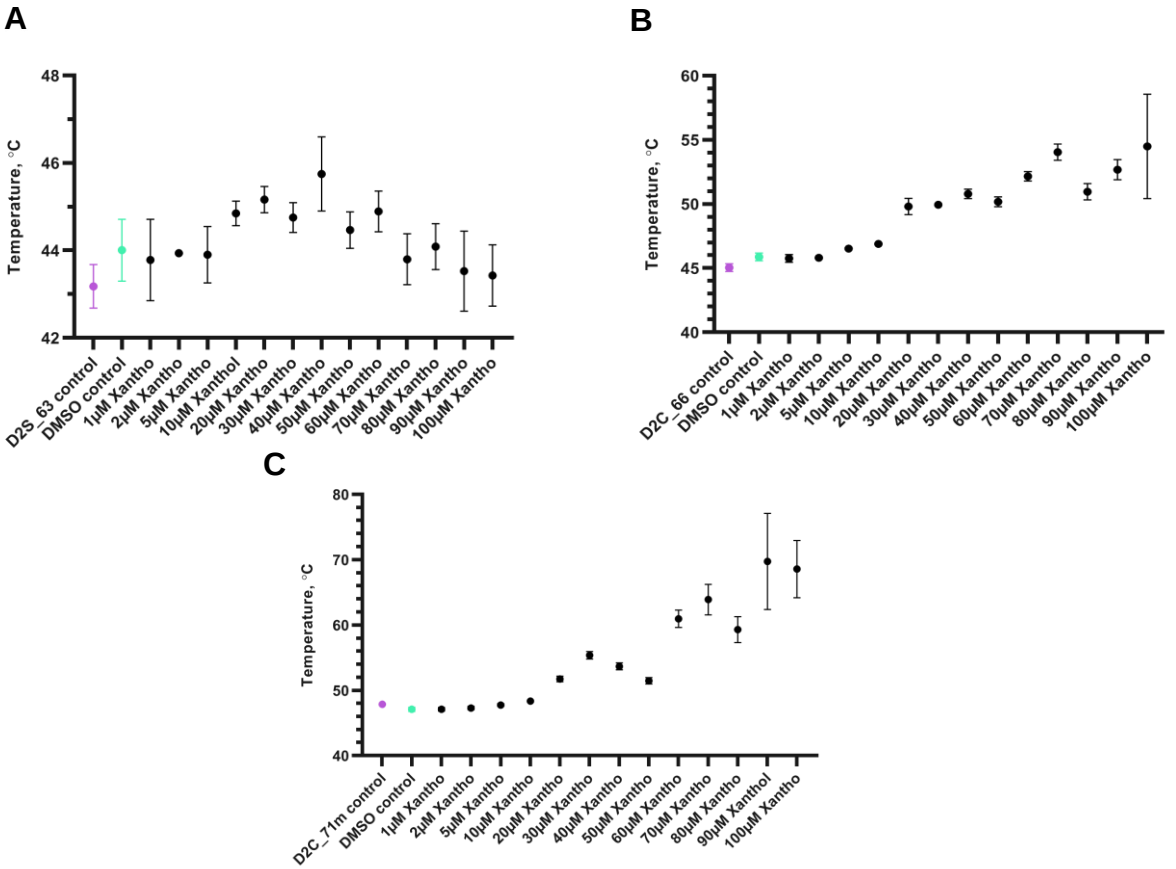

Figure 31. ***TSA of Dio2 constructs with Xanthohumol.*** *All assays contained <10% DMSO and varying concentrations of xanthohumol. (A) TSA of D2S_63 with xanthohumol. (B) TSA of D2C_66 with xanthohumol. (C) TSA of D2C_71 monomer with xanthohumol.*

The result from the assays indicates an increase in the binding temperature with increased concentrations of xanthohumol, between 5 – 50 µM in particular. However, an increase of error also appeared for the higher concentrations of xanthohumol signifying that there could be an increased likelihood of artefacts forming but the initial transitions at the lower temperatures indicates a Kd of ~ 5-10 µM, which is slightly higher but still comparable with the IC_{50} value of xanthohumol (~ 3µM).

3.4.2 Microscale Thermophoresis

After the xanthohumol TSA had produced some positive results but also indicated that there were potential artefacts being produced, an alternative method was proposed to assess the binding. For microscale thermophoresis assays, the protein buffer was exchanged to HEPES and the proteins were labelled with FITC. The proteins were then tested with increasing xanthohumol concentrations (0 - 140 µM, Fig A8) at 20, 30 and 40% laser (MST) power (Fig 32). Increasing the MST power increases the temperature gradient from 2 to 6°C and at a higher temperature gradient a greater signal change can usually been seen that can help in the binding events. As the binding of the Dio proteins had not been tested previously in an MST assay, a range of MST powers (low - high) were used to assess the quality of the data produced and the protein-ligand binding.

A

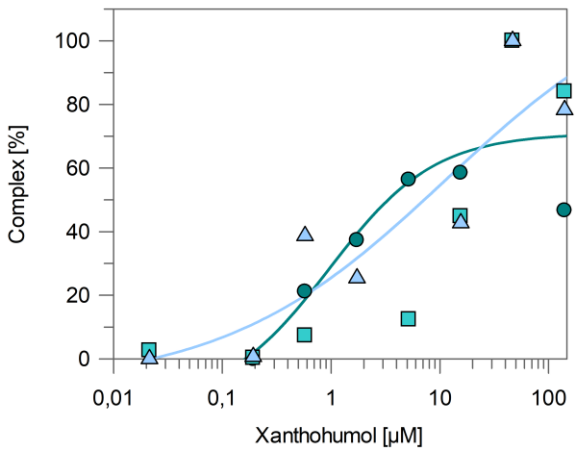

MST Power	Kd (µM)
20%	0.96 ±2.37
30%	/
40%	11.3 ±59.11

Continued next page

Figure 32 continued:

B

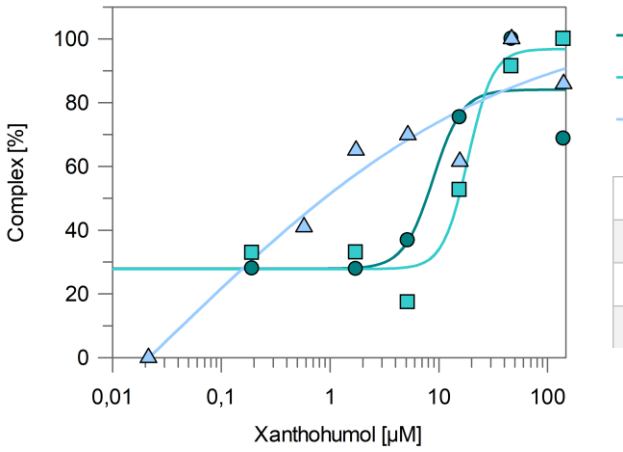

MST Power	Kd (µM)
20%	8.8 ±5.52
30%	18.5 ±5.81
40%	0.035 ±0.94

Figure 32. ***MST binding analysis of D2S_63 & D2C_66.*** *Both assays contained the same concentrations of xanthohumol, with a final DMSO concentration of 10%. (A) MST assay of 2.5 µM FITC labelled D2S_63. (B) MST assay of 2 µM FITC labelled D2C_66. Complete raw data for both assays in Table A9.*

The MST assay results indicates that for both constructs there is binding between xanthohumol and the protein seen particularly in the results from the assay with 20% MST power. The Kd from these assays is also within the range for the IC_{50} value of xanthohumol (1.5 – 3 µM) supporting the data produced. However, as the MST power was increased the results became more ambiguous indicating that a higher MST power was interfering with the binding and a lower MST power was more beneficial for the assay. Furthermore, after the MST assays had been performed, there was precipitation in the capillary for the 140 µM xanthohumol sample suggesting that there could have been protein aggregation that could have affected this result.

The MST assays, although indicative of Dio2 and xanthohumol binding, also demonstrated a limitation in the xanthohumol concentration range. Some samples had to be excluded from the final fit due to anomalous data however, this left an even smaller number of samples to use in the assessment of binding. The concentration range of xanthohumol was chosen to demonstrate a binding curve but complete saturation did not appear to be achieved particularly for D2S_63.

An MST assay was also performed for LZ_D3C (Fig 33) as the binding affinity between xanthohumol and this dimer protein should be stronger compared to the truncated monomeric Dio2 proteins.

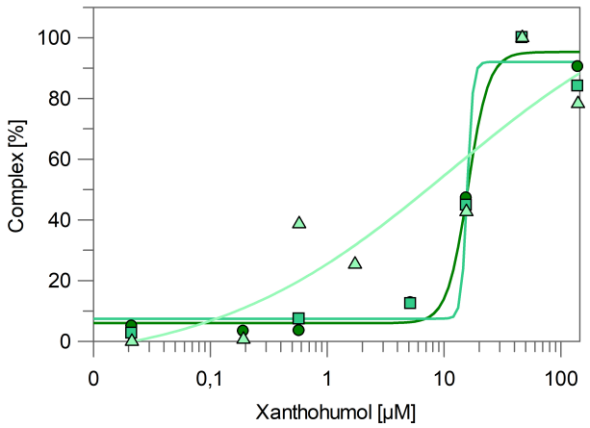

MST Laser Power	Kd (µM)
20%	15.9 ±1.39
30%	15.7 ±34.8
40%	11.3 ±59.1

Figure 33. ***MST binding analysis of LZ_D3C.*** *All samples contained 2.0 µM FITC labelled LZ_D3C and varying concentrations of Xanthohumol, with a final DMSO concentration of 10%. Complete raw data in table A10.*

The LZ_D3C and xanthohumol MST results indicates a weaker binding affinity, seen by the higher Kd, compared to the results seen for the Dio2 proteins. However, similarly to the previous assays, precipitation was seen in the higher concentrations of xanthohumol even after measures were taken to spin down the samples before applying them to capillaries. Furthermore, it is clear from these results that more xanthohumol samples are required at a concentration between 10 – 50 µM, as this seems to be the limiting factor in the binding measurements. Nevertheless, the results from the LZ_D3C binding assay are more convincing of xanthohumol binding as both the 20% and 30% MST powers indicate similar results. Further repeats of this assay would be needed with a smaller concentration range, unfortunately due to the labelling protocol required for this assay a large quantity of protein is needed which limited the final results.

3.4.3 Co-crystallisation

As some binding was evident in the assays produced, the substrates were used in co-crystallisation experiments with the Dio proteins (Fig 34). Both Dio2 and LZ_D3C proteins were crystallised with the substrates through soaking or by direct addition into the crystallisation set-up. For direct addition, the substrate would be mixed with the protein just before application by the Phoenix liquid handling system or by hand. For soaking, any crystals that were obtained were placed into a solution containing the substrate and cryo-protectant and incubated for varying time points. The crystals were then mounted as before and tested. Unfortunately, either no diffracting crystals were

produced or no density for the ligand could be seen in the resultant structures produced from soaking.

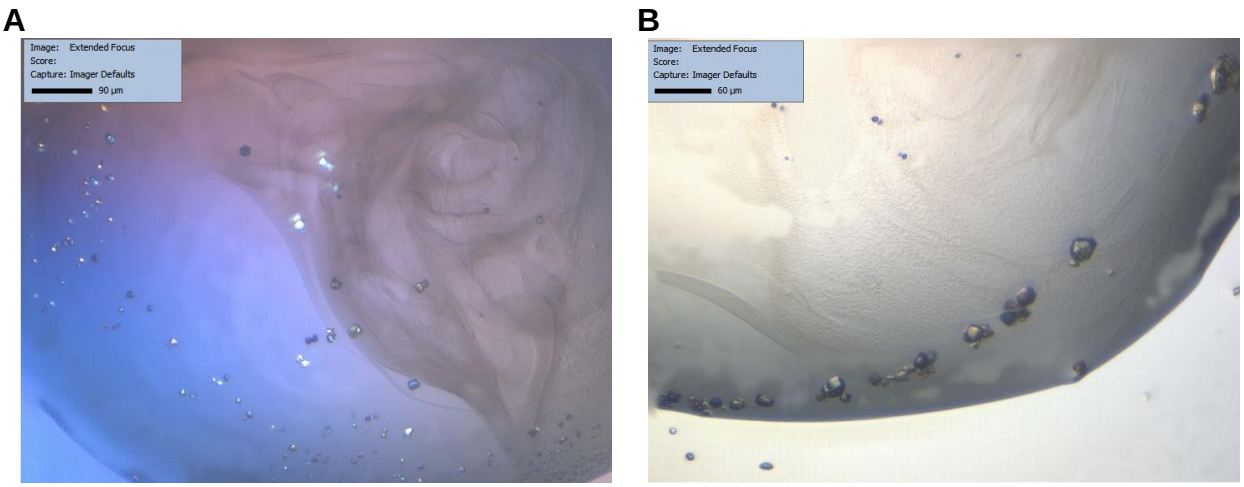

Figure 34. ***Co-crystallisation of Dio proteins with substrates.*** *(A) Micro crystals obtained from PACT (Qiagen) C12: 0.01 M Zinc Chloride, 0.1 M HEPES & 20% w/v PEG 6000. (B) Micro crystals obtained from Classics Suite Lite (Qiagen) G7: 0.1 M MES buffer, 0.01 M Zinc sulphate & 11.4% w/v PEG 550. Xanthohumol was used at a concentration of 0.5 mM for all plates.*

4.0 Discussion

4.1 Structural Characterisation of the Deiodinase isoforms

4.1.1 Deiodinase 2 specific loop

Structurally, all of the Dio_{cat} isoforms appear to be highly similar with many of the same secondary structure elements present. One of the major differences, seen only in the $Dio2_{cat}$ structure, is the addition of 15 residues between βN1 and βN2 in the Prx-like module (Fig 35a and b). This Dio2 specific insertion, known as the 'destruction sequence' from Schweizer *et al.,* 2014, could play a role in the ubiquitination and ultimate proteasomal degradation of Dio2. As previously mentioned in 1.4.1, Dio2 is the only isoform implicated in activity-induced inactivation (Halperin, 1994; Steinsapir *et al*., 1998) in which higher levels of TH substrate lead to a ubiquitinated inactive Dio2 (Gereben *et al*., 2000; Bianco *et al*., 2002; Sagar *et al*., 2007). As this longer loop region is not seen in Dio1 or Dio3, this further supports the hypothesis that this unique Dio2 feature could provide evidence for proteasomal degradation. Our structure shows that the loop is close to Cys^{205} and consequently coincides with the lack of a proximal Cys in the Dio2 sequence (SATU motif compared to SCTU in Dio1 and 3), whereby the selenylsulfide intermediate could instead form between the Sec^{130} in the active site and Cys^{205} (Fig 35c), before being reduced by a thiol cofactor; causing a conformational change of the nearby loop/destruction sequence creating a possible signal for ubiquitination. Previous studies on human Dio2 also identified this loop region as exclusive to this isoform (additional 18 residues) and a deletion mutant lacking this loop showed a lower turnover rate and a longer half-life compared to the wildtype hDio2 (Dentice *et al*., 2005; Sagar *et al*., 2007) supporting the hypothesis that TH binding can lead to inactivation and degradation of Dio2 via this loop.

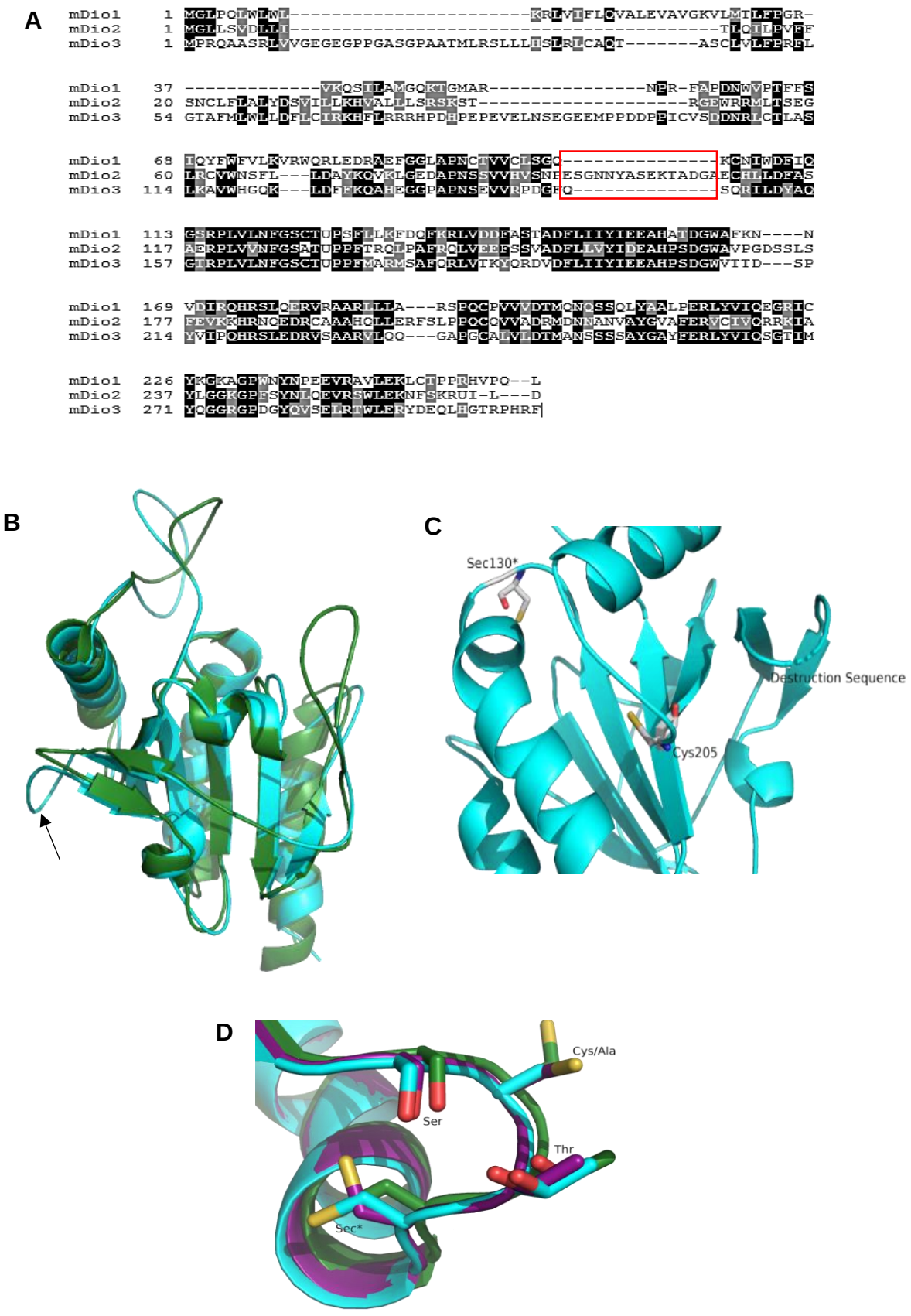

Fig 35. ***Dio isoform comparisons.*** *(A) Alignment of Dio sequences, highlighted box in red indicates the additional 15 residue loop in Dio2. (B) Overlay of* $Dio2_{cat}$ *(cyan) and* $Dio3_{cat}$ *(green) structures. Arrow indicates Dio2 specific loop. (C)* $Dio2_{cat}$ *structure with* Sec^{130}*,* Cys^{205} *and additional loop (destruction sequence) highlighted. (D) Dio1,2 & 3 SXTU active site motif.*

4.1.2 Active site residues

Additional differences between the isoforms are seen in particular with the residues surrounding the active site giving rise to possible explanations for regiospecificity and general activity. In the $Dio3_{cat}$ structure a Phe residue shields the Sec^{170}, effectively blocking the active site for TH substrates. The strained conformation of the Phe^{258} protruding from the α2/β3 loop blocks the active site and it was previously speculated that substrate binding or dimerization of the Dio3 protein could release this loop and allow access to the active site Sec (Schweizer *et al*., 2014). The residues on this α2/β3 loop are highly conserved amongst the isoforms signifying that they perhaps play a significant role in ligand binding. Moreover, in previous experiments, mutations that were performed on Phe^{258} and Tyr^{257} to limit conformational flexibility resulted in an inactivation of the Dio3 enzyme (Schweizer *et al*., 2014). However, in comparison this conformation of the Phe (Phe^{224}) is not seen in the $Dio2_{cat}$ structure (Fig 36a). Instead, the Phe^{224} in $Dio2_{cat}$ is shifted away from the Sec^{130} creating an opening with access to this active site. This indicates that this Ɵ2/β3 (α2/β3 on $Dio3_{cat}$) loop could be flexible but as the other conserved residues in this region have similar conformations, this leads to the conclusion that more than likely this is a Dio2 specific feature revealing a more open conformation of the active site compared to Dio3. The difference in the residue conformation points towards a clear difference in the general activity between Dio2 and 3 but it could also support the evidence that Dio2 is the major activating enzyme (Salvatore *et al*., 1996; Bianco *et al*., 2005) as this open active site state could allow easier access and orientation of the TH substrate, T_4. Further work with the $Dio1_{cat}$ homology model indicated that this Phe residue is not conserved, instead Dio1 has a Pro residue (Pro^{213}) (Fig 36b). As Dio1 is capable of deiodinating both the inner and outer rings of the THs, the presence of Pro^{213} creates an even more open active site for enabling a range of TH substrates to enter this space for catalysis. For example, by modelling the substrate T4 with the Dio structures, the wider active site for Dio1 demonstrates that the substrate is capable of different orientations compared to Dio2 and 3 as the position of the Phe could block the outer or inner deiodination (Fig 36c and d).

This open active site centre theory is further supported by the presence of an Arg residue in Dio3 (Arg^{275}). In contrast to Arg^{275} in Dio3, Ala and Lys replace this residue in Dio1 and 2, respectively (Fig 36e). The Arg residue was hypothesised in Schweizer *et al*., 2015 to be an Arg clamp that could interact with the carboxylate on the TH

substrate allowing catalysis to take place. Although in the $Dio2_{cat}$ structure, the Lys residue could have a similar function to Arg, the orientation points away from the Sec creating a wider active site centre in combination with Phe^{224}. This orientation and replacement of residues is more prevalent in Dio1, and the model suggests that the Ala^{230} and Pro^{213} creates an easy access for all of the TH substrates in varying orientations as there would be fewer interactions due to the wider opening resulting in a loss of regioselectivity compared to the other isoforms. However, the Ala^{230} is not conserved in other species of Dio1 compared to the conserved Lys and Arg in Dio2 and 3, respectively (Fig 36f) and most likely is a feature of the mDio1. The residues in place of Ala, include Ser and Pro which would still have little interaction with the substrates and orientation and the conserved Lys^{229} residue, as indicated by the homology model, would have no interaction with the substrates as the positioning of the residue points away from the active site (Fig 36e).

These results propose that this residue, supported in particular by Dio1 and 2, may not have a role in positioning and locking the TH substrate for catalysis but as an alternative the deiodinase specific insertion (loop-D), could potentially interact with the THs. The high B-factors for this loop allude to conformational flexibility suggesting this is a flexible lid above the active site that could potentially close over the substrates for catalysis. Previous work on Dio3 also suggested that the loop-D is similar to an Ω-loop, which can contribute to protein function (Fetrow, 1995; Bayse *et al*., 2020). Loop dynamic simulations from this work indicated that Asp^{211}, located on the loop-D, could be in a position to stabilise T_4 and enhance the selectivity of inner ring deiodination on Dio3. The lack of conservation in this residue on the flexible loop-D for Dio1 and 2 could provide further explanation on the mechanism for regioselectivity. However, this would need to be analysed further with a ligand bound structure as possible rearrangement of the active site cleft in combination with loop-D could provide more explanation to the specificity of the isoforms.

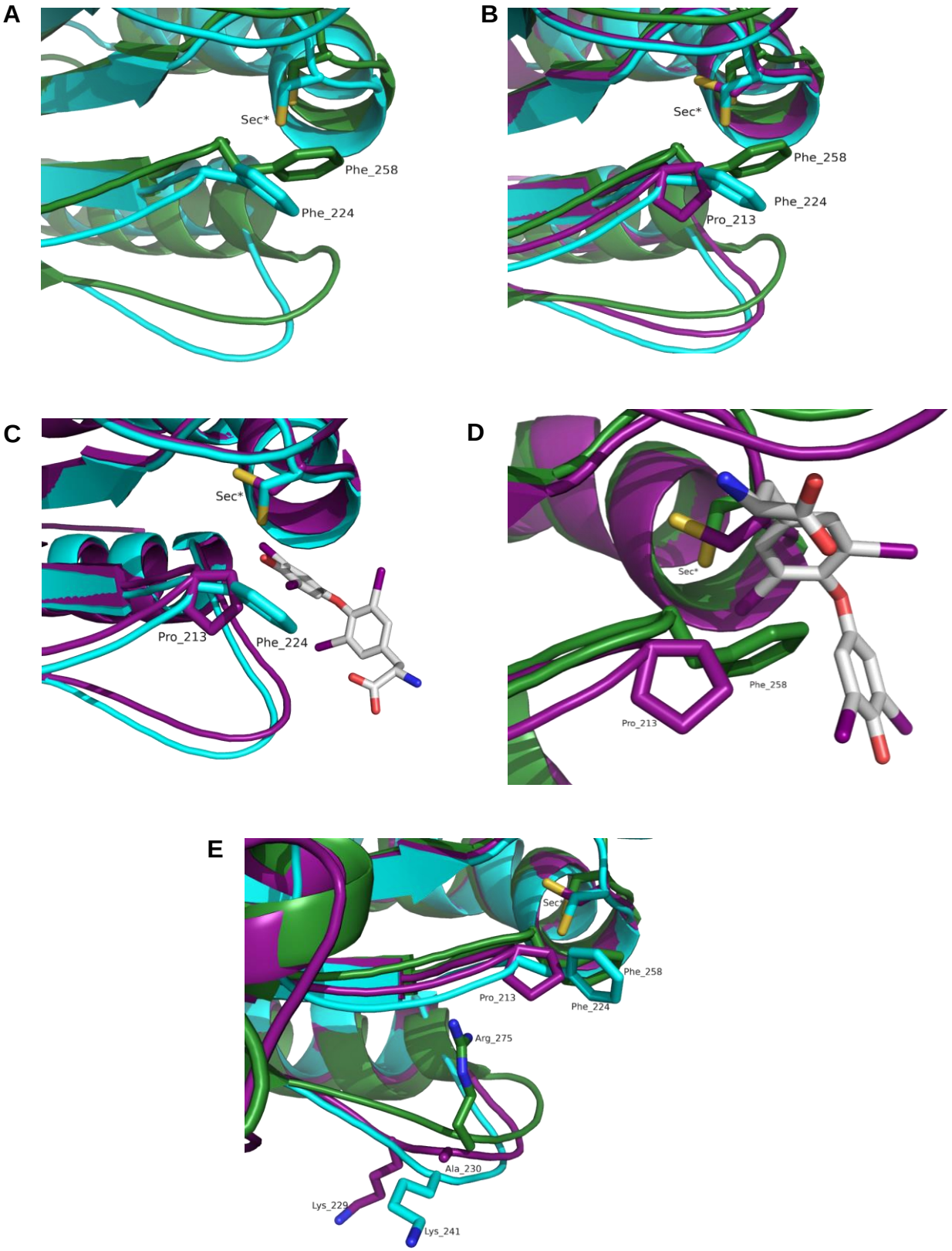

Continued next page

Figure 36 continued:

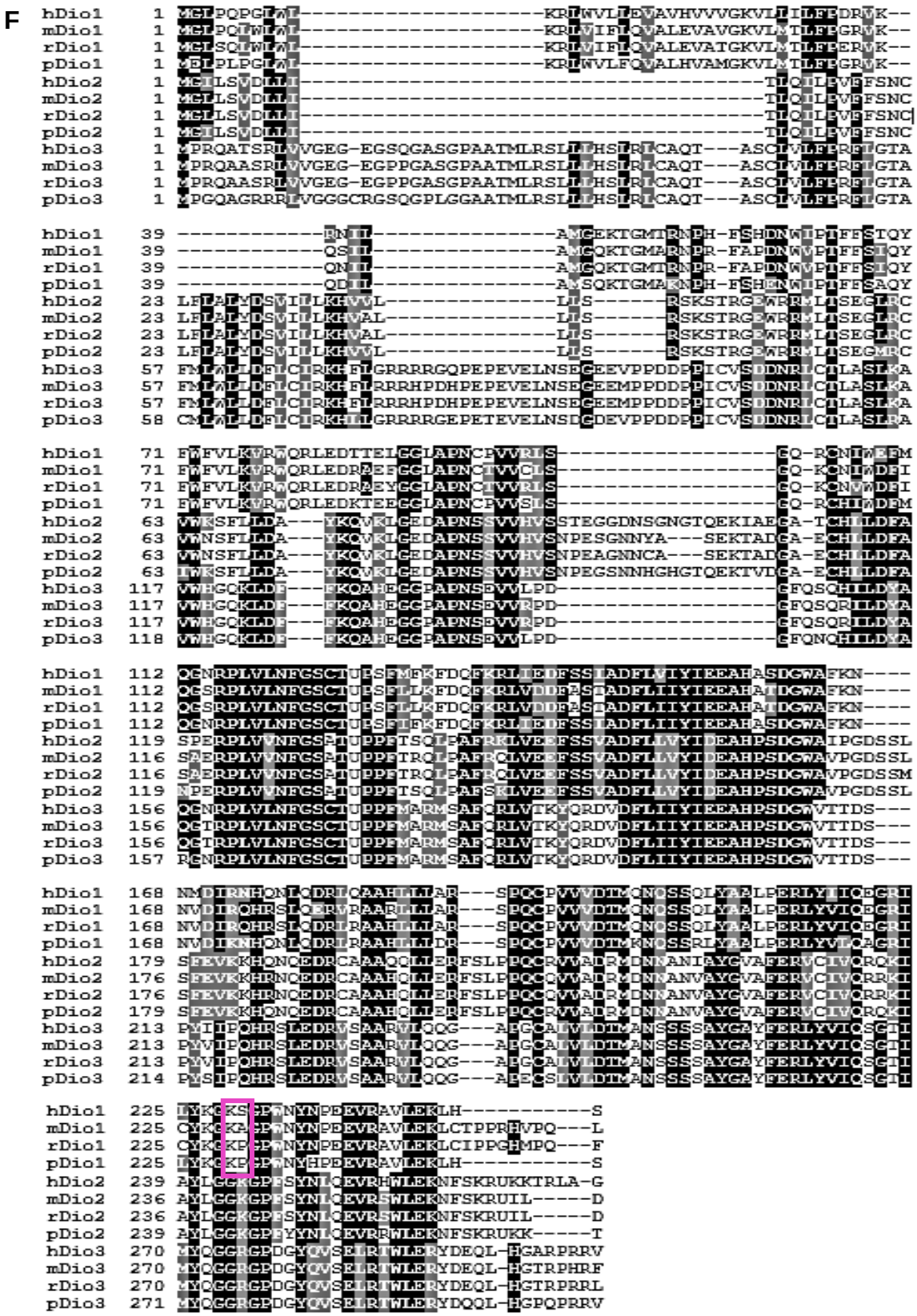

Fig 36. ***Dio active site.*** *(A) Overlay of Dio2$_{cat}$ (cyan) & Dio3$_{cat}$ (green) active site centres, demonstrating different Phe orientation. (B) Overlay of Dio1$_{cat}$ (purple), Dio2$_{cat}$ (cyan) & Dio3$_{cat}$ (green) structures, indicating Pro residue. (C) Dio1$_{cat}$ & Dio2$_{cat}$ with T$_4$. (D) Dio1$_{cat}$ & Dio3$_{cat}$ with T$_4$ (E) Overlay of Dio1,2 & 3 active site centres with highlighted residues. (F) Alignment of Dios from various species, h – human, m – mouse, r – rat, p – pig. Lys^{229} & Ala^{230} highlighted.*

4.1.3 Deiodinase specific insertion, loop-D

The residues at the anchor of the loop-D are highly conserved amongst the Dio isoforms, with considerable variation in the middle section of the loop. Previous mutation studies on Dio3 (Callebaut *et al*., 2003; Schweizer *et al*., 2014) identified important residues involved in this anchor section of the loop, in particular Glu^{200}, Tyr^{197}, Ser^{167} and Thr^{169} (Fig 37a). Mutation of these residues resulted in a possible disruption of hydrogen bonds between Glu^{200} with Thr^{169} and Tyr^{197}, that could allow too much flexibility in this loop meaning it cannot form the correct conformation for substrate binding or potentially breaks a proton transfer cascade (Bayse *et al*., 2020). As well as Glu, Trp and His are also highly conserved in loop-D (Fig 37b) and indicate a possible role in driving the dynamics for regioselective deiodination. The length and residues in the mid-section of the loop varies greatly between all the Dio isoforms (Fig 36e) and this particular region between the Trp and His residues could allow a specific arrangement of the loop that is able to orient the TH substrates for effective catalysis. However, the implications of these residues and specific orientation would need to be confirmed with new mutation studies and further structural work including the use of a TH substrate.

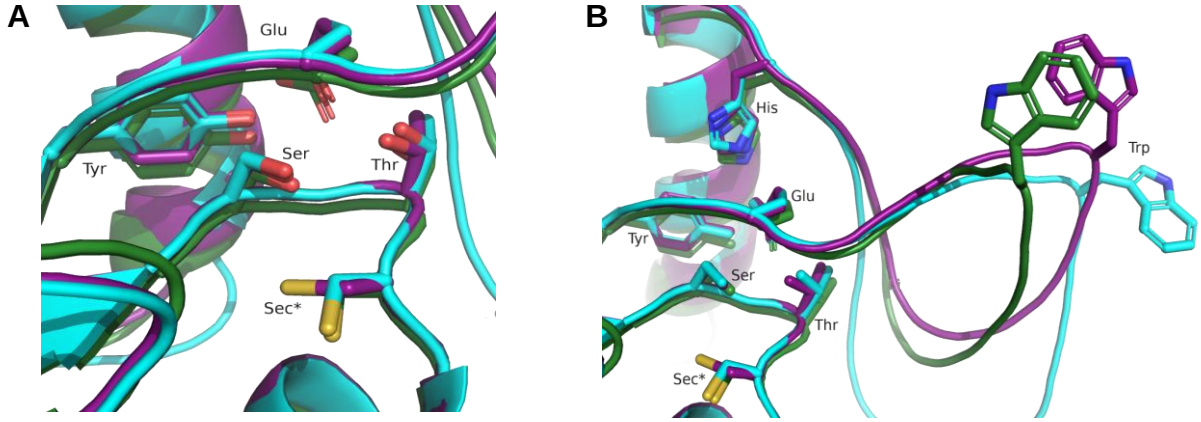

Fig 37. *Dio specific insertion, loop-D* *(A) Overlay of Dio isoforms showing conserved Glu, Tyr, Ser & Thr residues. (B) Overlay of Dio isoforms showing conserved Trp and His on loop-D.*

4.1.4 Proton transfer cascade

The conserved residues mentioned in 4.1.3 have also been implicated in a proton cascade, in which the proposed theory suggests that a proton from the Sec is passed along a hydrogen bond network of conserved residues in this Dio specific loop (His^{182}, Glu^{160}, Ser^{127}, Tyr^{157} and Thr^{129} on $Dio2_{cat}$) to the tyrosol position on the TH substrate (Fig 38). Two conserved His residues were identified as important for Dio activity,

His^{162} and His^{182} in $Dio2_{cat}$. The structure indicated that the His^{162} projects out from the loop-D towards the substrate binding site suggesting that, likewise to $Dio3_{cat}$, this histidine residue could act as a binding partner for the phenolic end of the TH substrate. The His^{162} in combination with a conformational change in loop-D could orientate and lock the TH substrate in place. Furthermore, the transfer of the proton from Sec along His^{182}, Glu^{160} and Ser^{127} could increase the nucleophilicity of the Sec and support the reaction kinetics whereby the Sec needs to be reduced by an intermediate cofactor.

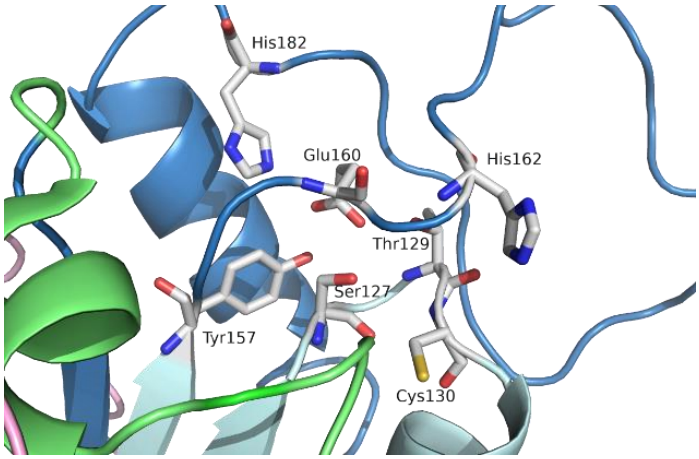

Fig 38. *Conserved proton cascade.* *Conserved residues involved in proton cascade on $Dio2_{cat}$.*

4.2 Dimerization of the Deiodinase isoforms

4.2.1 Natural dimer

Previous studies using fluorescence resonance energy transfer (FRET) and bioluminescence resonance energy transfer (BRET) have identified all the Dio isoforms as homodimers in vivo (Sagar *et al*., 2008) highlighting the transmembrane surface residues and part of the linker regions as important for mediating the dimerization, which is required for deiodinase activity and function. (Sagar *et al*., 2007; Schweizer *et al*., 2014). Interestingly, while purifying N-terminally truncated recombinant Dio2 constructs that predominantly behave as a monomer, dimeric species were also produced, as shown in 3.3.1. These dimeric species were only seen for the longer Dio2 constructs (D2_63/66/71), while the shorter constructs that contained less of the known linker region produced no dimer. This native dimer formation had only been seen once in previous literature (Schweizer *et al*., 2014) and was initially considered a possible artefact. However, with subsequent testing the

dimer product proved to be relatively stable, but a slight shift of form was seen; the monomer was able to produce a small amount of dimer over time and vice versa for the dimer species. This indicated that there could be a potential dynamic equilibrium between the monomeric and dimeric forms suggesting that the bonds for dimerization in these proteins are not complete although the significance of this observation remains to be investigated further. Nevertheless, the results showed that dimer formation was possible natively without the transmembrane region although the dimer formation may not be conducive to Dio activity as seen in previous work; through which a truncated Dio3 (loss of transmembrane) could still dimerize with a full length Dio3 to produce a dimer with the same affinity for substrate as the native dimer. Demonstrating that at least one transmembrane domain is needed for catalytic activity. This also confirms the results of the ligand interaction studies (3.4), in which the monomeric and the dimeric species produced for Dio2 showed no significant difference in protein-ligand interaction.

Although the production of the dimeric species for the Dio2 constructs was reproducible and validated by SEC, blue native PAGE and cross-linking, further studies of these dimers could be done via SEC MALS, a combination of size exclusion chromatography with multiangle light scattering or Dynamic light scattering (DLS) to corroborate the previous results. To further distinguish the potential size and shape of the homodimer small angle x-ray scattering (SAXS) could be used to produce a reasonable model of the dimer without producing a crystal.

4.2.2 Dimerization Interface

Although all the protein/protein interactions observed in the $Dio2_{cat}$ structure appeared to be crystal contacts (Fig 39a), confirmed by PDBePISA (Krissinel and Henrick, 2007), a tool used to study macromolecular interfaces and possible quaternary structures based on the uploaded PDB file. The protein, in particular the dimeric D2 species, could still offer insight into the potential residues involved in the dimerization via cross-linking. The results from this experiment indicated several lysine residues involved in the potential dimerization of the protein; Lys^{76}, Lys^{234}, Lys^{257}, Lys^{261} and Lys^{241} as the dominant interactor. These residues were mapped on the $Dio2_{cat}$ structure and allowed the identification of interaction interfaces (3.3.4, Fig 27). The aligned residues were also mapped on $Dio2_{cat}$ and $Dio3_{cat}$ and ran through HADDOCK

(High Ambiguity Driven protein-protein DOCKing) (Van Zundert *et al*., 2016) to try and identify alternative complex formations from other predicted proteins (Fig 39b and c). Other potential dimer structures included the use of two mirror image monomers with the transmembrane regions close together or alternatively one of the monomers is flipped 180° meaning although the transmembrane regions face the same direction they are on opposite sides of the dimer. In both cases, the active sites could not interact with one another and so there must be a structural change on dimerization within the active site region. In previous work, simulations of the $Dio3_{cat}$ structure as a dimer indicated that the N-terminus of the protein could wrap around and interact with the loop-D (Bayse *et al*., 2020) however, the work in this thesis supports the theory that the N-terminal transmembrane region may not directly contribute to the formation of the homodimer but is required for cell localisation and catalytic activity (Olvera *et al*., 2015; Schweizer and Steegborn, 2015). Alternatively, the C-terminus region of the Dio isoforms is relatively conserved and close to the dimerization interface in the proposed models. In these dimer formations, the residues of β3/β4 could interact with the N-terminal loop (linker region) causing a conformational change to the ϴ2/β3 loop creating an opening to the Sec within this hydrophobic pocket (Fig 39c) for potential TH substrates. The loop-D could then undergo further structural rearrangements creating a ‘lid’ over the active site, orientating/holding the TH substrate in place. Thereby creating an indirect link between the linker region, dimerization and loop-D, supporting the hypothesis that the linker could influence substrate specificity (Kuiper *et al*., 2003; Olvera *et al*., 2015; Schweizer and Steegborn, 2015). Overall, these possible dimer structures support and further refine the dimer model previously proposed by Schweizer *et al*., 2014 however, how dimerization occurs in the isoforms and what effect this has on catalytic activity remains speculative until elucidated from the structural characterisation of a deiodinase homodimer.

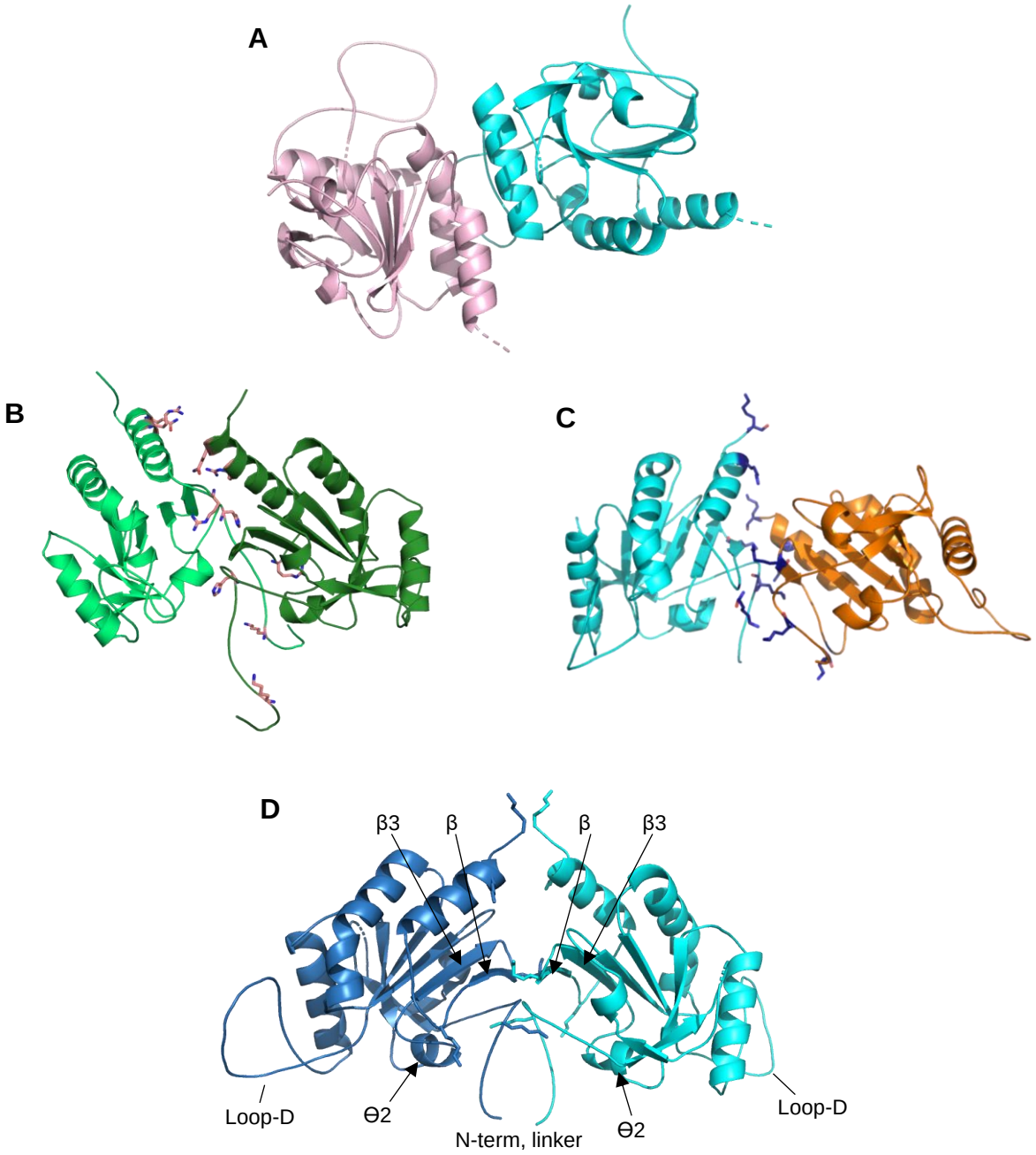

Fig 39. *Dimerization Interface.* *(A) Example of crystal contact from PISA for $Dio2_{cat}$. (B) Example of dimer interface for $Dio3_{cat}$ produced by HADDOCK. (C) Example of dimer interface for $Dio2_{cat}$ produced by HADDOCK. (D) $Dio2_{cat}$ dimer indicating specific regions associated with dimerization.*

4.2.3 Enforced dimer

As previously established, the N-terminal and linker region are needed for deiodinase activity and that the linker region, in particular, is required for dimerization. This was investigated further by creating an enforced dimer consisting of a leucine zipper (LZ) attached to a truncated form of Dio3 (78-304), containing the linker region. The LZ will act in place of the transmembrane domain (Fig 40), attached to the Dio3 construct and

drive the monomeric form of the protein into a dimeric form through the hydrophobic interactions of Leu residues in the parallel α-helices (Ramadevi *et al*., 1998; Jérôme and Müller, 2001). The production of this enforced dimer was not only to potentially produce a crystal structure of a dimeric form of Dio3 but also to test whether this generated dimer could still be a functional enzyme without a native transmembrane region. Therefore, this Dio3 dimer was used in conjunction with T_4 in an activity assay to determine the enzymes' ability to bind to TH substrate (3.3.3, Fig 24). The products were verified by liquid chromatography-tandem mass spectrometry and the results indicated an increase in rT_3 coinciding with the decrease of T_4 (Table A7). The activity of the Dio3 dimer further confirmed the role of the N-terminal transmembrane domain in catalytic activity of the Dio isoforms but also implied that the native transmembrane is possibly not needed for activity to occur as previously indicated. The role of the N-terminal transmembrane region could be to bring the catalytic regions of the homodimers together, a role that the LZ replaced, to effectively cause the conformational change needed for substrate interaction. Furthermore, the role of DTT dependence in the assay also supported the enzyme kinetics of the isoforms, in which an unknown thiol cofactor is needed as a reducing agent for the active site Sec, enabling catalysis to continue.

Overall, the assay indicated further potential in the use of the enforced Dio3 dimer in activity studies of the Dio isoforms, as the addition of the leucine zipper could also be applied to the truncated monomeric forms of Dio1 and 2. The activity assay could also be used to analyse possible further binding with other ligands and compounds of the Dios allowing further testing of prospective new drugs. However, the current assay is still limited, and additional comparisons would need to be made with monomeric forms of the Dio3 protein to support the evidence provided and show that the activity produced by the dimeric Dio3 is not an artefact. Further work could also be done with mutagenesis i.e. mutating the Cys^{170} to Ser to ascertain if a loss of activity/function of the enzyme occurs. Or with the use of inhibitors, such as xanthohumol, genistein (Dio1 specific) or iopanoic acid to investigate if these compounds could inhibit the activity of the enforced dimer.

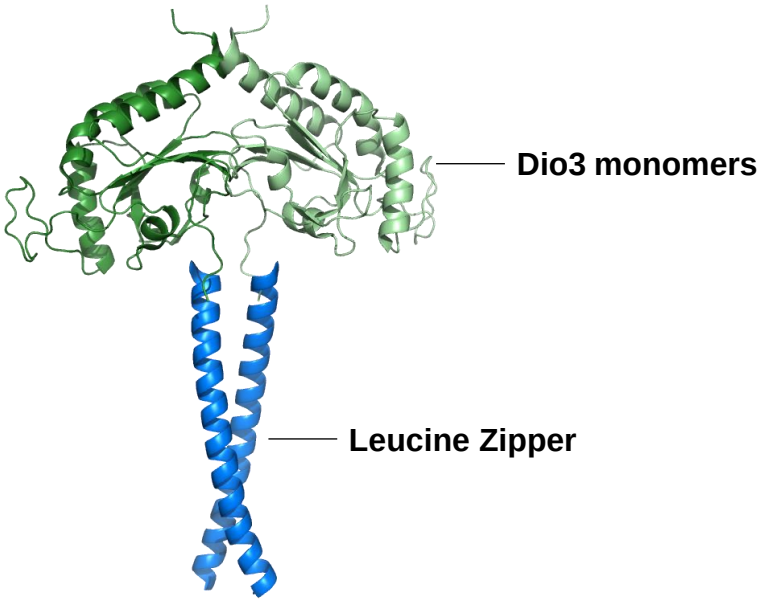

Fig 40. ***Modelling of enforced Dio3 dimer.*** *Example structure of mDio3cat in combination with a HY5 leucine zipper from Arabidopsis thaliana, PDB:2OQQ, (Yoon et al., 2007).*

4.3 Deiodinase ligands & compounds

4.3.1 Deiodinase binding

The analysis of binding between the Dio isoforms and TH substrates or potential compounds is an important feature in regards to understanding the functioning of the enzymes – what role do the specific regions of the protein play in binding, how does homodimerization support the catalytic activity and can binding still be seen without a full length native dimer? The mechanisms of catalysis for the Dio enzymes is still not fully understood likely contributing to the lack of modulators available for potential treatments against thyroid related diseases and cancer (Ciavardelli *et al*., 2014; Schweizer and Steegborn, 2015).

TSA and MST assays were used to investigate the protein-ligand interactions of both the Dio2 and 3 proteins with TH substrates or an inhibitor, xanthohumol with the goal of introducing these into crystallisation set ups. The TSA results with T_4/T_3 showed a lack of binding overall specifically for the Dio2 proteins, with only a small increase of melting temperature seen for the Dio3 dimer. Whereas, the results with xanthohumol indicated an increase in binding temperature for the Dio2 proteins. The outcome of these assays could be in part due to the T_4/T_3 substrates used and the NaOH solvent. The THs have particularly low solubility in water and experimentally are difficult to handle due to adhesion to plastic and glass (Schweizer *et al*., 2017). Furthermore,

initial TSA trials with the solvent, NaOH, implied a destabilisation of the protein was occurring causing a side effect to be seen in the TSA.

However, the absence of significant binding data with the THs could also be due to the truncated Dio proteins used in the assays. As previously stated, dimerization of the Dio isoforms is required for functionality of the enzymes; the truncated monomers of Dio2 and the non-native Dio3 dimer may be missing a certain structural component or even important residues required for the structural conformational changes needed to bind the THs. Nevertheless, as the activity assay for the Dio3 dimer indicated an ability for the enforced dimeric enzyme to bind to TH substrate, the ligand binding for TSA could be hampered by the use of the fluorogenic dye, Sypro Orange. This dye binds to the hydrophobic regions of the protein and as the ligand binding site is located in a hydrophobic pocket, the THs and the dye could compete for the binding site. The assessment of this competition would have to be tested with and without the fluorescent dye, which would negate the use of the TSA. Alternatively, the Sypro orange dye could be replaced by N-[4-(7-diethylamino-4-methyl-3-coumarinyl)phenyl] maleimide (CPM) (Alexandrov *et al*., 2008), a thiol-specific dye that could be used to evaluate protein-ligand binding for a full length Dio enzyme. Ultimately, the TSA indicated that the THs may not be a suitable addition to crystallography setups, as the results provided no evidence of increased protein stability.

As xanthohumol had indicated an increase in the melting temperature of the Dio2 proteins, this inhibitor was taken forward into MST assays. The results implied that a binding effect was seen between the protein and inhibitor however, this assay highlighted a few limitations and possible issues affecting the overall results. One major limitation was the concentration range of xanthohumol, and the precipitation seen in the upper limits of the concentration – a smaller range would be needed to see more evidence of conclusive binding. Furthermore, as the proteins have no internal fluorescence, they required hydrophobic labelling which could have hindered the results as it could cause non-specific binding to occur or interfered with the binding of xanthohumol. Additionally, as truncated forms of the Dio proteins were used, the binding could overall be too small to fully see via MST.

The overall outcome of the binding assays indicated that xanthohumol is stabilising the proteins, particular seen in the TSA results but whether complete binding is occurring would have to be investigated further. These results also partially support

the hypothesis that non-native Dio dimers can interact with the ligand but dimerization of the native Dio enzyme is needed specifically for strong TH binding. Alternate methods to study this interaction could be done with fluorescence anisotropy by labelling the ligand or by Isothermal titration calorimetry (ITC) but this would require a large sample quantity. However, the measuring of enzyme-ligand interaction may not be conducive to these methods as the main role of the Dio enzyme is not to hold a ligand for a period of time but to catalyse the iodination and release the ligand.

Further work on the protein-ligand interaction was performed computationally via HADDOCK or PLIP (protein-ligand interaction profiler) to try and identify how the THs could bind to the active site and the potential conformational changes needed. Unfortunately, the active site was not recognised as a potential binding site and even with the removal of loop-D from the structural PDB, this region was not identified as the ligand binding site. This work provides further evidence supporting the previous studies that a structural conformational change is required upon dimerization to allow access to the binding sites in the monomeric counterparts. Overall indicating that the structures obtained thus far are the ‘closed’ monomeric conformations of the Dio enzymes and dimerization creates an open enzyme for ligand binding.

Bibliography

Adams, P.D., Afonine, P. V., Bunkóczi, G., Chen, V.B., Davis, I.W., Echols, N., Headd, J.J., Hung, L.W., Kapral, G.J., Grosse-Kunstleve, R.W., McCoy, A.J., Moriarty, N.W., Oeffner, R., Read, R.J., Richardson, D.C., Richardson, J.S., Terwilliger, T.C. and Zwart, P.H. 2010. PHENIX: A comprehensive Python-based system for macromolecular structure solution. *Acta Crystallographica Section D: Biological Crystallography*. **66**(2), pp.213–221.

Afonine, P. V., Poon, B.K., Read, R.J., Sobolev, O. V., Terwilliger, T.C., Urzhumtsev, A. and Adams, P.D. 2018. Real-space refinement in PHENIX for cryo-EM and crystallography. *Acta Crystallographica Section D: Structural Biology*. **74**(6), pp.531–544.

Alexandrov, A.I., Mileni, M., Chien, E.Y.T., Hanson, M.A. and Stevens, R.C. 2008. Microscale Fluorescent Thermal Stability Assay for Membrane Proteins. *Structure*. **16**(3), pp.351–359.

Arrojo E Drigo, R. and Bianco, A.C. 2011. Type 2 deiodinase at the crossroads of thyroid hormone action. *International Journal of Biochemistry and Cell Biology*. **43**(10), pp.1432–1441.

Auf'mkolk, M., Koehrle, J., Hesch, R.D., Ingbar, S.H. and Cody, V. 1986. Crystal structure of phlorizin and the iodothyronine deiodinase inhibitory activity of phloretin analogues. *Biochemical Pharmacology*. **35**(13), pp.2221–2227.

Aw, D.K.L., Sinha, R.A., Tan, H.C., Loh, L.M., Salvatore, D. and Yen, P.M. 2014. Studies of molecular mechanisms associated with increased deiodinase 3 expression in a case of consumptive hypothyroidism *In*: *Journal of Clinical Endocrinology and Metabolism* [Online]. Endocrine Society, pp.3965–3971. [Accessed 22 July 2020]. Available from: https://pubmed.ncbi.nlm.nih.gov/24646062/.

Baqui, M., Botero, D., Gereben, B., Curcio, C., Harney, J.W., Salvatore, D., Sorimachi, K., Larsen, P.R. and Bianco, A.C. 2003. Human type 3 iodothyronine selenodeiodinase is located in the plasma membrane and undergoes rapid internalization to endosomes. *Journal of Biological Chemistry*. **278**(2), pp.1206–1211.

Baqui, M.M.A., Gereben, B., Harney, J.W., Larsen, P.R. and Bianco, A.C. 2000. Distinct subcellular localization of transiently expressed types 1 and 2 iodothyronine deiodinases as determined by immunofluorescence confocal microscopy. *Endocrinology*. **141**(11), pp.4309–4312.

Bates, J.M., St. Germain, D.L. and Galton, V.A. 1999. Expression profiles of the three iodothyronine deiodinases, D1, D2, and D3, in the developing rat. *Endocrinology*. **140**(2), pp.844–851.

Bayse, C.A., Marsan, E.S., Garcia, J.R. and Tran-Thompson, A.T. 2020. Thyroxine binding to type III iodothyronine deiodinase. *Scientific Reports*. **10**(1), pp.1–10.

Bergfors, T. 2003. Seeds to crystals.

Bernal, J. 2016. Deiodinases *In*: *The Curated Reference Collection in Neuroscience and Biobehavioral Psychology*. Elsevier Science Ltd., pp.392–398.

Berry, M.J. 1992. *Identification of Essential Histidine Residues in Rat Type I Iodothyronine Deiodinase*.

Berry, Maria J., Banu, L. and Larsen, P.R. 1991. Type I iodothyronine deiodinase is a selenocysteine-containing enzyme. *Nature*. **349**(6308), pp.438–440.

Berry, M. J., Kieffer, J.D., Harney, J.W. and Larsen, P.R. 1991. *Selenocysteine confers the biochemical properties characteristic of the type I iodothyronine deiodinase*.

Beyer, H.M., Gonschorek, P., Samodelov, S.L., Meier, M., Weber, W. and Zurbriggen, M.D. 2015. AQUA Cloning: A Versatile and Simple Enzyme-Free Cloning Approach D. Chatterji, ed. *PLOS ONE*. **10**(9), p.e0137652.

Bianco, A.C. and Kim, B.W. 2006. Deiodinases: implications of the local control of thyroid hormone action. *Journal of Clinical Investigation*. **116**(10), pp.2571–2579.

Bianco, A.C. and Larsen, P.R. 2005. Cellular and structural biology of the deiodinases. *Thyroid*. **15**(8), pp.777–786.

Bianco, A.C., Maia, A.L., Da Silva, W.S. and Christoffolete, M.A. 2005. Adaptive activation of thyroid hormone and energy expenditure. *Bioscience Reports*. **25**(3–4), pp.191–208.

Bianco, A.C., Salvatore, D., Gereben, B., Berry, M.J. and Larsen, P.R. 2002. Biochemistry, Cellular and Molecular Biology, and Physiological Roles of the Iodothyronine Selenodeiodinases. *Endocrine Reviews*. **23**(1), pp.38–89.

Callebaut, I., Curcio-Morelli, C., Mornon, J.P., Gereben, B., Buettner, C., Huang, S., Castro, B., Fonseca, T.L., Harney, J.W., Larsen, P.R. and Bianco, A.C. 2003. The iodothyronine selenodeiodinases are thioredoxin-fold family proteins containing a glycoside hydrolase clan GH-A-like structure. *Journal of Biological Chemistry*. **278**(38), pp.36887–36896.

Campos-Barros, A., Amma, L.L., Faris, J.S., Shailam, R., Kelley, M.W. and Forrest, D. 2000. Type 2 iodothyronine deiodinase expression in the cochlea before the onset of hearing. *Proceedings of the National Academy of Sciences of the United States of America*. **97**(3), pp.1287–1292.

Campos-Barros, A., Hoell, T., Musa, A., Sampaolo, S., Stoltenburg, G., Pinna, G., Eravci, M., Meinhold, H. and Baumgartner, A. 1996. Phenolic and tyrosyl ring iodothyronine deiodination and thyroid hormone concentrations in the human central nervous system. *The Journal of Clinical Endocrinology & Metabolism*. **81**(6), pp.2179–2185.

Casula, S. and Bianco, A.C. 2012. Thyroid hormone deiodinases and cancer. *Frontiers in Endocrinology*. **3**(JUN).

Celi, F.S., Dietrich, J.W., Zucchi, R., Senese, R., De Lange, P., Petito, G., Moreno, M., Goglia, F., Lanni, A., Vanvitelli, " L and Caserta, " 2018. 3,5-Diiodothyronine: A Novel Thyroid Hormone Metabolite and Potent Modulator of Energy Metabolism. *Frontiers in Endocrinology | www.frontiersin.org*. **1**, p.427.

Chaikuad, A., Knapp, S. and Von Delft, F. 2015. Defined PEG smears as an alternative approach to enhance the search for crystallization conditions and crystal-quality improvement in reduced screens. *Acta Crystallographica Section D: Biological Crystallography*. **71**(8), pp.1627–1639.

Ciavardelli, D., Bellomo, M., Crescimanno, C. and Vella, V. 2014. Type 3 deiodinase: Role in cancer growth, stemness, and metabolism. *Frontiers in Endocrinology*. **5**(DEC).

Citterio, C.E., Targovnik, H.M. and Arvan, P. 2019. The role of thyroglobulin in thyroid hormonogenesis. *Nature Reviews Endocrinology*. **15**(6), pp.323–338.

Croteau, W., Davey, J.C., Galton, V.A. and St. Germain, D.L. 1996. Cloning of the mammalian type II iodothyronine deiodinase. A selenoprotein differentially expressed and regulated in human and rat brain and other tissues. *Journal of Clinical Investigation*. **98**(2), pp.405–417.

Croteau, W., Whittemore, S.L., Schneider, M.J. and St. Germain, D.L. 1995. Cloning and expression of a cDNA for a mammalian type III iodothyronine deiodinase. *Journal of Biological Chemistry*. **270**(28), pp.16569–16575.

D'Arcy, A., Villard, F. and Marsh, M. 2007. An automated microseed matrix-screening method for protein crystallization. *Acta Crystallographica Section D: Biological Crystallography*. **63**(4), pp.550–554.

Davey, J.C., Becker, K.B., Schneider, M.J., St. Germain, D.L. and Galton, V.A. 1995. Cloning of a cDNA for the type II iodothyronine deiodinase. *Journal of Biological Chemistry*. **270**(45), pp.26786–26789.

Davis, I.W., Leaver-Fay, A., Chen, V.B., Block, J.N., Kapral, G.J., Wang, X., Murray, L.W., Bryan, W., Iii, A., Snoeyink, J., Richardson, J.S. and Richardson, D.C. 2007. MolProbity: all-atom contacts and structure validation for proteins and nucleic acids. *Nucleic Acids Research*. **35**, pp.375–383.

Dentice, M., Antonini, D. and Salvatore, D. 2013. Type 3 deiodinase and solid tumors: An intriguing pair. *Expert Opinion on Therapeutic Targets*. **17**(11), pp.1369–1379.

Dentice, M., Bandyopadhyay, A., Gereben, B., Callebaut, I., Christoffolete, M.A., Kim, B.W., Nissim, S., Mornon, J.-P., Zavacki, A.M., Zeöld, A., Capelo, L.P., Curcio-Morelli, C., Ribeiro, R., Harney, J.W., Tabin, C.J. and Bianco, A.C. 2005. The Hedgehog-inducible ubiquitin ligase subunit WSB-1 modulates thyroid hormone activation and PTHrP secretion in the developing growth plate. *NATURE CELL BIOLOGY*. **7**.

Echols, N., Grosse-Kunstleve, R.W., Afonine, P. V., Bunkóczi, G., Chen, V.B., Headd, J.J., McCoy, A.J., Moriarty, N.W., Read, R.J., Richardson, D.C., Richardson, J.S., Terwilliger, T.C. and Adams, P.D. 2012. Graphical tools for macromolecular crystallography in PHENIX. *Journal of Applied Crystallography*. **45**(3), pp.581–586.

Echols, N., Moriarty, N.W., Klei, H.E., Afonine, P. V., Bunkóczi, G., Headd, J.J., McCoy, A.J., Oeffner, R.D., Read, R.J., Terwilliger, T.C. and Adams, P.D. 2014. Automating crystallographic structure solution and refinement of protein-ligand complexes. *Acta Crystallographica Section D: Biological Crystallography*. **70**(1), pp.144–154.

Emsley, P. and Cowtan, K. 2004. Coot: Model-building tools for molecular graphics. *Acta Crystallographica Section D: Biological Crystallography*. **60**(12 I), pp.2126–2132.

Emsley, P., Lohkamp, B., Scott, W.G. and Cowtan, K. 2010. Features and development of Coot. *Acta Crystallographica Section D: Biological*

Crystallography. **66**(4), pp.486–501.

Van Den Ent, F. and Löwe, J. 2006. RF cloning: A restriction-free method for inserting target genes into plasmids. *Journal of Biochemical and Biophysical Methods*. **67**(1), pp.67–74.

Eravci, M., Pinna, G., Meinhold, H. and Baumgartner, A. 2000. *Effects of Pharmacological and Nonpharmacological Treatments on Thyroid Hormone Metabolism and Concentrations in Rat Brain** [Online]. Available from: https://academic.oup.com/endo/article-abstract/141/3/1027/2988156.

de Escobar, G.M., Obregon, M.J. and del Rey, F.E. 2008. Fetal and Maternal Thyroid Hormones. *Hormone Research*. **26**(1–4), pp.12–27.

Eswar, N., Webb, B., Marti-Renom, M.A., Madhusudhan, M.S., Eramian, D., Shen, M., Pieper, U. and Sali, A. 2006. Comparative Protein Structure Modeling Using Modeller. *Current Protocols in Bioinformatics*. **15**(1).

Ferreira, A.C.F., Lisboa, P.C., Oliveira, K.J., Lima, L.P., Barros, I.A. and Carvalho, D.P. 2002. Inhibition of thyroid type 1 deiodinase activity by flavonoids. *Food and Chemical Toxicology*. **40**(7), pp.913–917.

Fetrow, J.S. 1995. Omega loops; nonregular secondary structures significant in protein function and stability. *The FASEB Journal*. **9**(9), pp.708–717.

Gasteiger, E., Hoogland, C., Gattiker, A., Duvaud, S., Wilkins, M.R., Appel, R.D. and Bairoch, A. 2005. Protein Identification and Analysis Tools on the ExPASy Server *In*: *The Proteomics Protocols Handbook* [Online]. Humana Press, pp.571–607. [Accessed 26 September 2020]. Available from: https://link.springer.com/protocol/10.1385/1-59259-890-0:571.

Gereben, B., Bartha, T., Tu, H.M., Harney, J.W., Rudas, P. and Larsen, P.R. 1999. Cloning and expression of the chicken type 2 iodothyronine 5'- deiodinase. *Journal of Biological Chemistry*. **274**(20), pp.13768–13776.

Gereben, B., Goncalves, C., Harney, J.W., Larsen, P.R. and Bianco, A.C. 2000. Selective proteolysis of human type 2 deiodinase: A novel ubiquitin-proteasomal mediated mechanism for regulation of hormone activation. *Molecular Endocrinology*. **14**(11), pp.1697–1708.

Gereben, B., Zavacki, A.M., Ribich, S., Kim, B.W., Huang, S.A., Simonides, W.S., Zeöld, A. and Bianco, A.C. 2008. Cellular and molecular basis of deiodinase-regulated thyroid hormone signaling. *Endocrine reviews*. **29**(7), pp.898–938.

St. Germain, D.L. 1988. The effects and interactions of substrates, inhibitors, and the cellular thiol- disulfide balance on the regulation of type II iodothyronine 5'-deiodinase. *Endocrinology*. **122**(5), pp.1860–1868.

St. Germain, D.L., Schwartzman, R.A., Croteau, W., Kanamori, A., Wang, Z., Brown, D.D. and Galton, V.A. 1994. A thyroid hormone-regulated gene in Xenopus laevis encodes a type III iodothyronine 5-deiodinase (Proceedings of the National Academy of Sciences of the United States of America (August 2, 1994) 91 (7767-7771)). *Proceedings of the National Academy of Sciences of the United States of America*. **91**(23), p.11282.

Glinoer, D. and Cooper, D.S. 2012. The propylthiouracil dilemma. *Current Opinion in Endocrinology, Diabetes and Obesity*. **19**(5), pp.402–407.

Goldschmidt, L., Cooper, D.R., Derewenda, Z.S. and Eisenberg, D. 2007. Toward rational protein crystallization: A Web server for the design of crystallizable protein variants. *Protein Science*. **16**(8), pp.1569–1576.

Gomes-Lima, C., Wartofsky, L. and Burman, K. 2019. Can Reverse T3 Assay Be Employed to Guide T4 vs. T4/T3 Therapy in Hypothyroidism? *Frontiers in Endocrinology*. **10**, p.856.

Halperin, Y. 1994. Down-regulation of type II L-thyroxine, 5'-monodeiodinase in cultured GC cells: different pathways of regulation by L-triiodothyronine and 3,3',5'-triiodo-L-thyronine. *Endocrinology*. **135**(4), pp.1464–1469.

Huang, S.A. and Bianco, A.C. 2008. Reawakened interest in type III iodothyronine deiodinase in critical illness and injury. *Nature Clinical Practice Endocrinology and Metabolism*. **4**(3), pp.148–155.

Jerabek-Willemsen, M., Wienken, C.J., Braun, D., Baaske, P. and Duhr, S. 2011. Molecular interaction studies using microscale thermophoresis. *Assay and Drug Development Technologies*. **9**(4), pp.342–353.

Jérôme, V. and Müller, R. 2001. A synthetic leucine zipper-based dimerization system for combining multiple promoter specificities. *Gene Therapy*. **8**(9), pp.725–729.

Kabsch, W., T., B.A., K., D., A., K.P., K., D., S., M., G., R.R.B., P., E., S., F., K., W., W., K., W., K., W., K., W., K., P., K. and S., W.M. 2010. XDS. *Acta Crystallographica Section D Biological Crystallography*. **66**(2), pp.125–132.

Krissinel, E. and Henrick, K. 2007. Inference of Macromolecular Assemblies from Crystalline State. *Journal of Molecular Biology*. **372**(3), pp.774–797.

Kuiper, G.G.J.M., Kester, M.H.A., Peeters, R.P. and Visser, T.J. 2005. Biochemical mechanisms of thyroid hormone deiodination. *Thyroid*. **15**(8), pp.787–798.

Kuiper, G.G.J.M., Wassen, F., Klootwijk, W., Van Toor, H., Kaptein, E. and Visser, T.J. 2003. Molecular Basis for the Substrate Selectivity of Cat Type I Iodothyronine Deiodinase. *Endocrinology*. **144**(12), pp.5411–5421.

Larkin, M.A., Blackshields, G., Brown, N.P., Chenna, R., Mcgettigan, P.A., McWilliam, H., Valentin, F., Wallace, I.M., Wilm, A., Lopez, R., Thompson, J.D., Gibson, T.J. and Higgins, D.G. 2007. Clustal W and Clustal X version 2.0. *Bioinformatics*. **23**(21), pp.2947–2948.

Leonard, J.L. and Rosenberg, I.N. 1978. Subcellular distribution of thyroxine 5′-deiodinase in the rat kidney: A plasma membrane location. *Endocrinology*. **103**(1), pp.274–280.

Leonard, J.L. and Visser, T. 1986. Biochemistry of deiodination *In*: *Hennemann G (ed) Thyroid Hormone Metabolism*. Marce lDekker, New York, pp.189–229.

Leonard, J.L., Visser, T.J. and Leonard, D.M. 2001. Characterization of the Subunit Structure of the Catalytically Active Type I Iodothyronine Deiodinase. *Journal of Biological Chemistry*. **276**(4), pp.2600–2607.

Luiza Maia, A., Kim, B.W., Huang, S.A., Harney, J.W. and Larsen, P.R. 2005. Type 2 iodothyronine deiodinase is the major source of plasma T3 in euthyroid humans. *Journal of Clinical Investigation*. **115**(9), pp.2524–2533.

Maia, A.L., Goemann, I.M., Meyer, E.L.S. and Wajner, S.M. 2011. Type 1

iodothyronine deiodinase in human physiology and disease. *Journal of Endocrinology*. **209**(3), pp.283–297.

Mandel, S.J., Berry, M.J., Kieffer, J.D., Harney, J.W., Warne, R.L. and Larsen, P.R. 1992. Cloning and in vitro expression of the human selenoprotein, type I iodothyronine deiodinase. *Journal of Clinical Endocrinology and Metabolism*. **75**(4), pp.1133–1139.

Mandel, S.J. and Davies, T.. 2011. *Thyrotoxicosis* (Eds S Melmed KS Polonsky PR Larsen & HM Kronenberg, ed.). Elsevier.

Marsili, A., Zavacki, A.M., Harney, J.W. and Larsen, P.R. 2011. Physiological role and regulation of iodothyronine deiodinases: A 2011 update. *Journal of Endocrinological Investigation*. **34**(5), pp.395–407.

Martínez-Iglesias, O., Ruiz-Llorente, L., Contreras Jurado, C. and Aranda, A. 2014. Thyroid Hormone Receptors and their Role in Cell Proliferation and Cancer *In*: *Cellular Endocrinology in Health and Disease*. Elsevier Inc., pp.1–17.

McCoy, A.J., Grosse-Kunstleve, R.W., Adams, P.D., Winn, M.D., Storoni, L.C. and Read, R.J. 2007. Phaser crystallographic software. *Journal of Applied Crystallography*. **40**(4), pp.658–674.

Mondal, S. and Mugesh, G. 2017. Novel thyroid hormone analogues, enzyme inhibitors and mimetics, and their action. *Molecular and Cellular Endocrinology*. **458**, pp.91–104.

Mullur, R., Liu, Y.Y. and Brent, G.A. 2014. Thyroid hormone regulation of metabolism. *Physiological Reviews*. **94**(2), pp.355–382.

National Institute of Diabetes and Digestive and Kidney Diseases 2016. Hyperthyroidism (Overactive Thyroid) | NIDDK. [Accessed 25 June 2020]. Available from: https://www.niddk.nih.gov/health-information/endocrine-diseases/hyperthyroidism.

National Institute of Diabetes and Digestive and Kidney Diseases 2013. Hypothyroidism (Underactive Thyroid) | NIDDK. [Accessed 25 June 2020]. Available from: https://www.niddk.nih.gov/health-information/endocrine-diseases/hypothyroidism?dkrd=hispt0299.

Notredame, C., Higgins, D.G. and Heringa, J. 2000. T-coffee: A novel method for fast and accurate multiple sequence alignment. *Journal of Molecular Biology*. **302**(1), pp.205–217.

Olvera, A., Mendoza, A., Villalobos, P., Mayorga-Martínez, L., Orozco, A. and Valverde-R, C. 2015. The variable region of iodothyronine deiodinases directs their catalytic properties and subcellular localization. *Molecular and Cellular Endocrinology*. **402**, pp.107–112.

Ramadevi, N., Rodriguez, J. and Roy, P. 1998. A Leucine Zipper-Like Domain Is Essential for Dimerization and Encapsidation of Bluetongue Virus Nucleocapsid Protein VP4. *Journal of Virology*. **72**(4), pp.2983–2990.

Reinhard, L., Mayerhofer, H., Geerlof, A., Mueller-Dieckmann, J. and Weiss, M.S. 2013. Optimization of protein buffer cocktails using Thermofluor. *Acta Crystallographica Section F: Structural Biology and Crystallization Communications*. **69**(2), pp.209–214.

Renko, K., Hoefig, C.S., Hiller, F., Schomburg, L. and Köhrle, J. 2012. Identification of iopanoic acid as substrate of type 1 deiodinase by a novel nonradioactive iodide-release assay. *Endocrinology*. **153**(5), pp.2506–2513.

Renko, K., Schäche, S., Hoefig, C.S., Welsink, T., Schwiebert, C., Braun, D., Becker, N.-P., Köhrle, J. and Schomburg, L. 2015. An Improved Nonradioactive Screening Method Identifies Genistein and Xanthohumol as Potent Inhibitors of Iodothyronine Deiodinases. *Thyroid*. **25**(8), pp.962–968.

Rial, D. V. and Ceccarelli, E.A. 2002. Removal of DnaK contamination during fusion protein purifications. *Protein Expression and Purification*. **25**(3), pp.503–507.

Rosene, M.L., Wittmann, G., Arrojo E Drigo, R., Singru, P.S., Lechan, R.M. and Bianco, A.C. 2010. Inhibition of the type 2 iodothyronine deiodinase underlies the elevated plasma TSH associated with amiodarone treatment. *Endocrinology*. **151**(12), pp.5961–5970.

Ruf, J. and Carayon, P. 2006. Structural and functional aspects of thyroid peroxidase. *Archives of Biochemistry and Biophysics*. **445**(2), pp.269–277.

Sagar, G.D.V., Gereben, B., Callebaut, I., Mornon, J.-P., Zeöld, A., da Silva, W.S., Luongo, C., Dentice, M., Tente, S.M., Freitas, B.C.G., Harney, J.W., Zavacki, A.M. and Bianco, A.C. 2007. Ubiquitination-Induced Conformational Change within the Deiodinase Dimer Is a Switch Regulating Enzyme Activity. *Molecular and Cellular Biology*. **27**(13), pp.4774–4783.

Sagar, G.D.V., Gereben, B., Callebaut, I., Mornon, J.P., Zeöld, A., Curcio-Morelli, C., Harney, J.W., Luongo, C., Mulcahey, M.A., Larsen, P.R., Huang, S.A. and Bianco, A.C. 2008. The thyroid hormone-inactivating deiodinase functions as a homodimer. *Molecular Endocrinology*. **22**(6), pp.1382–1393.

Salvatore, D. 2011. Deiodinases: Keeping the thyroid hormone supply in balance. *Journal of Endocrinology*. **209**(3), pp.259–260.

Salvatore, D., Harney, J.W. and Reed Larsen, P. 1999. Mutation of the Secys residue 266 in human type 2 selenodeiodinase alters 75Se incorporation without affecting its biochemical properties. *Biochimie*. **81**(5), pp.535–538.

Salvatore, D., Low, S.C., Berry, M., Maia, A.L., Harney, J.W., Croteau, W., St. Germain, D.L. and Larsen, P.R. 1995. Type 3 iodothyronine deiodinase: Cloning, in vitro expression, and functional analysis of the placental selenoenzyme. *Journal of Clinical Investigation*. **96**(5), pp.2421–2430.

Salvatore, D, Tu, H, Harney, J W, Larsen, P R, Salvatore, Domenico, Tu, Helen, Harney, John W and Larsen, P Reed 1996. *Type 2 Iodothyronine Deiodinase Is Highly Expressed in Human Thyroid*.

Samuels, H.H., Forman, B.M., Horowitz, Z.D. and Ye, Z.S. 1988. Regulation of gene expression by thyroid hormone. *Journal of Clinical Investigation*. **81**(4), pp.957–967.

Sanders, J.P., Van der Geyten, S., Kaptein, E., Darras, V.M., Kühn, E.R., Leonard, J.L. and Visser, T.J. 1997. Characterization of a Propylthiouracil-Insensitive Type I Iodothyronine Deiodinase [1]. *Endocrinology*. **138**(12), pp.5153–5160.

Schweizer, U., Schlicker, C., Braun, D., Köhrle, J. and Steegborn, C. 2014. Crystal structure of mammalian selenocysteine-dependent iodothyronine deiodinase

suggests a peroxiredoxin-like catalytic mechanism. *Proceedings of the National Academy of Sciences of the United States of America*. **111**(29), pp.10526–31.

Schweizer, U. and Steegborn, C. 2015. New insights into the structure and mechanism of iodothyronine deiodinases. *Journal of Molecular Endocrinology*. **55**(3), pp.R37–R52.

Schweizer, U., Towell, H., Vit, A., Rodriguez-Ruiz, A. and Steegborn, C. 2017. Structural aspects of thyroid hormone binding to proteins and competitive interactions with natural and synthetic compounds. *Molecular and cellular endocrinology*.

Shevchenko, A., Tomas, H., Havliš, J., Olsen, J. V. and Mann, M. 2007. In-gel digestion for mass spectrometric characterization of proteins and proteomes. *Nature Protocols*. **1**(6), pp.2856–2860.

Shimizu, R., Yamaguchi, M., Uramaru, N., Kuroki, H., Ohta, S., Kitamura, S. and Sugihara, K. 2013. Structure-activity relationships of 44 halogenated compounds for iodotyrosine deiodinase-inhibitory activity. *Toxicology*. **314**(1), pp.22–29.

Sparta, K.M., Krug, M., Heinemann, U., Mueller, U. and Weiss, M.S. 2016. XDSAPP2.0. *Journal of Applied Crystallography*. **49**(3), pp.1085–1092.

Steinsapir, J., Harney, J. and Larsen, P.R. 1998. Type 2 iodothyronine deiodinase in rat pituitary tumor cells is inactivated in proteasomes. *Journal of Clinical Investigation*. **102**(11), pp.1895–1899.

Toyoda, N., Berry, M.J., Harney, J.W. and Larsen, P.R. 1995. Topological analysis of the integral membrane protein, type 1 iodothyronine deiodinase (D1). *Journal of Biological Chemistry*. **270**(20), pp.12310–12318.

Toyoda, N., Kaptein, E., Berry, M.J., Harney, J.W., Larsen, P.R. and Visser, T.J. 1997. Structure-Activity Relationships for Thyroid Hormone Deiodination by Mammalian Type I Iodothyronine Deiodinases. *Endocrinology*. **138**(1), pp.213–219.

Tu, H.M., Legradi, G., Bartha, T., Salvatore, D., Lechan, R.M. and Larsen, P.R. 1999. Regional expression of the type 3 iodothyronine deiodinase messenger ribonucleic acid in the rat central nervous system and its regulation by thyroid hormone. *Endocrinology*. **140**(2), pp.784–790.

Unger, T., Jacobovitch, Y., Dantes, A., Bernheim, R. and Peleg, Y. 2010. Applications of the Restriction Free (RF) cloning procedure for molecular manipulations and protein expression. *Journal of Structural Biology*. **172**(1), pp.34–44.

Valverde-R, C., Croteau, W., LaFleur, G.J., Orozco, A. and St. Germain, D.L. 1997. Cloning and Expression of a 5′-Iodothyronine Deiodinase from the Liver of <i>Fundulus heteroclitus. *Endocrinology*. **138**(2), pp.642–648.

Vasil'ev, A.A. and Engman, L. 1998. Iodothyronine Deiodinase Mimics. Deiodination of o,o'-Diiodophenols by Selenium and Tellurium Reagents. *Journal of Organic Chemistry*. **63**(12), pp.3911–3917.

Visser, T.J. 1988. Metabolism of thyroid hormone. *New Comprehensive Biochemistry*. **18**, pp.81–103.

Visser, T.J., Van Der Does Tobe, I., Docter, R. and Hennemann, G. 1976. Subcellular localization of a rat liver enzyme converting thyroxine into tri iodothyronine and

possible involvement of essential thiol groups. *Biochemical Journal*. **157**(2), pp.479–482.

Visser, T.J., Leonard, J.L., Kaplan, M.M. and Larsen, P.R. 1982. Kinetic evidence suggesting two mechanisms for iodothyronine 5'-deiodination in rat cerebral cortex. *Proceedings of the National Academy of Sciences of the United States of America*. **79**(16 I), pp.5080–5084.

Wienken, C.J., Baaske, P., Rothbauer, U., Braun, D. and Duhr, S. 2010. Protein-binding assays in biological liquids using microscale thermophoresis. *Nature Communications*. **1**(7), pp.1–7.

Wu, Y. and Koenig, R.J. 2000. Gene regulation by thyroid hormone. *Trends in Endocrinology and Metabolism*. **11**(6), pp.207–211.

WW, du M., G, M., C, W. and PG, J. 2001. Reactions of Organoselenenyl Iodides With Thiouracil Drugs: An Enzyme Mimetic Study on the Inhibition of Iodothyronine Deiodinase. *Angewandte Chemie (International ed. in English)*. **40**(13).

Yoon, M.K., Kim, H.M., Choi, G., Lee, J.O. and Choi, B.S. 2007. Structural basis for the conformational integrity of the Arabidopsis thaliana HY5 leucine zipper homodimer. *Journal of Biological Chemistry*. **282**(17), pp.12989–13002.

Van Zundert, G.C.P., Rodrigues, J.P.G.L.M., Trellet, M., Schmitz, C., Kastritis, P.L., Karaca, E., Melquiond, A.S.J., Van Dijk, M., De Vries, S.J. and Bonvin, A.M.J.J. 2016. The HADDOCK2.2 Web Server: User-Friendly Integrative Modeling of Biomolecular Complexes. *Journal of Molecular Biology*. **428**(4), pp.720–725.

Appendix

Table A1: Kinetics of Deiodinases
Summary of Deiodinase kinetics from 1.3.2

Construct	Km	Vmax	Preferred Substrate
Dio1	High nM – low µM	pmol/mg/min	rT_3
Dio2	Low nM	≤Dio1	T_4
Dio3	nM	-	T_3

Figure A2: Chemical structures of compounds from 1.6, produced using MarvinSketch. (A) Gold thioglucose. (B) Xanthohumol. (C) Genistein. (D) Propylthiouracil. (E) Methylthiouracil. (F) Methimazole. (G) Iopanoic acid. (H) Amiodarone.

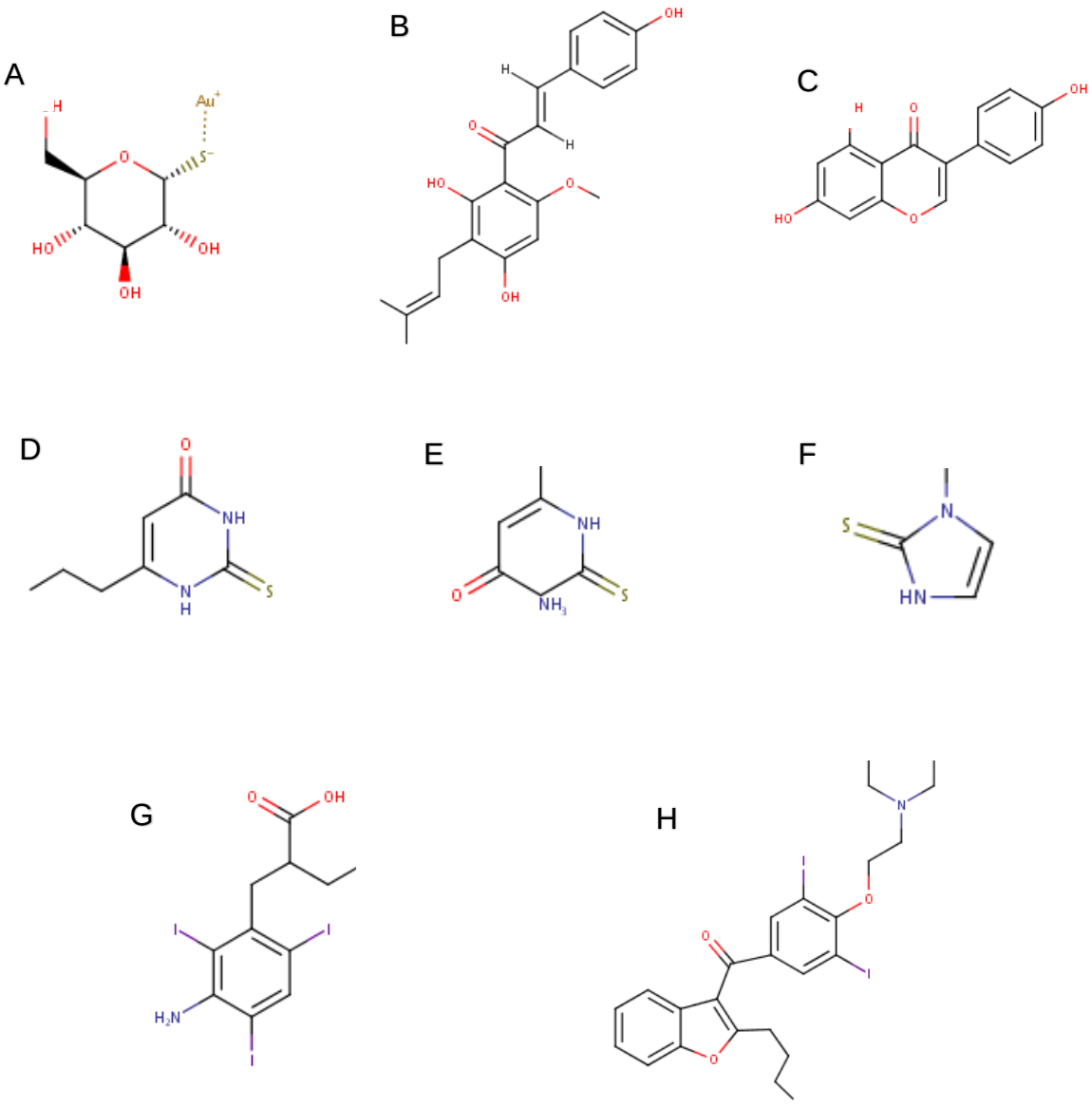

Table A3: Oligonucleotide primers for PCR

Dio	Construct	Primer
hDio1 (*E.coli*)	52-249	Forward: 5'-TCTTCTGGTGAGAATCTTTATTTTCAGGGAAGGAACCCCCATTTCAGC-3' Reverse: 5'-TCAGCTTCCTTTCGGGCTTTGTTAACTGTGGAGCTTTTCCAGAA-3'
	75-249	Forward: 5'-ATTCTTCTGGTGAGAATCTTTATTTTCAGGGATTGAAGGTCCGTTGGC-3' Reverse: 5'-TCAGCTTCCTTTCGGGCTTTGTTAACTGTGGAGCTTTTCCAGAA-3'
	77-249	Forward: 5'-GCATCGCGAACAGATCGGTGGTGTCCGTTGGCAGCGACTA-3' Reverse: 5'-TCGACCCCGGGTCCCATATGTTAACTGTGGAGCTTTTCCAGA-3'
	86-249	Forward: 5'-GCATCGCGAACAGATCGGTGGTACTGAGCTAGGGGGTCTG-3' Reverse: 5'-TCGACCCCGGGTCCCATATGTTAACTGTGGAGCTTTTCCAGA-3'
	104-249	Forward: 5'-GCATCGCGAACAGATCGGTGGTAGGTGCAACATTTGGGAGT-3' Reverse: 5'-GGTCGACCCCGGGTCCCATATGTTAACTGTGGAGCTTTTCCAGA-3'
mDio2 (*E.coli*)	80-262	Forward: 5'-GCGCATCGCGAACAGATGGGTGGTGATGCTCCCAATTCCAGTG-3' Reverse: 5'-CTCAGCTTCCTTTCGGGATTTGTTACTATCTCTTGCTGAAATTCTTCTC-3'
	90-262	Forward: 5'-GGAATTCCATATGTCCAATCCTGAATCAGG-3' Reverse: 5'-CGCGGATCCTCATCTCTTGCTGAAATTC-3'
	103-262	Forward: 5'-TCGCGAACAGATCGGTGGATCCACCGCTGATGGGGCCGAA-3' Reverse: 5'-GGTGGTGGTGGTGGTGCTCGAGTCATCTCTTGCTGAAATTCTTCTCC-3'
mDio3 (*E.coli*)	78-304	Forward: 5'-GCTTTGTTAGCAGCCGGATCCCTCATTAGAATCGATGTGGCCTAGTACC-3' Reverse: 5'-AAATCAGATGCTGCGTCATATTCTGAAAAACGACCACCCTGAGCCCG-3'
LZ	N/A	Forward: 5'-GTTAGCAGCCGGATCCCTCGAGGTTTTTCAGAATATGACGCAGCATC-3' Reverse: 5'-GCATCGCGAACAGATCGGTGGTGCTTATCTGAGCGAACTGGAAAATC-3'

Table A4: Oligonucleotide primers for site directed mutagenesis

Construct	Mutation	Primer
D2S_63, D2S_66 & D2C_71	KK180AA	Forward: 5'-CTCTGTCTTTTGAGGTTGCGGCGCACCGGA-3' Reverse: 5'-CCTCTTGGTTCCGGTGCGCCGCAACCTCAA-3'
D2S_63/66	KK180AA	Forward: 5'-CTCTGTCTTTTGAGGTTGCGGCGCACCGGAACCAAGAGG-3' Reverse: 5'-CCTCTTGGTTCCGGTGCGCCGCAACCTCAAAAGACAGCG-3'
D2C_71	EK101AA	Forward: 5'-GTAACAATTATGCCTCGGCGGCGACCGCTGATGG-3' Reverse: 5'-CCATCAGCGGTCGCCGCCGAGGCATAATTGTTAC-3'
LZ_D3C	EGEE89AGAA	Forward: 5'-GTAGAGCTCAACAGTGCAGGCGCGGCGATGCCCCCTGACGAC-3' Reverse: 5'-GTCAGGGGGCATCGCCGCGCCTGCACTGTTGAGCTC-3'

Table A5: Molecular weight, pI & extinction coefficient of proteins

Protein	Molecular Weight (kDa)	pI	Extinction Coefficient (M^{-1} cm^{-1})
Dio1 Full length	29	8.8	~ 53,000
D2S_49	24	5.9	~ 31,000
D2S_63	22.3	5.8	~ 25,500
D2C_66	22	5.7	~ 20,000
D2C_71	21.4	5.9	~ 20,000
D2S_80	20.4	5.7	~ 18,600
D2S_90	19.4	5.8	~ 18,600
D2S_99	18.4	6.1	~ 17,000
D2S_103	18	6.0	~ 17,000
LZ_D3C (dimer)	60	5.3	~ 65,000

Fig A6: LZ_D3C vector map. Created using Snapgene software (*Insight Science*).

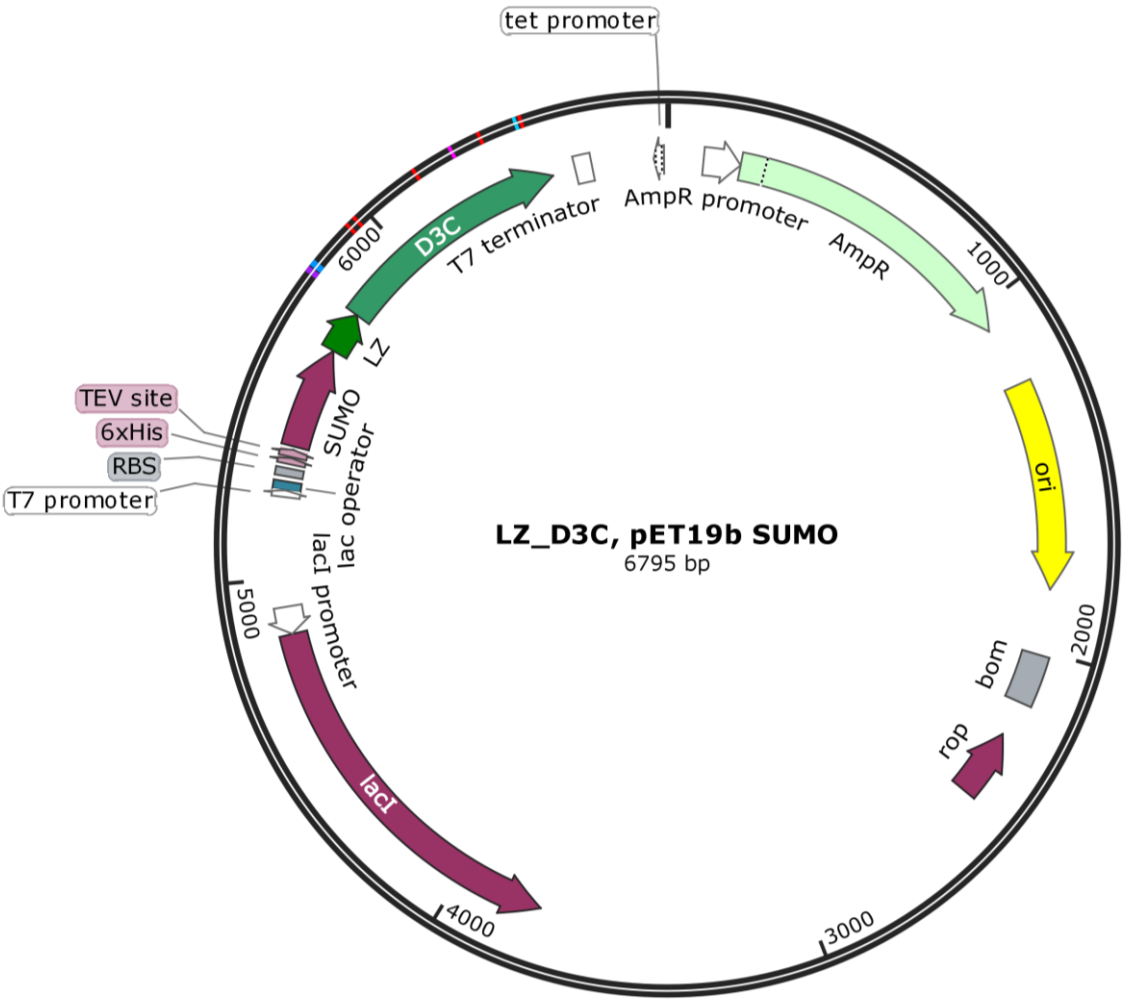

Table A7: Results from Mass Spectrometry of the LZ_D3C activity assay indicating area ratio of TH substrates.

Highlighted samples produced anomalous results and were excluded from the final calculations.

	T4 area ratio	T3 area ratio	rT3 area ratio	3,5-T2 area ratio
D3C_0h 5 µg	1764.90899	0.36261	0.02378	0.084
D3C_0h 5 µg	1837.38729	0.37668	0.02649	0.08238
D3C_1h 5 µg	1642.94978	0.36757	0.02996	0.07537
D3C_1h 5 µg	1381.7426	0.30949	0.03218	0.05479
D3C_2h 5 µg	1815.92698	0.43671	0.08655	0.07565
D3C_2h 5 µg	1536.36263	0.35775	0.03961	0.0686
D3C_0h 10 µg	1780.8399	0.35955	0.02383	0.07575
D3C_0h 10 µg	1851.45668	0.38312	0.02599	0.08484
D3C_1h 10 µg	1780.6288	0.39491	0.04126	0.07729
D3C_1h 10 µg	1621.60041	0.35523	0.03488	0.07529
D3C_2h 10 µg	1646.43926	0.37567	0.05517	0.07249
D3C_2h 10 µg	1555.81191	0.38403	0.04907	0.07636
D3C_0h 10 µg w/o DTT	1855.01345	0.37606	0.02599	0.09039
D3C_0h 10 µg w/o DTT	1762.94834	0.62181	0.17213	0.11651
D3C_1h 10 µg w/o DTT	1777.83865	0.37972	0.031	0.08981
D3C_1h 10 µg w/o DTT	1716.24179	0.36275	0.03026	0.09908
D3C_2h 10 µg w/o DTT	1634.06718	0.35471	0.02829	0.09164
D3C_2h 10 µg w/o DTT	1667.24943	0.36817	0.02666	0.09671
D3C_0h 20 µg	1809.27282	0.37303	0.02536	0.08502
D3C_0h 20 µg	1726.11667	0.37462	0.02532	0.07724
D3C_1h 20 µg	1615.26033	0.3866	0.06367	0.07543
D3C_1h 20 µg	1641.90956	0.38097	0.05834	0.06813
D3C_2h 20 µg	1142.75163	0.29658	0.06967	0.0559
D3C_2h 20 µg	1696.30733	0.40495	0.0951	0.07599
Control – w/o D3C	1906.94495	0.39576	0.02699	0.06321

Figure A8: Xanthohumol concentrations used in MST assays.

Created using the concentration finder software from Nanotemper Technologies. This was used to find the xanthohumol concentrations that would produce the optimum binding curve and also enable the DMSO concentration to remain low (< 10%).

Cap number	Concentration (µM)
1	140
2	46.67
3	15.56
4	5.19
5	1.73
6	0.58
7	0.19
8	0

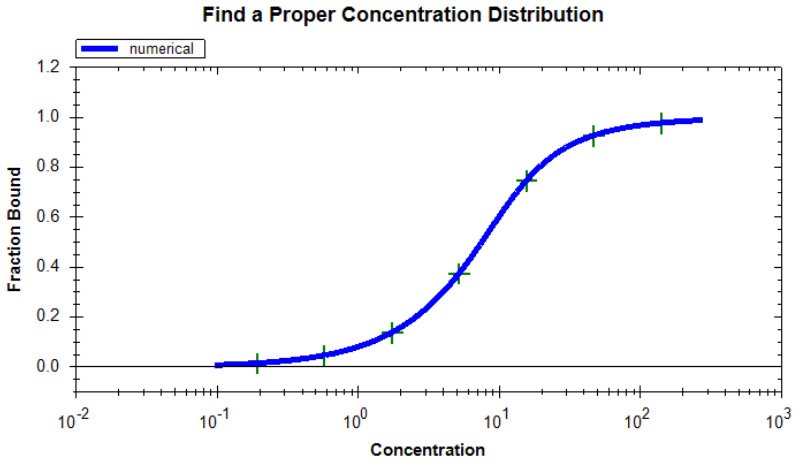

Table A9: Results from MST assay for Dio2 proteins and Xanthohumol.
Anamalous results highlighted in orange and excluded from final fit.

D2S_63 MST results (20% Laser power)		D2S_63 MST results (30% Laser power)		D2S_63 MST results (40% Laser power)	
Xanthohumol [µM]	0-100% results	Xanthohumol [µM]	0-100% results	Xanthohumol [µM]	0-100% results
140	46.66	140	84.0680	140	78.2771
46.67	100.0	46.67	100.0	46.67	100.0
15.56	58.4570	15.56	44.8637	15.56	42.6840
5.19	56.3160	5.19	12.4382	5.19	7.6163
1.73	37.3220	1.73	0.0	1.73	25.3843
0.58	21.1250	0.58	7.3155	0.58	38.6973
0.19	0.0	0.19	0.2843	0.19	0.6752
0.0	76.3230	0.0	2.6439	0.0	0.0

D2C_66 MST results (20% Laser power)		D2C_66 MST results (30% Laser power)		D2C_66 MST results (40% Laser power)	
Xanthohumol [µM]	0-100% results	Xanthohumol [µM]	0-100% results	Xanthohumol [µM]	0-100% results
140	68.7140	140	100.0	140	85.9205
46.67	100.0	46.67	91.3920	46.67	100.0
15.56	75.4210	15.56	52.6078	15.56	61.5313
5.19	36.8340	5.19	17.3700	5.19	69.8539
1.73	27.8350	1.73	32.9992	1.73	65.0437
0.58	0.0	0.58	0.0	0.58	41.0208
0.19	27.9730	0.19	32.8207	0.19	64.2653
0.0	96.0830	0.0	42.4614	0.0	0.0

Table A10: Results from MST assay for LZ_D3C protein and Xanthohumol.

LZ_D3C MST results (20% Laser power)		LZ_D3C MST results (30% Laser power)		LZ_D3C MST results (40% Laser power)	
Xanthohumol [µM]	0-100% results	Xanthohumol [µM]	0-100% results	Xanthohumol [µM]	0-100% results
140	90.4260	140	84.0680	140	78.2771
46.67	100.0	46.67	100.0	46.67	100.0
15.56	47.2210	15.56	44.8637	15.56	42.6840
5.19	12.7020	5.19	12.4382	5.19	7.6163
1.73	0.0	1.73	0.0	1.73	25.3843
0.58	3.4560	0.58	7.3155	0.58	38.6973
0.19	3.30	0.19	0.2843	0.19	0.6752
0.0	5.0010	0.0	2.6439	0.0	0.0

Acknowledgements

I would like to take this opportunity to thank everyone who supported and guided me during my doctorate.

First of all I would like to thank Prof. Dr. Clemens Steegborn for providing me with the opportunity to not only work on an interesting project but also for the chance to come to Germany and work with some amazing people. Thank you for the discussions, motivation and perseverance in the project and in me.

I would like to thank all the members of the AG Steegborn group, past and present. Notable names include, Dr. Michael Weyand, Dr. Matthew Fuszard, Dr. Andrea di Fonzo, Dr. Christian Kambach, Dr. Sébastien Moniot and Dr. Allegra Vit. Thank you for the many discussions and helpful feedback throughout the years. Many thanks go to the amazing Sabrina, Susanne, Lisa and Norbert for all of your support and help with my project and in the lab. I would like to also thank Renate, Gabi and Anke for all of their continued assistance and help in many matters, you made my life in Germany much easier! To all of the colleagues of AG Steegborn and past students, you have made my time in Bayreuth so enjoyable and the incredible working atmosphere and dynamic is something I will never forget.

I would like to specifically thank my office colleagues, ‘the boys’, Julian Pfahler and Jonathan Quast. Our office became synonymous with the sound of laughter and lively discussions. You both were always there with thoughtful insights, a shoulder to lean on and even a helping hand (sometimes helping me out from under the desk). The experience in our ‘V.I.B office’ was one of a kind and something I’m forever grateful for.

I would also like to take this opportunity to thank the AG Höcker and AG Möglich groups for creating an amazing atmosphere in and outside of the department. We all became a weird, wonderful (if not sometimes dysfunctional) family and I have enjoyed all of our moments together. I would like to specifically thank Sooruban Shanmugaratnam for his patience, kindness and even laughter in the lab; and also Dr. Robert Stabel for his continued support and friendship over the years through work, life and even climbing.

I would like to also thank the MX team of Helmholtz Zentrum Berlin for their discussions and support during and outside of our beamtimes. I would like to further thank the Thyroid Trans Act, without their funding and support this project would not be possible.

My biggest thanks goes to my biggest supporters, my friends and family. Even though I'm sure many of you still are not quite certain what I actually do, you have always supported me in my endeavours with comforting words, encouragement and genuine happiness in celebrating my achievements. So, to my amazing family and those unfortunately no longer with us (Grandad Bob), I hope I have made you proud.

And finally, I would like to thank my parents. My Dad supported me during all of my education, pushed me to try my hardest and always allowed me to dream big. You brought up being a Doctor to me many years ago, and although I maybe haven't taken the route you had in mind, I want you to know you planted the seed and I'm grateful for your help over the years. And of course I would like to thank my Mum, I wouldn't be where I am today without her. Every triumph and hardship I have had, she has been there every step of the way encouraging me and picking me back up. She never once told me I was incapable of achieving what I wanted in life and always believed in me. Thank you for giving me the confidence to stand up for myself and be heard. You are my greatest advocate and defender, and quite literally my loudest supporter. This completion of my doctorate isn't just my accomplishment, it is also yours.

Eidesstattliche Versicherungen und Erklärungen

(§ 8 Satz 2 Nr. 3 PromO Fakultät)

Hiermit versichere ich eidesstattlich, dass ich die Arbeit selbstständig verfasst und keine anderen als die von mir angegebenen Quellen und Hilfsmittel benutzt habe (vgl. Art. 64 Abs. 1 Satz 6 BayHSchG).

(§ 8 Satz 2 Nr. 3 PromO Fakultät)

Hiermit erkläre ich, dass ich die Dissertation nicht bereits zur Erlangung eines akademischen Grades eingereicht habe und dass ich nicht bereits diese oder eine gleichartige Doktorprüfung endgültig nicht bestanden habe.

(§ 8 Satz 2 Nr. 4 PromO Fakultät)

Hiermit erkläre ich, dass ich Hilfe von gewerblichen Promotionsberatern bzw. –vermittlern oder ähnlichen Dienstleistern weder bisher in Anspruch genommen habe noch künftig in Anspruch nehmen werde.

(§ 8 Satz 2 Nr. 7 PromO Fakultät)

Hiermit erkläre ich mein Einverständnis, dass die elektronische Fassung der Dissertation unter Wahrung meiner Urheberrechte und des Datenschutzes einer gesonderten Überprüfung unterzogen werden kann.

(§ 8 Satz 2 Nr. 8 PromO Fakultät)

Hiermit erkläre ich mein Einverständnis, dass bei Verdacht wissenschaftlichen Fehlverhaltens Ermittlungen durch universitätsinterne Organe der wissenschaftlichen Selbstkontrolle stattfinden können.

…….

Ort, Datum, Unterschrift